Department of Small Animals and Horses
University of Veterinary Medicine Vienna
Clinic of Equine Hospital
(Head: Univ.-Prof. Dr. med. vet. Florien Jenner, Dipl. ACVS/ECVS)

Development of a 3D joint-on-a-chip model to mimic healthy and osteoarthritic equine joints - a pilot study

Master Thesis

for the degree of

Master of Science (MSc.)

University of Veterinary Medicine Vienna

submitted by
Sabina Gansberger, BSc

Vienna, May 2021

Supervisors:

Univ.-Prof. Dr. med. vet. Florien Jenner, Dipl.ACVS, Dipl.ECVS

AND

Dr. med. vet. Iris Ribitsch, PhD, Priv.-Doz.

University of Veterinary medicine Vienna

Department of Small Animals and Horses

Clinic of equine Hospital

AND

Dr. Mario Rothbauer, MSc

Medical University of Vienna

Department of Orthopedics and Trauma Surgery

Karl Chiari Lab of Orthopaedic Biology

Reviewer:

Assoc. Prof. Dr. Thomas Kolbe

University of Veterinary Medicine Vienna

Institute of In-vivo and In-vitro Models

Biomodels Austria

Table of Contents

List of Abbreviations

3D	Three dimensional
36b4/Rplp0	ribosomal phosphoprotein P0
ACAN	aggrecan
ADAMTS	a disintegrin and metalloproteinase with thrombospondin motif
CAD	computer-aided design
cDNA	complementary Desoxyribonucleic acid
Col1	cartilage-related gene collagen type I
Col2	collagen type II
ColX	collagen Type X
COMP	cartilage oligomeric matrix protein
DAMP	danger associated molecular pattern
DMEM	Dulbecco`s modified eagle's medium
ECM	extra cellular matrix
EtOH	ethanol
FCS	fetal calf serum
FDA	fluorescein diacetate
GAG	glycosaminoglycan
GAPDH	glyceraldehyde 3-phosphate dehydrogenase
Hif	hypoxia-inducible factor
Ihh	Indian hedgehog
IL	interleukin
INF	interferon
LIF	leukemia inhibitory factor
MAPK	mitogen-activated protein kinase
MIA	monosodium iodoacetate
MMP	matrix metalloproteinase
MMP-13	metalloproteinase 13
MSC	mesenchymal stem cell
NK-κB	nuclear factor-kappa B
NSAID	nonsteroidal anti-inflammatory drug
OA	osteoarthritis
PBS	phosphate buffered saline
PDMS	polydimethylsiloxane
PG	proteoglycan
qPCR	quantitative polymerase chain reaction
PI	propidium iodide
PPIA	peptidylprolyl isomerase A
Runx2	Runt-related transcription factor 2
SNP	single nucleotide polymorphism
Sox9	SRY-related high mobility group-box gene 9
TNF-α	tumor necrosis factor-α

1 Introduction

Osteoarthritis (OA) is a highly prevalent joint disease[1]. It is the most common form of arthritis and is a major cause of disability[2]. The term osteoarthritis is derived from the Greek words *osteo* (bone) and *arthron* (joint)[3]. It can be found in any joint, but is particularly prevalent in the hip, knee(s), hand(s) and spine[4]. Any articular injury can lead to the onset of OA[1]. Characteristic for OA pathophysiology is the degeneration or loss of articular cartilage of the joint[5]. The disease is associated with pain and impaired locomotion in late stages. OA may not be a single disease but rather reflects a common response to joint tissue damage induced by mechanical or biological factors[6,7].

1.1 Epidemiology

Osteoarthritis is one of the most frequently occurring diseases of the musculoskeletal system. It is considered the most common form of arthritis[8]. In 2017 globally approximately 300 million people were affected by this disease, which is approximately 4 % of the population. This makes it one of the most diagnosed diseases in human general practice[5]. In 2020 it was the fifth leading cause of disability world-wide[9]. Especially in elderly people OA is responsible for impaired locomotion[10]. Due to aging of the population, it is believed that the incidence of OA will increase further. OA is expected to be the single greatest cause of disability by the year 2030[2]. Hence, osteoarthritis leads to high socioeconomic costs. It was estimated that the annual economic burden exceeds 185 million US dollar world-wide[11].

However, OA is not only a prevalent disease of humans but of most mammalian species, including domesticated animal species such as horses, sheep, cats and dogs[12,13].

1.1.1 Osteoarthritis in horses

In equine patients orthopaedic disorders such as osteoarthritis are very common. At equine hospitals 54 – 60 % of all presented lameness's are related to this disease[1,14,15]. OA has a high impact on the equine industry not only because of treatment costs but also as reason for dropping out from athletic use. It is consider one of the major causes of horse retirement[8]. Mainly older horses are affected but due to excessive training also young athletes are often affected by this disease[16]. In young racehorses (2-3 years) every third was found to have cartilage

lesions and osteoarthritis[13]. Reasons for this could be premature training start or excessive and prolonged mechanical loading[8,13].

1.2 Structure and function of a normal joint

Joints are highly complex structures composed of a number of connective tissues which all contribute to normal joint function and transmission of mechanical loads. The main components of a joint are articular cartilage, the subchondral bone, the synovium which produces the synovial fluid and the peri-articular soft tissues including ligaments and tendons[17]. In diseased state these connective tissues undergo changes in structure, function and metabolism[14].

1.2.1 Synovium

The connective vascular tissue lining the inner surface of a joint is called synovium[6]. It is a specialized connective tissue and seals the synovial cavity and fluid from surrounding tissues in synovial joints[18]. The main functions of the synovium include lubrication, immune responses and phagocytosis[19]. All articular surfaces except for the articular cartilage and focal areas of the bone are covered by this tissue[6]. The synovial lining has neither a conventional basement membrane nor a true epithelium for separating the joint cavity from the synovial vasculature[3]. The synovium consists of cells from the subsynovial stroma (fibrous, areolar and fatty tissues) and the synovial intima. The later is lined by synoviocytes, which are classified into three major cell types: type A, B and C cells[6]. Type A cells contain vacuoles and are of macrophage origin[19], type B cells are derived from fibroblasts and type C cells appear to be an intermediate from type A and B. Most abundant in the synovium are type B cells, which have a secretory fibroblast-like function and synthesise important macromolecules such as lubricin and hyaluronan[6,19]. Lubricin are molecules rich in collagen and proteoglycans and are embedded within the ECM. They act as semi-permeable membrane and mediate transport of solutes[19]. Synoviocytes are responsible for the exchange between the blood and the synovial fluid as well as for the production of its components[3].

1.2.2 Subchondral Bone

The subchondral bone is histologically and biochemically very similar to bone in other locations. However, the organisation of the subchondral bone plate is very specific. Compared to bones in other anatomical locations, the plate is thinner and its haversian system is oriented

parallel to the joint surface and not parallel to the long axis of the bone[6]. The subchondral bone is lying immediately beneath the calcified cartilage and can be separated into the subchondral bone plate and the trabecular bone[20]. The plate is very porose and is invaded by channels, containing blood vessels and nerves, which directly link it to the cartilage. The number and diameter of this channels depends on the magnitude of compression within and between the joints[20]. Distal to the plate is the subchondral trabecular bone, which is important for shock absorption and stabilisation of the normal joint[6,20]. Compared to the plate it is more metabolic active and it was found that it may be important for the nutrient supply to the cartilage[21]. The subchondral trabecular bone is inhomogeneous in structure and changes with distance to the cartilage[22]. The subchondral bone is uniquely adapted to mechanical forces acting on the joint through different density patterns, mechanical properties, adjustable scale parameters and bone remodelling upon mechanical stress[20].

1.2.3 Articular Cartilage

Articular cartilage (hyaline cartilage) is a specialized type of connective tissue which is extremely complex. It is aneural, avascular and alymphatic, which means that nutrient supply to the cells happens by diffusion from the synovial fluid [23]. Cartilage covers the subchondral plate and is composed of a fluid and solid phase and chondrocytes[24]. Moreover, organized collagen and proteoglycan arrangements, as well as water, are key components. Cartilage has a very high water content (around 70 %, depending on the age) and it is freely exchanged with the synovial fluid[6]. The main functions of articular cartilage are load-bearing, shock absorption and articulation of joints. It allows for simultaneous motion and weight-bearing with negligible friction[25,26]. The elastic deformation properties of hyaline cartilage allow for withstanding of compression forces considerably higher than the normal body weight[27]. The ability of cartilage to withstand the high forces acting on articular surfaces depend on its structure, the water content and the biochemical composition[28].

The only cell type found in articular cartilage are chondrocytes. They are highly specialized and are important for cartilage development and maintanaince[29]. They originate from mesenchymal stem cells (MSCs) and make less than 2 % of the total cartilage volume and their density varies with the distance from the surface as does the composition of the surrounding macromolecules[17].

Articular cartilage is divided into four histologically and phenotypically distinct zones: the superficial (tangential or gliding) zone, the middle (transitional) zone and the deep (radial) zone as well as the calcified zone[3]. The zones are differentiated based on the different cell morphology and collagen organisation. Especially the superficial zone is of interest due to its high density of biologically active cells and the surface-to-surface contact. It provides lubrication and contains elongated cells which are responsible for the production of lubricin, hyaluronate and other anti-adhesive molecules[6]. Cells in this zone are usually smaller and flatter and they are present in a greater density compared to cells in deeper zones[29]. Chondrocytes found in the middle zone show a round morphology. They produce important extracellular matrix components that provide the tissue with its unique biomechanical properties[6]. In the deep zone, chondrocytes are usually larger. The deep zone is the tissue boundary to the subchondral bone[17]. Each zone has different structural properties which protect against compression, shear and tensile forces. The compression capacity of the deep zones is much higher than that of the superficial zones[24].

1.2.3.1 Chondrocytes

Chondrocytes live in a relatively acidic and hypoxic environment[6]. In healthy joints they have a low metabolic activity and possess limited regenerative capacity[10,23]. Through the production of important extracellular matrix components such as aggrecan and collagen type II, they enable resilience of the joints[24]. The balance between catabolic and anabolic processes of chondrocytes is one of the most important things that maintain a healthy cartilage[8]. They rarely form cell-cell contacts for communication between cells. However, they respond to a variety of external and internal stimuli such as mechanical loading, hydrostatic pressure and growth factors[29]. Phenotypic stability of chondrocytes is important for maintaining the homeostasis of articular cartilage and is lost during OA. Chondrocytes react to abnormal biomechanical and biochemical environment by taking part in cartilage matrix destruction and acquire a fibroblast-like and hypertrophy-like phenotype[30]. Chondrocyte hypertrophy is a normal development stage in endochondral ossification during bone formation[31]. However, in OA the differentiation of chondrocytes toward hypertrophy is aberrant and is characterized by an increased expression of matrix-degrading enzymes[30]. The shift towards hypertrophy happens in a disorganised way. It is characterised by epigenetic changes[32] and abnormal gene expressions[33] that lead to phenotypic instability. In none-diseased state chondrocytes express cartilage specific genes, like SRY-related high mobility group-box gene 9 (Sox9), aggrecan (ACAN) and collagen type

II (Col2)a1, at a relatively low level, this enables a low matrix turnover. During early stages of OA it comes to an increase in anabolic processes with an increased expression of these cartilage specific genes and factors that drive the hypertrophic phenotype Runt-related transcription factor 2 (Runx2) and hypoxia-inducible factor (Hif)-2α. In later phases of OA the expression of cartilage specific markers decreases and expression of hypertrophic genes increases, such as Runx2, collagen Type 10 (Col10)a1 and matrix metalloproteinase (Mmp)13[30].

1.2.3.2 Extracellular matrix of cartilage - Collagens and Proteoglycans

The major structural components of the extracellular matrix (ECM) in articular cartilage are collagen type II and proteoglycans (PGs)[34]. They are responsible for the specialized biomechanical properties of hyaline cartilage such as load-bearing and shock absorption[8]. Type II collagen is produced by chondrocytes during early development. Resynthesis of fibrils after degradation only occurs limited in adults[6].

Collagens in articular cartilage differ from those found in other anatomical locations. In cartilage, collagen type II is accounting for more than 90 % of the fibral network[3]. It is more glycosylated than type I collagen and forms fibrils that are not uniform. They are larger in the center and the deep zones of the matrix where they are radially oriented and anchor the cartilage to the underlying bone plate. Whereas fibrils in the superficial zone are orientated parallel to the joint surface and have a protective function. This reflects the diverse biomechanical demands on different areas of the joint[6].

Proteoglycans are important for load distribution upon compression. They consist of proteins and polysaccharides[6]. Various types can be found in articular cartilage. The largest is aggrecan and it is also the most abundant polyglycan in articular cartilage[3]. It interacts with hyaluronan to form aggregates. This bond is stabilized by linker proteins which are similar in humans and horse[6]. Aggrecan has three globular domains. Glycosaminoglycans (GAGs) and oligosaccharide chains are attached to its core protein[26]. The GAGs attract cations and water which leads to swelling of the tissue and is counteracted by the fibrillar collagen network. This gives the articular cartilage its high tensile strength and robustness[34].

1.2.3.3 Nutrition

The articular cartilage of adults lacks blood vessels. Nutrients are transported from the synovial vessels to the synovial fluid and from there they penetrate the cartilage[6]. It is based on diffusion and is facilitated by compression-relaxation cycles. Joint movement is important to enable sufficient nutrient supply, since it was shown that diffusion alone is insufficient. This would explain why cartilage degrades in immobilized joints[35]. Metabolic waste products are cleared in opposite direction[26]. Also subchondral bone vessels may penetrate the calcified cartilage and supply it with nutrients[36]. Without the direct nutrient supply through blood vessels or lymph, chondrocytes depend mainly on anaerobic metabolism[29]. Chondrocytes consume much less oxygen than most other cell types. Chondrocytes mainly depend on the Embden-Meyerhof-Parnas pathway of glycolysis, which is oxygen independent[35]. In cartilage hypoxic conditions are found, which facilitates the differentiation of MSC into chondrocytes rather than osteocytes[37]. Oxygen tension falls with distance from articular surfaces. Tension at the deep zones of cartilage was determined to be roughly 1 %[35]. Zhou et al. found that the oxygen consumption rate in articular cartilage at 21 % oxygen is 10.6 ± 1.4 nmoles/10^6 cells/hour and that it is relative independent from oxygen tension[35]. The diffusivity of small molecules in cartilage is round 40 to 50 % of their diffusivity in aqueous solutions[35].

1.3 Osteoarthritis

1.3.1 Etiopathogenesis

OA is a multifactorial disorder with numerous causes, include aging, obesity, genetic predisposition, accumulation of microtrauma or one major trauma[10]. Genetic alterations causing OA are for example abnormal TGF-beta/Smad, Wnt/beta-catenin or Ihh (Indian hedgehog) signaling pathways, which lead to an imbalance between anabolic and catabolic activity of chondrocytes and results in irreversible degradation of the ECM[12]. Genetic studies have identified multiple genetic risk factors for OA. However, the odds ratios for most identified single nucleotide polymorphism (SNP) associations are low, and mainly apply only to one form of this disease[10]. Moreover, the mechanisms underlying these genetic risks are often unidentified[12]. In horses, repeated microtrauma is the most common factor to cause OA[6].

1.3.2 Pathophysiology and progression

Osteoarthritis is defined as a chronic degenerative joint disease with intermittent inflammatory episodes induced by normal wear and tear or through injury or abnormal mechanical loading[2]. Characteristic for OA is the degeneration or complete loss of articular cartilage, subchondral bone sclerosis and the formation of new bone on the joint surfaces and margins[4]. However, all joint tissues undergo morphological changes depending on the diseased state (Figure 1)[12].

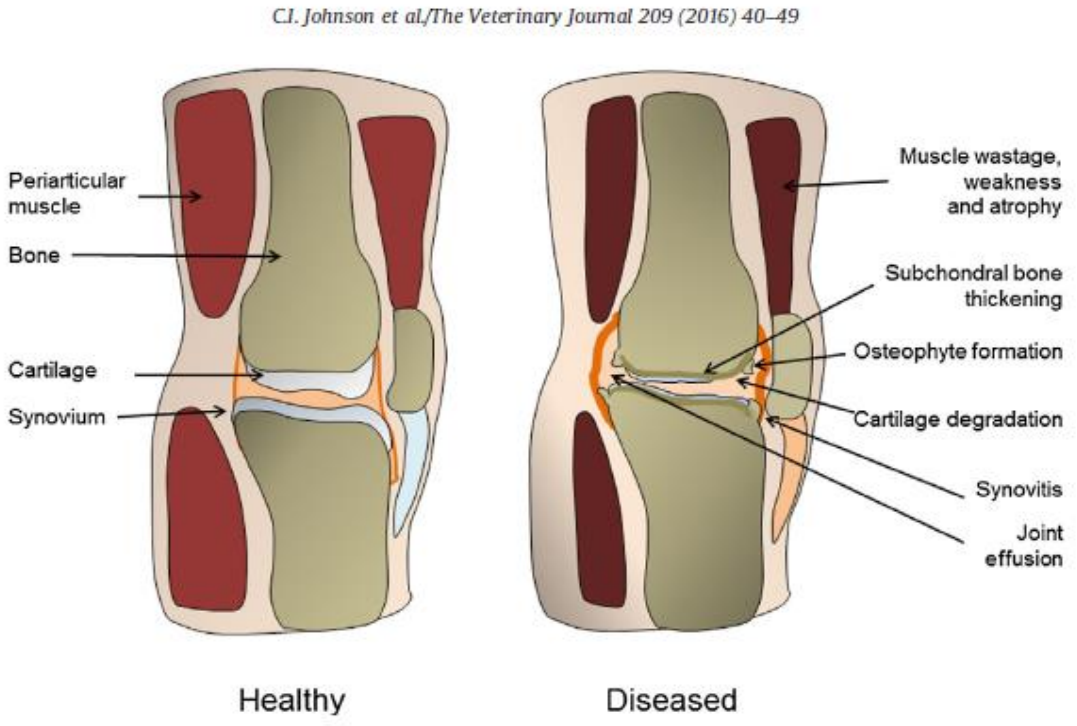

Figure 1: ***Depiction of a healthy and a diseased synovial joint****. Showing the changes in the entire organ upon diseased state: bone weakening and wearing, synovial thickening and swelling, subchondral bone thickening, osteophyte formation and cartilage degeneration. Additionally, weakening and inflammation of tendons and laxation of ligaments can be observed (Johnson et al., 2016).*

First, the ECM undergoes remodeling through changes of the molecular composition as well as organisation. Water molecules are attracted by negatively charged glycosaminoglycan chains which get exposed through the disruption of the extracellular matrix. Consequently, water content increase and thus swelling of the cartilage is observed. Followed by fibrillation of the cartilage surface. With that, the resistance against external forces is decreased and

deep clefts within the cartilage are formed[10]. Resulting from the loss of cartilage, friction between joint surfaces increases, which causes pain, limited motion and other OA associated symptoms. As the damage progresses, cartilage as well as subchondral bone fragments, are released into the joint space where they induce an inflammatory response[13]. OA is characterised as a disease of the whole joint[38]. It has long been seen as primary disease of the articular cartilage, but recently it has been shown that synovial inflammation and subchondral bone damage can initiate OA and have an impact on disease progression[38,39].

1.3.2.1 The role of the subchondral bone in OA

The subchondral bone plays a considerable role in the progression of osteoarthritis, because it dampens the mechanical force acting on the joint and acts as a source of inflammatory mediators, which are responsible for degeneration of the deep cartilage layer[40,41]. Upon disease state biochemical, biomechanical and structural changes are observed at the osteochondral junction in joints. This includes loss of integrity, meaning that the barrier between the synovial cavity and the subchondral bone gets compromised, and osteochondral plasticity, where adjacent structures create new tissues with aberrant functions and morphologies[42]. Fissures in the articular cartilage, which arose during OA often extend into the subchondral plate. Following fragmentation subchondral and synovial compartments become floated with tissue debris, cells and fluids[43]. Through osteochondral junctions' osteoblasts, osteoclasts, osteocytes and the bone-lining cells can communicate with the cartilage[42]. During OA disease progression this communication is enhanced. Through tissue disruption subchondral tissue becomes exposed to molecules produced by chondrocytes, e.g. vascular endothelial growth factor[44]. Other examples are cytokines and growth factors to enhance nerve growth and sensitivity, osteoclast activity and formation of new bone structures. On the other hand chondrocytes become exposed to differentiation factors through the invasion of vascular channels into the articular cartilage from the subchondral tissue[42]. Moreover, chondrocyte hypertrophy has been connected to endochondral ossification[44].

1.3.2.2 The role of the synovium in OA

Synovial tissue inflammation is present in all stages of OA[45] and plays an important role in cartilage degradation (Figure 2). During OA it comes to a loss of the lubrication function of the synovium, this has increased wearing and heating of the joint as consequence[19]. Hyper physiological mechanical stress leads to primary synovitis[46]. Synoviocytes release high amounts of

degradative enzymes and inflammatory mediators involved in matrix depletion. Examples of these are cytokines, prostaglandins and metalloproteinases[47]. However, synoviocytes synthesize also soluble mediators important in OA progression such as cytokines like IL-1, eicosanoids and proteinases[46]. These mediators in turn attract immune cells, induce an phenotypic shift in in chondrocytes and enhance angiogenesis[2]. Immune cells are present in the synovium that contribute to the inflammation process, such as synovial $CD4^+$T cells, which secrete TNF-α and IL-6[48]. The predominant immune cells in OA synovium are T-cell lymphocytes and mast cells. To a lesser extent also B cells, plasma cells and mast cells are found[48]. In response to cytokines it comes to an influx of leucocytes from the vascular compartments into the synovium. Macrophages start to infiltrate the synovium and form multinucleated giant cells, which enhance phagocytosis. Mainly synovial macrophages are responsible for the innate immune activation and cytokine production during OA, but also chondro- and synoviocytes play a role[49]. Moreover, alterations in the normal function of type B synoviocytes are observed during disease. They start to release pro-inflammatory cytokines which leads to a shift in chondrocyte activity to produce degrading enzymes. Type B synoviocytes can transform into fibrocytes upon inflammation[19].

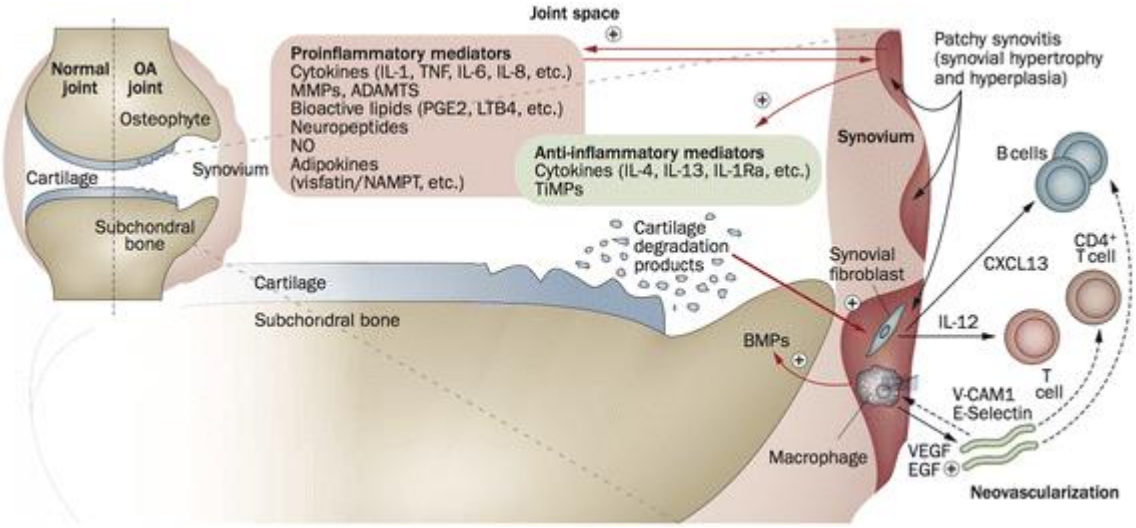

*Figure 2**: Involvement of the synovium in osteoarthritis**. Phagocytosis of cartilage breakdown products by synovial cells leads to an amplification of synovial inflammation. Activated synovial cells produce pro-inflammatory cytokines and catabolic mediators responsible for cartilage breakdown. Activation of synovial T-, B-cells and macrophages further enhance inflammatory responses. To counteract this anti-inflammatory cytokines get produced (Mathiessen et al., 2017)*

1.3.2.3 The role of cartilage in OA

Articular cartilage shows the greatest morphological changes of all tissues involved in OA. In healthy joints, chondrocytes maintain the balance between matrix degradation and repair, induced by mechanical stimuli and cytokines. Physiological loading increases the anabolic activity of chondrocytes. This leads to increased proteoglycan synthesis, cell proliferation, aggrecan expression and collagen type II expression and that prevents cartilage destruction[51]. It was found that in rats moderate exercise can protected against the development of OA compared to normal cage activity[52]. It was also reported that mechanical stimulation influences the differentiation of mesenchymal stem cells into chondrocytes and modulates cartilage homeostasis[50].

Mechanical stimulation has a regulatory impact on development and long-term maintenance of articular cartilage[53], including matrix biosynthesis and transcriptional networks in chondrocytes[23]. Metabolic changes in chondrocytes play a major role in cartilage degradation. In OA catabolic processes predominate, hence the balance is shifted towards degradation[51]. In figure 3 the effects of mechanical loading on chondrocytes are shown. Abnormal loading leads to upregulation of MMPs and ADAMTs through various pathways, which induces cartilage damage. Moreover, long-term exposure to inflammatory stimuli and stress through extensive mechanical loading induce a phenotypic change in chondrocytes towards a fibroblast-like and hypertrophy-like phenotype. This shift is characterised by an aberrant gene expression[30]. Abnormal mechanical stress on the joint triggers intracellular signalling by mechanoreceptors. These receptors are found at the surface of cells in joint tissue, especially chondrocytes and cells of the subchondral bone[64]. Following activation of mechanoreceptors, inflammatory mediators (prostaglandins, chemo- and cytokines) are synthesised and released. Proinflammatory pathways such as nuclear factor-kappa B (NK-κB) and mitogen-activated protein kinase (MAPK) are activated through mechanical stress (Figure 3)[40]. During early disease states, the proteoglycan synthesis is upregulated but matrix destruction is massive resulting in a loss of matrix. Non-physiological loading promotes the degradation of EMC through the production of MMP-13 and other enzymes[26,53]. With increased cartilage loss the viscoelastic properties become insufficient to withstand normal loading forces. This leads to cartilage fissures and remodelling of the bone and articular soft tissue[6]. Altered joint biomechanics, which lead to mechanically induced tissue destruction, can be responsible for chronic inflammation. Mechanotransduction stress signalling can lead to cytokine production and cell-derived DAMPs[63].

Chondrocytes react to pro-inflammatory cytokines released by synoviocytes and osteochondral cells. Upon stimulation they shift their metabolism towards production of cartilage degrading enzymes and inhibition of tissue repair and regeneration[19]. Chondrocytes exhibit a momentary proliferative response and increased matrix synthesis in an attempt to repair the damage caused by pathological stimuli. Characteristic for this stage is chondrocyte cloning and formation of clusters as well as hypertrophic cloning[13]. Chondrocytes are further stimulated to secret catabolic factors. This is a key factor in cartilage depletion[10]. Collagen and proteoglycan networks break down, which disturbs cartilage integrity. Consequently, chondrocytes undergo apoptosis and complete loss of articular cartilage is initiated[6].

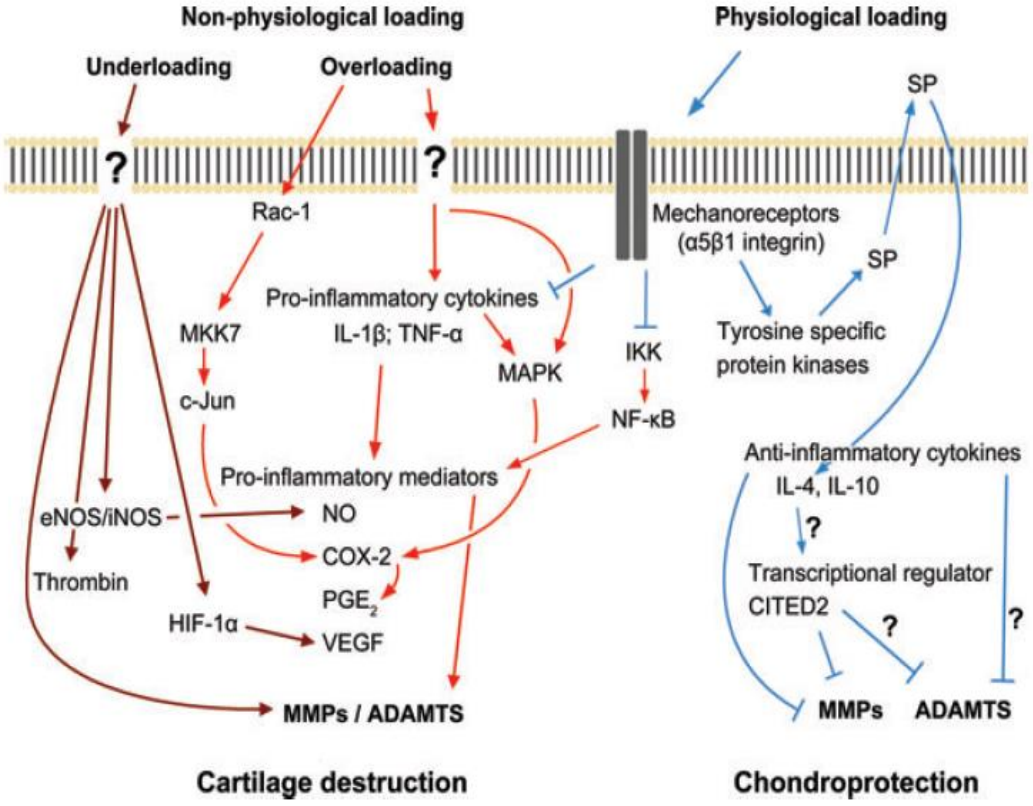

Figure 3: ***Effects of mechanical loading on chondrocytes****. Non-physiological loading includes over as well as underuse. The abnormal loading leads to upregulation of MMPs and ADAMTs through various pathways and that induces cartilage damage. On the other hand, physiological loading blocks these pathways and protects cartilage from destruction (Sun, 2010).*

During daily activities, articular cartilage is subjected to complex dynamic mechanical loading, including shear, tensile stress and compression. A study by Mosher et al. showed that a 20 minutes run leads to transient cartilage strains of about 20 % in the weight bearing regions of

the femur and strains of about 30 % in regions of the tibia[54]. During walking peak strains of 7 to 23 % are found in the tibiofemoral contact area[55]. Hence, cartilage strains depend on anatomical locations and specific activity undertaken. These biomechanical forces lead to matrix deformation, volume changes, shear stresses, intra-tissue fluid flow, streaming potential and hydrostatic pressure gradients and other physical phenomena[28]. Nonetheless, the body manages to prevent destruction of cartilage, as long as the forces are not too excessive[6]. During physical activity load on articular cartilage in humans can vary between seven to ten MPa[56] reaching up to 20 MPa at intense activity[25]. It is unknown at which range the physiological load intensity ends and where the non-physiological starts. In bovine cartilage explants, it was found that the critical point was reached for a single impact at a force of 15-20 MPa where apoptosis of chondrocytes and collagen damage was induced. Other studies found chondrocyte apoptosis already happened at a peak stress of 4.5 MPa and degradation of collagen was observed at 7-12 MPa[57]. The last study indicates that chondrocyte apoptosis may precede cartilage matrix damage. A study which used repetitive loading of 5 MPa at 0.3 Hz elucidated that impact damage is also cumulative in joints[58]. However, also immobility can have a destructive impact on cartilage homeostasis because it also induces catabolic processes in the chondrocytes[51]. Immobility leads to cartilage thinning, tissue softening and reduced proteoglycan content over time[59]. Various mechanisms such as the transmission of forces to surrounding tissues and fluid distribution, axial strains on the cartilage are minimized[24].

1.3.2.4 Osteoarthritis and Inflammation

OA related symptoms and the progression of the disease are associated with the degree of inflammation[65]. The term osteoarthritis implies that this disease involves inflammation. However, for a long time, it was believed that OA is a non-inflammatory arthropathy. This was due to the fact that in OA patients compared to ‘inflammatory joint diseases’ such as rheumatoid arthritis, the levels of pro-inflammatory cytokines is rather low[66]. Only since recent years, it is recognized that a persistent low-grade inflammation and activation of innate inflammatory pathways are central mediators of OA pathogenesis[63].

Roughly 12 % of all OA cases are secondary to prior joint injury. This includes disruption of anterior cruciate ligaments, meniscus injuries and intra-articular fractures[67]. Joint trauma leads to cellular and molecular alterations, which can lead to cartilage destruction over time. One example of these alterations is the release of inflammatory mediators immediately post injury[65].

Furthermore, an aberrant wound-healing is found. This accounts to the chronic low-grade inflammation in OA. Under normal conditions, wound healing is initiated by danger-associated molecular patterns (DAMPs), which induce blood clotting, inflammation, cellular proliferation and tissue remodelling[63]. They interact with pattern recognition receptors and stimulate the innate immune system response. The activated signalling cascade leads to production of chemo- and cytokines, growth factors and matrix proteases, which stimulate cell proliferation and tissue remodelling[68].

1.3.2.5 The role of Cytokines

Pro-inflammatory cytokines such as interleukin (IL) -1, tumor necrosis factor-α (TNF-α), IL-6 and leukemia inhibitory factor (LIF) play an important role in the pathogenesis of osteoarthritis[39]. They are responsible for functional changes in cartilage, synovium and subchondral bone[69]. Anti-inflammatory cytokines, like IL-4, IL-10 and interferon (INF) -y may block the actions of the pro-inflammatory cytokines. To a low-level cytokines are needed to maintain normal homeostasis. However, in OA the balance is disrupted[70]. Cytokines and growth factors play a central role in OA induction and development. IL-1β and TNF-α are first produced by synoviocytes and diffuse via the synovial membrane into the articular cartilage[69]. They are responsible for cartilage destruction and drive further inflammatory responses. Cytokine receptors are expressed on chondrocytes, synoviocytes and other cell types of the joint and are significantly elevated in number in OA[69,71]. Cytokines pass across the subchondral bone and create an important cross-talk between bone cells and chondrocytes[72]. Activation of cytokine receptors has deleterious effects on the chondrocyte metabolism[6]. In response chondrocytes and synoviocytes start to produce other cytokines, such as LIF, IL-6 and IL-8. Moreover, catabolic factors such as proteases and proinflammatory cytokines get produced[69]. Especially IL-1 was identified to play a major role in cartilage matrix destruction. Elevated levels were found in patient (human and horse) synovial fluids[39]. Moreover, IL-1 is involved in the formation of inadequate repair tissue in cartilage and decreases the synthesis of type II collagen as well as proteoglycans. Additionally, the synthesis of metalloproteinases is inhibited which further promotes catabolic metabolism[73].

1.4 Clinical manifestation

Clinically OA is characterized in horses through varying levels of lameness, which often is bilateral[8,13]. In human as well as in veterinary patients major symptom of OA include joint instability, pain, stiffness, swelling, reduced range of motion, inflammation and radiographic joint space narrowing[4,13,51]. Only a weak correlation between the magnitude of pain and the severity of cartilage degradation is present in osteoarthritis[6]. Osteoarthritis can be found in any joint in the body and can lead to a reduced mobility. The joint pain is typically aggravated by activity and relived by rest. However, in advanced disease states, OA can also induce pain at rest[74].

1.4.1 Diagnosis and Biomarkers

Physical examination (degree of pain and remaining mobility) and radiology are currently the only available diagnostic modalities for OA. However, they fail to detect early disease states[11,75]. Biomarkers are defined as any substance, structure, or process that allows for the prediction of an incidence or disease[76]. Due to the high prevalence of OA finding suitable biomarker became very important. Biomarkers for OA include metabolic markers found in blood, urine and synovial fluid, miRNA and special proteins such as collagen[77,]. Since the synovial fluid is one of the first joint components that gets altered upon disease, it is an interesting source for biomarkers. Examples are upregulation of cytokines like interleukin 6 (IL-6), IL-1B and tumor necrosis factor alpha (TNF-α). Interesting serum biomarkers are Collagen Type X (ColX) or COMP[77,78]. Both are important for cartilage stabilisation and become upregulated during OA[11].

1.4.2 Treatment

Currently, no treatment is available to stop the progressive loss of articular cartilage and fully restore joint functionality[55]. Thus, there is a large unmet need for novel treatment approaches and disease-modifying regenerative therapies for OA[79].

At the moment disease management focuses on the treatment of symptoms, mainly the relief of pain and stiffness. Systemic treatments include nonsteroidal anti-inflammatory drugs (NSAIDs) and nutraceuticals. NSAIDs are used for pain management. They are considered effective and easy to administer. However, they can cause side effects such as gastrointestinal ulceration and kidney disease[80]. Moreover, intra-articular therapies can be performed. An example would be the application of corticosteroids, which are considered potent, effective and

inexpensive[81]. Other examples for intra-articular therapies are biological therapies, where e.g. Il-1 receptor antagonist or mesenchymal stem cells are administered. Biological therapies rely on immune-modulatory and regenerative properties[82]. Alternatively, shockwave therapy or physical therapy can be a treatment option[83,84].

1.5 Models for osteoarthritis

Many aspects of osteoarthritis are still unclear. Model organisms such as mice, rats, guinea pigs, rabbits, sheep, goats and horses are commonly used to study OA[85]. Throughout the years various models were established to study the complexity of the joint and the interplay between biochemical, mechanical and inflammatory factors, which regulate cartilage matrix homeostasis[55]. The higher the functional alignment of the model to the native tissue and observed pathogenesis, the higher the translation value of the model[86].

1.5.1 The horse as a model for OA

The horse is an ideal model for OA, since the pathogenesis, clinical presentation and articular biology is equivalent to humans[1,8]. As it is also observed in humans OA incidences increase with age in equines[16]. Furthermore, the similar cartilage thickness, cellular structure, biochemical composition and mechanical properties are of advantage compared to small-sized animals[1,85]. The average articular cartilage thickness is 1.5 to 2 mm in horses and 2.2 to 2.5 mm in humans. In small sized animals the mean thickness is much lower, eg in rabbits it is only 0.3 mm[87]. In addition, the loading forces acting on equine joints are of a similar or even greater magnitude than in humans[88]. An advantage of using the horse as a model is the availability of naturally occurring, early-stage diseased tissue following a veterinary surgical intervention. Whereas from humans only tissue of advanced disease progression state is a source of samples for *in vitro* models[12]. All these facts make the horse a suitable model for studying OA. By studying this disease in horses not only veterinary but also human patients will benefit.

1.5.2 In vivo models

In vivo models provide a good insight into osteoarthritis. However, none of the currently available *in vivo* OA models is able to mimic all features of OA. They are often designed to investigate a specific feature of osteoarthritis[86].

1.5.2.1 Knock-in and knock-out models

OA models that involve genetic manipulation are mainly conducted in mice, due to various benefits such as their short life cycles, breeding efficiency and biological similarities to human OA pathogenesis[89]. Knock-in and knock-out models are mainly used to investigate the specific role of a certain molecule[86]. The group of Neuhold et al. found that the degeneration of articular cartilage in transgenic mice is enhanced, similar to what is observed during OA, after constitutively activation of MMP-13 expression in a gain of function model[90].

1.5.2.2 Cytokine-induced models

In vivo models are mainly used to study the onset of OA. These models are typically generated by the injection of chemicals such as collagenase, quinolone, or monosodium iodoacetate (MIA)[86]. The intraarticular injection often leads to rapid induction of osteoarthritis. However, chemically induced *in vivo* models often fail to mimic natural observed OA pathogenesis. Therefore, their translation value is rather low[86].

1.5.2.3 Load-based models

Load-based models are used to determine the physiological pressure acting on cartilage during motion. It was found that depending on the joint and the species the mean contact pressure lies between 3 and 9 MPa[12,91]. Obesity-induced OA models have been developed, since increased body weight is one of the major risk factors for OA development[86]. These experiments are mainly conducted in mice fed with a high-fat diet. It was found that these mice had a higher susceptibility for OA compared to mice with a normal diet[92].

1.5.2.4 Surgical models

In this type of model a trauma is introduced to the joint to trigger the OA pathogenesis. The trauma is achieved through an injury which is typically caused by impaired joint mechanics. The trauma can be induced noninvasively or invasively[86]. A widely used surgical model is based on destabilisation of the medial meniscus, which leads to abnormal stress on the cartilage surface. The group of Blanchet et al. observed chondrogenesis of the joint capsule and subchondral bone erosions following joint trauma. Moderate to severe OA was observed eight weeks post-surgery[93].

1.5.3 In vitro models

In vivo models have the main disadvantage that they are costly, time-consuming and ethnically questionable. Guided by the 3R principle, to replace, reduce and refine animal work - *in vitro* models are more and more used and developed[9]. Moreover, *in vitro* models have the advantage that they are highly reproducible, compared to *in vivo* models[94].

1.5.3.1 Monolayer cultures

Current models for osteoarthritis also include 2D cultures of chondrocytes to investigate e.g. cytokine stimulation. Chondrocyte monolayers are very easy to use and therefore belong to the most widely used models[86]. It has been shown that the addition of cytokines to the culture medium leads to osteoarthritic changes in gene expression, such as a decrease of collagen type 2 and aggrecan and an increase of MMP-13 expression[95]. Pearson et al. treated synovialfibroblasts with chondrocyte-conditioned medium to investigate the crosstalk between synovium and cartilage. They found that a modest chondrocyte-derived IL-6 concentration leads to increased IL-6 secretion by synoviocytes upon treatment[96]. However, the drawbacks of these types of models are that the plastic surface does not represent the *in vivo* situation. It has been observed that especially chondrocytes undergo dedifferentiation if they are cultured in monolayers. Therefore, 2D models are nowadays only used as a supplement to 3D models[86].

1.5.3.2 Explant models

Explant models are *ex vivo* models. They are directly derived from *in vivo* tissue during surgery. Therefore, they maintain cells in their natural 3D environment and allow for interactions between tissues, which makes them advantageable over monoclutures[97]. Currently, different culture methods are used, e.g. the submerging method, where the tissue is completely submerged in medium, or the sponge method were the tissue is cultured on a collagen or gelatine sponge that is soaked with medium[98]. In OA research they are often used to investigate compressive load on articular cartilage. With them the cell response can be examined in the natural ECM environment and matrix depletion can be observed[99]. Single impact, static or dynamic loads with varying frequency and amplitude can be investigated. For load-based analysis this is the simplest type of model[12,100]. The great advantage of these models is that they are simple and easy to produce. However, a major drawback is the limited availability of samples that can

be obtained from one donor[99]. Moreover, there is always the risk that the cells die when the tissue is removed from the specimens[97].

1.5.3.3 3D models

3D models are most widely used since they mimic the native environment of chondrocytes much better than 2D models and do not have the limitations of explant models concerning the finite biological source[97]. Typically for 3D cartilage engineered tissues, chondrocytes or stem cells are seeded into biomaterial scaffolds[86]. Hydrogels used in *in vitro* cell culture experiments have different properties and depending on cell type and study set up different scaffolds need to be chosen. Modelling of cartilaginous tissues is often performed by seeding chondrocytes into 3D matrices and scaffolds like alginate, agarose, poly-glycolic acid, or poly-lactic acid[59]. For biomechanical studies, agarose hydrogels are the most frequently used materials[101]. However, it was reported that agarose gels lack adhesive motifs and necessary cell-matrix interactions for optimal mechano-transduction[102]. Chondrocytes in agarose gels exhibit lower cell proliferation rates and GAG secretion compared to other hydrogels such as collagen or alginate. It is assumed that this is because agarose lacks native ligands which would allow for interaction with mammalian cells. Also, the metabolic behaviour of the cells is greatly influenced by the hydrogel. Chondrocytes seeded in agarose have a two-fold higher oxygen consumption compared to cells seeded in collagen. Collagen gels provide a more native surface for the cells. This is due to the fact that collagen is a major component of cartilage EMC and processes ligands that enhance cellular attachment[103]. Hunter et al. showed that bovine chondrocytes seeded in fibrin-based hydrogels responded differently with respect to GAG production, total collagen production and dynamic stiffness in comparison to dynamically compressed agarose-chondrocyte constructs[104]. There are different types of 3D OA models, e.g. inflammatory models or models to test potential OA therapies. For example Chen et al. investigated the therapeutic effects of hyaluronic acid and platelet-rich plasma in a 3D OA model[105].

1.5.4 Mechanical stimulation of models

The field of mechanobiology is widely expanding since mechanical loading is responsible for many degenerative and regenerative processes. The main focus lies in understanding how mechanical loading influences cell behaviour[12,102]. In many studies, mechanical stimulation is applied to cartilage tissue to mimic *in vivo* conditions with the aim to gain an understanding of the physiological and pathological effects of biomechanical stimulation[55,106–108]. These studies

showed that the response of chondrocytes to mechanical loading *in vitro* is indeed very similar to native cartilage[28]. However, results of *in vitro* studies must be interpreted with caution because mechanical stimulation in such experiments often causes large stress amplitudes and gradients and often fails to mimic the load distribution *in vivo*[34,51].

Various types of mechanical stimuli can be applied to models, but it has been shown that only dynamic deformation stimulates a biological response in chondrocytes[24]. Most commonly uniaxial compression is applied[28]. Other examples of mechanical stimulation used in previous studies are hydrodynamic shear, hydrostatic pressure, tension and compression[28,109]. The effect of dynamical compression on cartilage depends on the frequency and the amplitude of the load stimuli applied[110,111].

1.5.5 Microfluidics and organ-on-a-chip

Organs-on-a-chip are a relatively new technology. Microfluidic chips allow for the simulation of microenvironments at tissue, cellular or molecular level[61,112]. They consist of culture reservoirs and connected channels with an in- and outlet for continuous nutrient supply and waste removal[113]. Key features of these models are that they provide a microenvironment that specifically offers a structure and response that defines a tissue or even an organ[86]. The devices are often only a few square centimeters in size and allow for exact control of micro- to picoliter amounts. In these systems biomechanical and biochemical cues can be highly controlled. Microfluidic chips allow for easy integration of optical imaging systems due to the usage of transparent materials such as polydimethylsiloxane (PDMS) and glass slides[23, 114].

At the moment the development for OA microfluidic devices is still in the early stages[86]. Rosser et al. developed a nutrient gradient-based 3D chondrocyte culture-on-a-chip. The chondrocytes remained metabolically active over a time span of three weeks. Moreover, a high expression of collagen type II, aggrecan and Sox9 was measured which is also naturally found in chondrocytes. With that, the model proved to mimic some basic characteristic of native cartilage. Through challenging the cell construct with inflammatory cytokines the authors were able to simulate a response similar to OA[115]. Microfluidic chips have also been used to study the influence of mechanical loading on chondrocyte-laden hydrogels. Occhetta et al. applied hyper physiological compression to a 3D human cartilage-on-a-chip model (Figure 4). The compression led to an increased expression of inflammatory mediators and catabolic enzymes, as well as chondrocyte hypertrophy, which represents an osteoarthritic phenotype[9]. Another approach

in modelling OA was conducted by the group of Lin et al. They used pluripotent stem cells and a dual-flow bioreactor to create an osteochondral tissue chip. After 28 days of differentiation real-time PCR, as well as histological examination, confirmed that the osteochondral tissue was successfully mimicked. To induce OA, they challenged the cartilage component with IL-1β. The results indicated that functional crosstalk between the two tissues could be established under normal as well as under pathological conditions. Moreover, they showed that this system was suitable for drug screening[38]. The big advantage of microfluidic chips is that they enable the crosstalk among different tissue types as well as mechanical loading and thereby a whole joint can be mimicked. The development of a dynamic joint-on-a-chip could offer a promising alternative to animal testing enabling the investigation of dynamic compression on cartilage development, maintenance and the onset of OA.

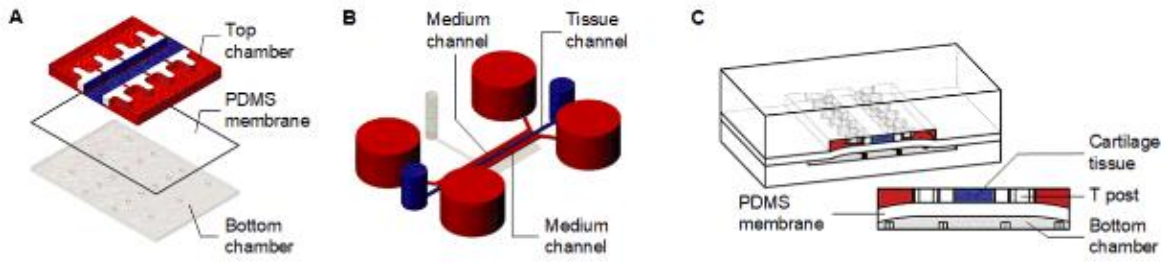

Figure 4: ***Schematic representation of the cartilage-on-a-chip device*** *A) the chip consists out of a top and a bottom layer which are separated by a PDMS membrane; B) the top layer of the chip consists of a tissue channel (blue) and flanking it two medium channels (red); C) the bottom compartment can be pressurized and by that compressive stress is exerted onto the microtissue (Occetta et al., 2019).*

1.5.6 FLUIGENT System – pressure controller for mechanical stimulation

The FLUIGENT MFCS PRESSURE CONTROLLER system is a pressure-based flow control system. The system can be combined with a LINK module, the so-called Flow EZ™, which provides automation, live monitoring and recording of data. It allows for mechanical stimulation patterns on 3D cell cultures on a microfluidic platform. This system is suitable for the creation of a cartilage-on-a-chip model because it allows for controlled investigation of chondrocyte response to external stimuli. This involves measurement of chondrocyte deformation under compression compared to no pressure[116,117].

2 Material and Methods

2.1.1 Culture medium

For the preparation of 500 mL culture medium following ingredients were mixed (Table 1):

Table 1: Ingredients of cell culture medium

Volume [mL]	Item	Company
435	Dulbecco`s Modified Eagle Medium (DMEM)	Life Technologies Europe B.V., Netherlands
50	Heat-inactivated Fetal calf serum (FCS)	Sigma Aldrich, USA
5	Penicillin-Streptomycin	Sigma Aldrich, USA
5	Amphotericin B	Biochrom, England

Prepared culture medium was stored at 4 °C and preheated in a water bath (37 °C) before usage.

2.1.1.1 Inflammation medium

For the preparation of the inflammation medium, 10 ng of TNFα (rh TNF-alpha 10 µg, LOT 354650, ImmunoTools, Germany) and 10 ng of IL-beta (IL-1beta/IL1F2, 10 µg, LOT 354600, ImmunoTools, Germany) was added per mL of normal culture medium.

2.2 Cell Bank – sample preparations

Cells were isolated of 3 euthanised horses (biological replicates) with written owner consent. The horses were not diagnosed with osteoarthritis and were euthanized due to reasons not related to this project. After extraction tissues (cartilage and synovial membrane) were immediately transferred into falcon tubes (15mL tube, 120x17mm, PP, Sarstedt, Germany) containing sterile phosphate-buffered saline (PBS) (Dublecco's Phosphate Buffered Saline, Sigma Aldrich, USA) to prevent drying out. Further processing of the tissues was performed under a laminar airflow hood (Safety Cabinet Herasafe KS18, Thermo Fisher Scientific, USA).

2.2.1 Chondrocytes

Chondrocytes were extracted from cartilage tissue of euthanised horses. Cartilage was obtained from the knee joint. The cartilage fragments were placed into a small petri-dish (Cellstar® Cell Culture Dishes, PS, 100x20mm, with vents, sterile, Greiner Bio-One GmbH, Germany). Using a scalpel, the cartilage was minced into small pieces (1 mm^3) and transferred into a 1 mg/mL collagenase solution (Collagenase from Clostridium histolyticum, Sigma Aldrich, USA) in a beaker. The beaker was placed into an incubator at 37 °C (HERAcell 240i, Thermo Scientific©, USA) for digestion under constant stirring. After 6 hours the mixture was filtered through a cell strainer (EASYstrainer, 100 µm, Greiner Bio-one, Austria). The digestion reaction was stopped by addition of the same amount of FCS containing medium as collagenase solution. Obtained chondrocytes were washed twice in PBS(+) and centrifuged at 400g for 5 minutes. The cell pellet was resuspended in cell culture medium and seeded into T175 flasks (TC Flask T175, Stand., Vent. Cap, Sarstedt, Germany) and cultured in a humidified atmosphere at 37 °C and 5 % CO_2. The next day cells were washed to remove any non-adherend cells and remaining debris.

2.2.2 Synoviocytes

Extracted synovial membrane tissue were placed with the inner lining faceing down into a petri-dish filled with trypsin (0.05 Trypsin-EDTA, Life Technologies Limited, UK). After 20 minutes, cells were carved from the synovial membrane using a cell scraper (Cell Scraper, 28 cm length, Greiner Bio-One GmbH, Germany) and were resuspended in medium before seeding them on T175 flasks.

2.2.3 Mesenchymal stem cells (MSCs)

MSCs were extracted from the bone marrow of the sternum. The marrow was filtered using a sterile cell strainer and mixed 1:1 with PBS. 30 mL of this mixture were carefully layered on 15 mL FICOLL and centrifuged (Rotanta 460 R, Andreas Hettich, Germany) for 30 minutes at 330 g without breaking. Afterward the buffy coade was aspirated and resuspended in 1:10 PBS and centrifuge at 450 g for 5 minutes at 20 °C. The washing step was repeated and after that the obtained mononuclear cell fraction was seeded an a T175 flask in culture medium.

2.3 Cell culture routine

2.3.1 Medium change

Culture medium was exchanged twice a week, if not otherwise stated. First, the old medium was removed using a sterile serological pipette (serological pipette, 5ml/10ml/25ml, Sarstedt, Germany). Then the flask was washed by carefully adding PBS(+), gentaly swaying and removal of PBS. Then 20 mL of fresh medium was added and the flask was placed back into an incubator.

2.3.2 Cell harvest (trypsinization)

Cells were harvested after confluency of around 80 to 90% was reached. First, all medium was removed from the T175 Flasks. Two washing steps with PBS(-) followed. Afterward 6 mL of trypsin were added and the flask was placed for 5 minutes in an incubator. After the incubation detachment of the cells was checked under a light microscope (OLYMPUS CKX41, Olympus Optical CO., LTD., Japan). Tapping on the bottom of the flask facilitated cell detachment. When the detachment was successful, 6 mL of medium was added to stop the trypsinization process. The cell suspension was transferred into a 15 mL falcon tube (Screw cap tube 15 mL, Sarstedt, Germany) and centrifuged at 450 g and 20 °C for 5 minutes. In the next step, the supernatant was removed and the pellet was resuspended in 10 mL PBS(+) and centrifuged at the same settings as above. After the centrifugation steps, the supernatant was carefully removed and the cell pellet was resuspended in 5 mL fresh medium.

2.3.3 Cell count

Cell concentration and viability were determined by transferring 10 µL of the cell suspension into a 1.5 Eppendorf tube. 10 µL of Trypan blue (Trypan Blue Stain 0.4%, Gibco, USA) were added. From this mixture 10 µL were pipetted into one side of a countess counting chamber (Countess cell counting chamber slides, Invitrogen, USA) and 10 µL into the other side. The slide was then placed into the corresponding slot of the Countess counter (Countess II Automated Cell Counter, Thermo Fischer Scientific, USA). Using the function “count cells” the cell number was determined per milliliter. The same step was repeated for the other side of the counting chamber slide and then the mean of the two cell counts was calculated to determine the concentration of the cell suspension.

2.3.4 Freezing and thawing of cells

2.3.4.1 Freezing

After the cells reached a confluency of 80 percent they were frozen. This was done by first harvesting of the cells from the flasks as described above. Depending on the approximate cell number the pellet was resuspended in 2 to 5 mL freezing medium. 1 mL of the suspension was transferred into a fresh cryotube (CryoPure tube 2.0 mL with QuickSeal screw cap, Sarstedt, Germany). The freezing medium consisted out of 90% FCS and 10 % DMSO (Dimethyl sulfoxide, Sigma Aldrich, USA) was used. As soon as the freezing medium was added the cryotubes were placed into pre-cooled freezing containers (Nalgene® Mr. Frosty® Cryo 1 °C Freezing Containers, Cat. No. 5100-0001, Thermo Fisher Scientific, USA) which were then stored at -80 °C for 24h before transferring them to -150 °C.

2.3.4.2 Thawing

For the thawing process cell were quickly warmed to room temperature by either placing them into a water bath or by warming them with the hands. 1 mL of medium was added and through pipetting mixed with the cell suspension. As soon as all ice completely thawed the cells were transferred into a flask containing the appropriate amount of medium. The flask was then placed into an incubator at 37 °C.

2.4 Microfluidic chip design and manufacturing

For the design of the microfluidic chips AutoCAD (computer-aided design) software, 2020 (autodesk.com/products/autocad/, 11.02.2021) was used. Which allowed for the creation of 2D drawings. The design was adapted from previous studies of Dr.nat.techn. Mario Rothbauer (Figure 5).

The microfluidic chip consists of several PDMS (SuperClear Silicone Sheet 5HT6240GK 0.5 mm, MVQ Silicones GmBH, Germany) layers. Using a cutter machine (Microfab Roland Plotter CAMM-1 GS-24, Roland DG Corporation, Germany) the 0.5 mm thick PDMS foil was cut according to the chip design. Excess foil was removed using a forceps. For the bonding of the individual layers, plasma oxidation reaction was performed. The bottom layer and a glass slide (Microscope Slides, Marienfeld, Germany) were placed into a plasma cleaner (Plasma Cleaner PDC-002-CE, Harrick Plasma Inc, USA). Through a pump, a vacuum was established

within the cleaner chamber and the layers were plasma treated for 2 minutes. After that the PDMS layer was placed on top of the glass slide with the treated surfaces facing each other. This needed to happen rather fast for better bonding results. Through gentle pressure on the system, the bonding was enhanced further. Afterwards the chip was fixed with clamps and placed into an 80 °C incubator for 10 minutes. The same steps were repeated with the next layers until the microfluidic chip had the desired size. Care was taken to align the individual layers as exactly as possible on top of each other to keep the systems optimal function. After the last layer was placed the microfluidic chip remained for at least 30 min or overnight in the incubator to increase bonding stability.

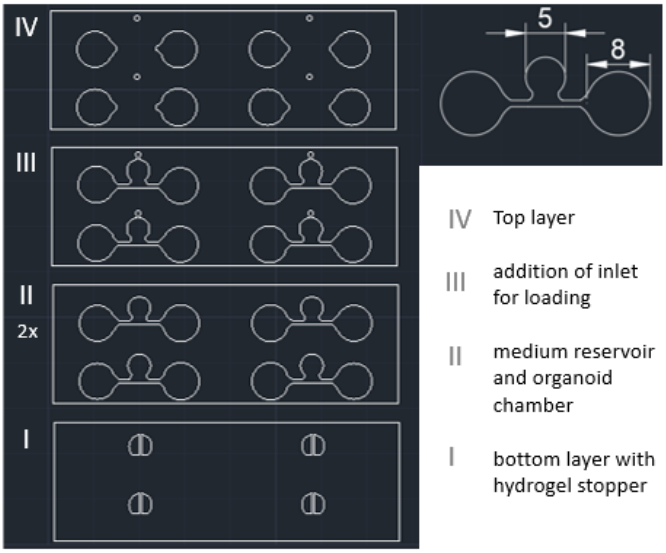

Figure 5: ***Microfluidic chip design.*** *The microfluidic chips consisted out of 5 PDMS layers. The organoid chamber had a diameter of 5 mm with a chamber volume of 40 µL and the medium reservoirs had a diameter of 8 mm. One chip hosted four of these culture complexes. Design adapted from Dr. Mario Rothbauer.*

In order to investigate the effects of mechanical stimulation on chondrocytes, a novel microfluidic joint-on-a-chip was designed. A pneumatic chamber was added which could be dilated by applying air pressure was installed. Through this, a compressive force acts on the chondrocyte laden hydrogel which simulates a mechanical stimulus comparable to movement. In figure 6 the AutoCAD design of the two mechanical microfluidic chips is shown.

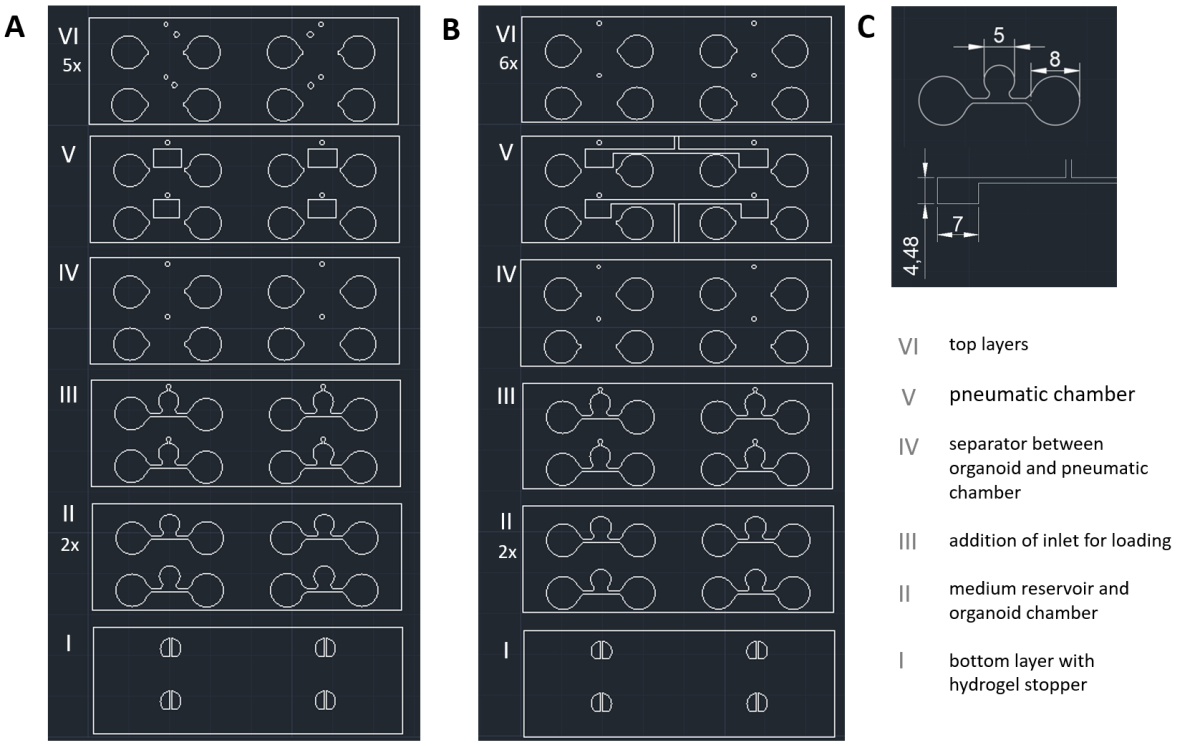

Figure 6: ***Design of the mechanical stimulation microfluidic chips****. A) first design B) second design C) magnification of the organoid chamber with connected medium reservoirs and the pneumatic chamber. Dimensions are given in millimeter*

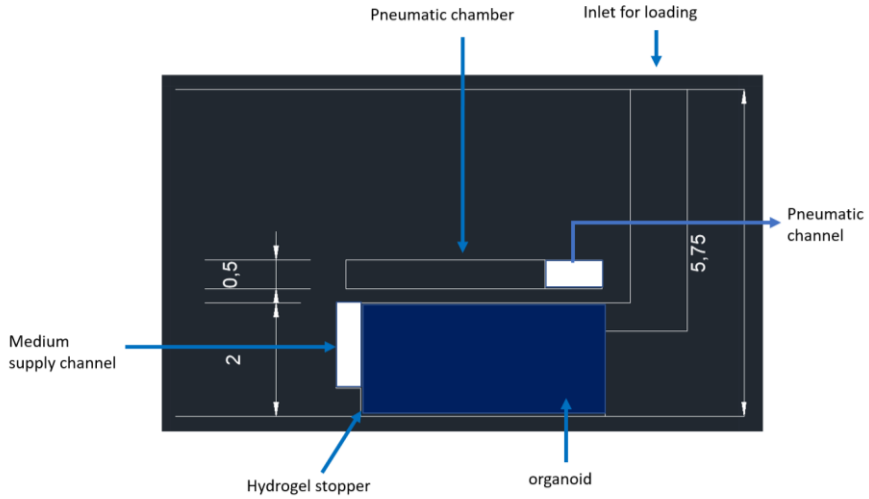

Figure 7: ***Cross-section of a microfluidic chip:*** *showing design version 2. Not indicated is the glass slide on the bottom and the removable glass slide on top of the chip. Dimensions in mm.*

The microfluidic chip was built out of eleven PDMS layers in the first draft and twelve in the second. The additional layer was added to make sure that the pneumatic chamber only dilated downwards to the organoid chamber. The bottom layer, which is bonded to a glass slide has a hydrogel stopper (Figure 7). This little step prevents the hydrogel from spilling into the medium channel during loading.

The following three layers contain the cut outs for the organoid chamber and the connected medium reservoirs and channels. The layer covered the organoid. In the first draft, this layer was 0.5 mm thick. The same height as the other layers. In the second draft this was changed to a 0.25 mm. This should further help directing all the applied pressure to the bottom. This separating layer harboured the inlets for loading the hydrogel and the medium reservoirs. The layer comprised the pneumatic chamber. To optimize pressure application the pneumatic layer was changed so that two systems could be simultaneously stimulated and to give a better interface through the inlet on the side of the chip instead of on top. The size of the pneumatic-chamber was not changed between the first and the second draft. To cover the system, five to six top layers were used.

2.5 Loading of microfluidic chips and Hydrogels

Microfluidic chips were UV treated for 1h before usage. To avoid migration of the cells from the hydrogels the organoid chambers were coated with filtered lipidure (Lipidure, CM5206, Lot# 180223, NOF Corporation, USA). After approximately 2 minutes the lipidure was removed and the chip was left at room temperature to allow evaporation of any remaining coating reagent. The microfluidic devices were placed into sterile petri-dishes for protection.

For the cultivation equine cells in passage, two or three were used. Cells were loaded into hydrogels at a concentration of 3 $*10^6$ cells per mL if not otherwise stated. This cell concentration was chosen according to a previous chondrocyte study conducted by Julie Rosser in 2019[115]. After polymerisation of the hydrogel, the cell culture medium was filled into the medium wells on the microfluidic device, before placing them into an incubator. Medium was changed every day. The cell constructs were harvested for further analysis after 14 days.

2.6 MTT assay – access cell metabolic activity

For one MTT assay reaction, 200 µL of culture medium were mixed with 40 µL of MTT reagent (CellTiter 96© Aqueous One Solution Reagent, LOT# 0000282592, Promega GmbH, Germany). The total volume was added to the cell construct and incubated for 1 hour. Afterward, the color was checked visually. A purple color change of the construct indicated that the cells were still alive.

2.7 Live/dead staining with FDA and PI

In order to evaluate the viability of the seeded cells in the hydrogel, live/dead staining was performed using fluorescein diacetate (FDA), staining with a green fluorescent dye (494-517 nm) and propidium iodide (PI), staining with red fluorescent dye (528-617 nm). This fluorescence-based assay allows for two-color discrimination of living-cell populations from those that are dead. First a FDA stock solution was prepared by dissolving 5 mg of FDA (Fluorescein diacetate, Lot#MKBR3002V, Sigma Aldrich, USA) in 1 mL acetone. For the PI stock solution 2 mg of PI (Propidium iodide, Lot#MKCB0899V, Sigma Aldrich, USA) were dissolved in 1 mL PBS. The staining solution was freshly prepared before usage by mixing 5 mL PBS with 8 µL FDA stock solution and 50 µL PI stock solution. The hydrogels to be tested were placed on a 24 well plate (TC-Plate 24 well, standard, F, Sarstedt, Germany), covered with 1 mL of staining solution and incubated in the dark for 5 minutes. For the analysis an inverted fluorescence microscope (EVOS FL Auto, life technologies, USA) with Texas Red and GFP filters was used. Analysis of the FDA/PI assay was performed via the software Image J.

Table 2: Working solution of the FDA/PI assay

Volume [µL]	Reagent
1000	PBS
1.6	FDA
20	PI

2.8 Gene expression analysis

For the gene expression analysis cell constructs were released from the microfluidic chips by cutting the PDMS top layers with a scalpel and using tweezers to remove the layers. The construct was transferred into a fresh Eppendorf tube and shock frozen in liquid nitrogen for 1 minute. Samples were stored at -80 °C until RNA extraction was performed.

2.8.1 RNA extraction

For the RNA extraction first, a lysis buffer was prepared by mixing 500 µL of Trizol (TRIzol LS Reagent, Invitrogen, USA) and 5 µL of β-mercaptoethanol (2-Mercaptoethanol, Sigma Aldrich, USA) to each sample. Chloroform (Chloroform, Sigma Aldrich, USA) was added in a ratio of 1:5 to the samples and mixed via vortexing (RS-VA 10, Phoenix Instruments, Germany). The samples were incubated at room temperature for 5 minutes and occasionally vortexed. After the incubation, the samples were centrifuged at 4 °C and 13,000 g for 15 minutes. After the centrifugation three phases were visible: a clear upper phase, a whitish interphase and a pink bottom phase. The upper phase was transferred into a new tube (1.5 ml SafeSeal tube, Sarstedt, Germany) without disturbing the interphase. The upper phase contains the RNA. To precipitate the RNA the same volume of DEPC water (DEPC-Treated Water, Thermo Fischer Scientific, USA) was added to the tube. To lose less RNA working on ice was recommended. Isopropanol (Isopropanol 99.5 %, Acros Organics, USA) was added to the mixture according to the formula: total volume * 0.8. In addition 1 µL of dye (GlycoBlue, Thermo Fischer Scientific, USA) were added and mixed by vortexing before incubation on ice for 20 minutes. Following the incubation another centrifugation step was performed with the following settings: 13,000 g, 4°C, 30 minutes. If a low amount of RNA was to be expected the centrifugation time was increased to 1 hour. After the centrifugation a blue RNA pellet was visible at the bottom of the tube. The supernatant was carefully removed and the pellet was resuspended in 75 % EtOH (Ethanol , Scharlau, Germany) same amount as the trizol the sample has been been lysed in. Afterward, the samples were again centrifuged at 4°C and 14,000 g for 5 minutes. The supernatant was removed and the remaining liquid was allowed to evaporate at room temperature by opening the tube for 5 to 10 minutes. After the EtOH completely evaporated 20 µL of Nuclease free water (Nuclease-Free Water, Thermo Fischer Scientific, USA) was added to the pellet. The samples were either directly processed further or stored at – 80 °C.

2.8.2 DNase Treatment and determination of RNA yield

For the DNase digestion, a Master Mix was prepared containing the reagents given in table 3. To each sample, 10 µL of the Master Mix were added before incubating them at 37 °C for 30 minutes on a heating block (Thermocell cooling and heating block, Bioer, China). Afterward, 3 µL of resuspended DNase inactivation reagent (DNase Inactivation reagent, Thermo Fischer Scientific, USA) were added per sample and they were incubated for 2 minutes at room temperature. The samples were occasionally mixed and centrifuged at 2000 g for 5 minutes.

Table 3: Master Mix for DNase digestion; amount given per sample

Reagents	Amount per sample [µL]
10x DNase Buffer	3
rDNase	1
Nuclease free water	6

After the centrifugation 2 phases were visible. The upper clear phase contained the RNA and was transferred into new tubes. Using a nanophotometer (NanoPhotometer N60, Implen, Germany) the RNA concentration was measured before the samples were stored at -80 °C. For more exact measurements of samples where a low RNA yield was expected Qubit (Quibit 4 Fluorometer and RNA IQ Assay, Thermofischer, USA) measurement was performed following the user instructions.

2.8.3 quantitative Polymerase Chain Reaction (qPCR)

RNA samples were tested for expression of different cartilage and inflammation markers. For normalisation of the results expression levels of housekeeping genes were measured (table 4).

Table 4. Equine primer sequences designed by Sinan Gültekin PhD.

Gene name	Forward Primer	Reverse Primer
Cartilage marker		
Col2	CAACAACCAGATCGAGAGCA	CATTCAGGGTGGCAGAGTTT
Sox9	GAGGAAGTCGGTGAAGAACG	GTTGGGGGAGATGTGTGTCT
ACAN	TGGGAGAGCAGATGTCAGTG	GTTCTGGAGGCTGGGATGTA
Differentiation marker		
Col1a2	TCCATCTGGAGAGCCTGGTA	CACCTGGTAGACCACGTTCA
Inflammation marker		
MMP13	TGGTCCAGGAGATGAAGACC	GATGGCATCAAGGGATAAGG
IL6	ATGGCAGAAAAAGACGGATG	GGGTCAGGGGTGGTTACTTC
Housekeeping genes		
GAPDH	GTTTGTGATGGGCGTGAAC	GATGCCAAAGTGGTCATGG
18S	TTTCGATGGTAGTCGCTGTG	CTTGGATGTGGTAGCCGTTT
PPIA	ACCCTACCGTGTTCTTCGAC	ATCCTTTCTCCCCAGTGCTC
36b4(Rplp0)	TGCATTCTCGCTTCCTGGAG	TCCACAGACAAAGCCAGGAC

For the qPCR Master Mixes were prepared according to table 5. Two nanograms of RNA were used per sample. cDNA synthesis and subsequently qPCR reaction was performed by Rev-Trans QPCR One-Step Eva Green kit (Bio&Sell, Germany).

Table 5: Master Mix for qPCR; amount given per sample

Reagent	Amount [µL]	Company
Enzyme	2.5	RevTrans-qPCR EvaGreen© Enzyme Mix , Bio&Sell, Germany
Primer 1	0.4	Microsynth, Switzerland
Primer 2	0.4	Microsynth, Switzerland
Nuclease free water	4.7	Thermo Fischer Scientific
RNA	2	-

The PCR reaction had three steps: hold, PCR and the melting curve step. Following settings were used for each stage:

- Hold stage: 50 °C for 15 min and 95 °C for 5 min.
- PCR stage repeated 45 times: 95 °C for 20 s, 55 °C for 30 s, and 72 °C for 20 s.
- Melting curve stage: 60 °C for 1 min, 95 °C for 15s.

Temperature changes were performed at a rate of 1.6 °C per second. For each gene a negative control was added, where the RNA was replaced by nuclease-free water. The transcript levels of genes of interests were normalized to transcript levels of the housekeeping genes.

2.9 Pilot experiment 1 – Hydrogel comparison

In order to investigate which hydrogel is most suitable for this study the 3 cell types (MSC, chondrocytes, synoviocytes) of the joint were seeded into either collagen type I or fibrin hydrogel. Moreover, agarose or agarose - collagen type II blended hydrogels were compared concerning their suitability for chondrocytes.

2.9.1 Preparation of the hydrogel

2.9.1.1 Fibrin hydrogel

A stock solution was produced by dissolving the corresponding amount of fibrinogen (Fibrinogen from human plasma, Sigma-Aldrich, USA) in PBS. For low concentrations (< 5 mg/mL) the stock solution was filtered using a sterile 0.22 µm filter (Millex®GP Filter unit 0.22 µm, Merck Millipore Ltd., Ireland). For higher concentration sterilization was performed through UV light. For polymerization, the fibrinogen stock solutions were in a ratio of 1:1 to the thrombin-medium-cell suspension (Thrombin from human plasma 20U, Lot#37784921, Sigma Aldrich, USA) mix at a ratio of 1:1. The polymerization happened immediately after mixing.

For the preparation of the TISSEEL(Firbin Sealant, Baxter, USA) fibrin hydrogels, the stock solutions were diluted with medium (Table 7) to achieve the desired concentration. Polymerization was induced through mixing with the thrombin-cell suspension mix.

2.9.1.2 Collagen type I hydrogel

PureCol gel solution (PureCol EZ Gel solution, Lot#SLCG2035, Sigma Aldrich, USA) was mixed with the cells suspension to reach a final concentration of 2.2 mg/mL. Polymerization happened at 37 °C in the incubator after 30 minutes.

2.9.1.3 Agarose hydrogel

Agarose powder (Agarose, low gelling temperature, Lot# SLCG4128, Sigma Aldrich, USA) was weigh to produce a stock solution with double concentration of the final hydrogel. The powder was dissolved in PBS by placing the beaker into a microwave and heating the mixture until the liquid boiled and appeared completely clear. To prevent the agarose from polymerising before loading the beaker was placed onto a heating plate at 40 °C. The mixture was mixed in a ratio of 1:1 to the medium/cell suspension to achieve the final concentration and loaded onto the chip. Care was taken to work fast to avoid early polymerisation.

2.9.1.4 Agarose hydrogel blended with Collagen type 2

Agarose stock solutions were produced as described above. In a 1:1 ratio, the agarose solution was mixed with a medium/cell/collagen mixture. Collagen (Collagen from chicken sternal cartilage, type II (Miller) powder, Lot # 029M4168V, Sigma Adlrich, USA) was previously dissolved in distilled water (Aqua, B. Braun, Germany).

2.9.2 Collagen type 1 hydrogels vs fibrin hydrogels

In order to investigate which hydrogel is most suitable for this study the 3 cell types (MSC, chondrocytes, synoviocytes) of the joint were seeded into either 2.2 mg/mL collagen type I or 2.5 mg/mL fibrin hydrogels. Moreover, different cell concentrations were tested, namely $3 * 10^6$ cells/mL, $6 * 10^6$ cells/mL and $9 * 10^6$ cells/mL.Hydrogel constructs were loaded onto a microfluidic chip.

2.9.3 Stability of fibrin hydrogels

Experiments were performed without cells to see if the hydrogels at higher fibrin concentrations were handleable, to see if a contraction happens and if so to see if the polymer concentration had an influence on the contraction. Three different fibrin concentrations were tested, namely,

10 mg/mL, 20 mg/mL and 40 mg/mL. The experiments were performed with 40 µL drops on 24 well plates, to mimic the volume of the microfluidic chip culture chamber. The drops were covered with medium and placed into an incubator. The stability of the gels was checked every other day over a period of 2 weeks.

2.9.4 Comparison of fibrin hydrogels

Fibrin hydrogels were tested from two different companies: Sigma Aldrich and TISSEEL. For each three different concentrations were tested (Table 6) on MSC, chondrocytes and synoviocytes. This experiment was conducted together with Sarah Hackl, another Master student of the group, whose project focused on establishing a co-culture microfluidic chip for osteoarthritis research.

Table 6: Tested conditions for comparison of different fibrin hydrogels

Fibrin [mg/mL]	Thrombin [U]
Sigma Aldrich	
25	5
50	10
100	20
TISSEEL	
45.5	10
68.25	5
79.6	5

Hydrogel droplets of 40 µL were produced and placed into a 24 well plate. Hydrogels were examined on a macro- and microscopic level every other day. After 12 days of cultivation a FDA/PI and MTT assay was performed.

2.9.5 Comparison of agarose hydrogels and hydrogel blended with Collagen type 2

Most papers that applied mechanical force to chondrocytes use agarose hydrogels as scaffolds. However, literature[102,103] suggested that a combination of agarose and collagen hydrogels may provide a more natural environment for chondrocytes. Two different concentrations were tested, namely 2 % and 4 % agarose hydrogels. Three different combinations of blended

hydrogels were tested (Table 7). Hydrogel tests were performed in 24 well plates. Chondrocytes were seeded in a concentration of $3*10^6$ million cells/mL. Cells were harvested after 10 and 20 days. Each time a qPCR, MTT and FDA/PI assay was performed. Life/dead quantification was performed in image J following a tutorial by Allevi3D[118].

Table 7: Experimental setup for test of blended hydrogels

Agarose	Collagen type 2 [mg/mL]
2 %	2.5
2 %	5
4 %	5

2.10 Pilot experiment 2 – Characterisation of agarose and fibrin hydrogels

2.10.1 Cell homogeneity in hydrogels - cell tracker

Chondrocytes were treated with cell tracker fluorescence dye (CellTracker™ Green CMFDA Dye, ThermoFischer Scientific, USA) in order to investigate if the seeded cells are homogenously distributed within the hydrogels loaded on the chips. For this 10 µL of the cell-tracker solution were added to 20 mL medium without FCS and pipetted to the cells. After 45 minutes incubation, the cells were trypsinized as described before. cell counting was performed and the pellet was dissolved to reach a cell concentration of $6*10^6$ cell/mL. As described before a 4 % agarose gel was produced. The agarose was mixed 1:1 with the cell suspension to reach a final cell concentration of $3*10^6$ cells in a 2 % agarose gel. The mixture was loaded onto a microfluidic chip and using a fluorescence microscope the cell distribution was examined.

2.10.2 Relative diffusion and diffusion rate

Diffusion rates of three different fibrin (TISSEEL 45.5 mg/mL, 68.25 mg/mL, 79.6 mg/mL) hydrogel concentrations and two agarose (2 %, 4 %) hydrogel concentrations were tested. Hydrogels (without cells) were prepared as described above and loaded onto a microfluidic chip. A 1 µL/mL fluorescein (FD20S-250MG Fluorescein isothiocyanate-dextran, Lot # SLCD1285, average mol wt 20,000, Sigma Aldrich, USA) solution was pipetted into the medium channel and via a time laps foto session over one hour pictures were taken every 3 minutes using a fluorescence microscope. To measure the diffusion, rate the fluorescence intensity of each

time point was measured using Imag J software (version 2.1.1) and a linear fit was applied to the results.

For determination of the diffusion rate in µm per minute the time laps results were loaded into Image J. The contrast was changed make the diffusion front clearly visible. The same settings were used for each sample and time point. Using lines (indicated by the arrows in Figure 8) the progression of the diffusion was measured. This was performed at three locations for each hydrogel concentration for timepoint 0, 30 min and 60 min. The measured lengths were converted into µm. Through this the mean diffusion rate in µm per minute for each hydrogel was calculated.

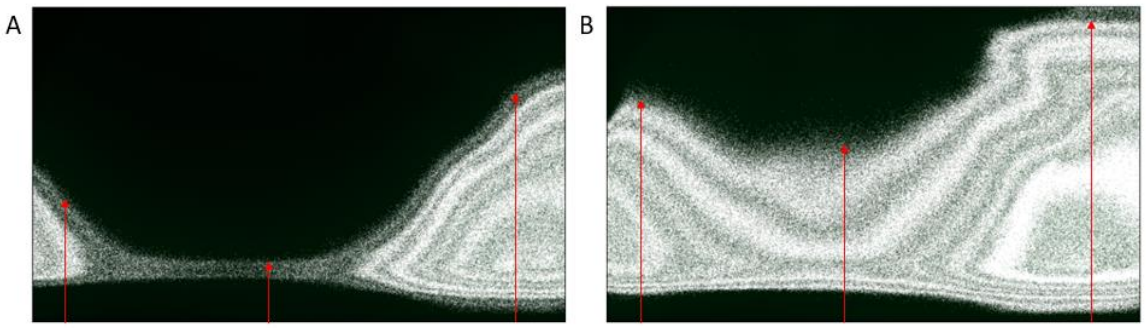

*Figure 8: Example of **diffusion rate** measurement; showing contrast time laps pictures of a 2 % agarose hydrogel at time point (A) zero and (B) after 30 minutes. Arrows show the diffusion change at three different locations.*

2.10.3 Rigidity test

Using a tonometer (TonoVet Tonopen XL, iCare, Finland) the resistance of different concentrations of fibrin and agarose hydrogels (same as in 2.12.2) were measured. For the measurements hydrogels were loaded onto a silicon form (Figure 9), which was produced by mixing 40.5 mL of silicon base reagent (DOWSIL 184 silicone elastomer base, Dow Chemical Company, USA) with 4.5 mL of the silicon base curing agent (DOWSIL 184 silicone elastomer curing agent, Dow Chemical Company, USA). The pipette was used to mix the two components, before purring of the solution into the 3D mold. After 10 minutes the mold was smacked onto the table to get rid of bubbles. The silicon took two days for full polimerisation. With a spatula, the silicon was separated from the mold and placed into a beaker to be autoclaved. The hydrogels were produced as described above (without cells) and loaded onto the silicon form. After polymerisation the mean resistance of the hydrogels was measured using the tonometer. The tonometer performs six consecutive measurement via a probe. It discards the

highest and the lowest value measured and calculates the mean from the remaining values. Three hydrogels were tested per condition.

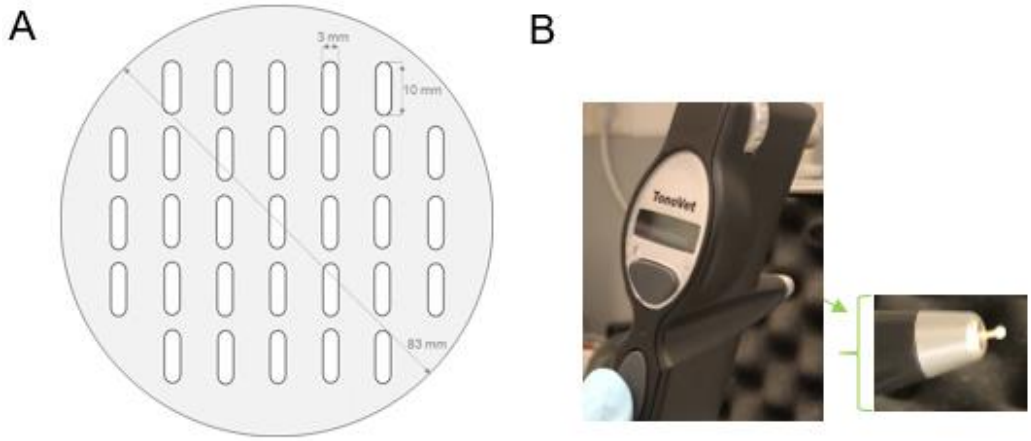

Figure 9: A) ***Design of the silicon form*** *used for the rigidity test. The design was adapted from previous studies by DVM Gil Oreff; B)* ***Tonometer*** *used for rigidity measurements and a magnification of the probe*

2.11 Pilot experiment 3 – Mechanical stimulation on a chip

2.11.1 Pressure control system – FLUIGENT

For the mechanical stimulation of the cells, a pressure control system was used. For this, the Fluigent LineUp™ Series was chosen. The setup is depicted in Figure 10. The LineUp™ series consisted of a compressor (FLPG Plus, Fluigent, France), four flow modules (LineUp™ Flow EZ, Fluigent, France), a switch module (P-Switch LineUp™ Fluigent, France) and a link module (LineUp™ Link, Fluigent, France). The link module connected the flow controllers with the computer. Via Microfluidics Automation Tool (MAT, version 20.0.0.3, Fluigent, France) various pressure and flow patterns could be selected.

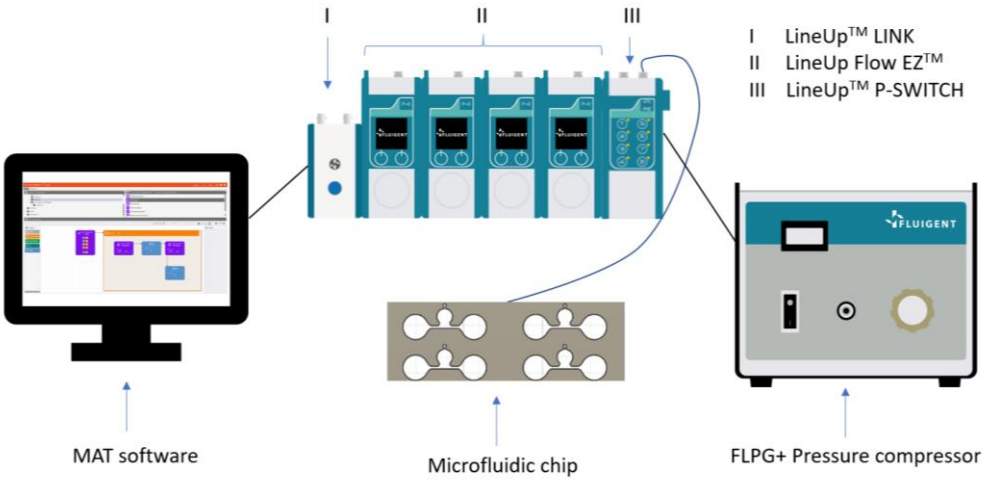

Figure 10: ***Setup of the Fluigent LineUp Series system.*** *The LineUp™ LINK module provides a connection to the microfluidic automation tool (MAT) software. The LineUp Flow EZ™ modules are Flow controller allows for pressure-based fluid control. The LineUp™ P-SWITCH is a pneumatic valve controller. Adapted from: (https://www.fluigent.com/product/microfluidic-components-3/lineup-series/, 15.04.2021)*

2.11.2 Compression capability characterization

Depending on the applied pressure different compression force is transmitted to the cell construct. The Fluigent system allows for a variety of programmable pressure patterns. Positive as well as negative pressure can be applied. Pressure patterns can have a sine, square, sawtooth, triangle, or customed shape. Offset and amplitude can be chosen in the range of -800 mbar to 1000 mbar. For the characterisation of this system, pressure curves were created for various conditions.

2.11.2.1 Transmission

To test if there is any time delay in signal transduction to the microfluidic chip, different pressure patterns and frequencies were tested. Pressure patterns were regulated via the MAT software and time was measured when the signal appeared at the system. For this, the automatically generated datalog files were used.

2.11.2.2 Compression of the organoid chamber upon pressure application

The amount of deflection from applied pressure on the organoid chamber was measured by filling a 1 µL/mL fluorescein solution into the system. Using a fluorescence microscope, pictures were taken at 0 to 1000 mbar pressure in steps of 100 mbar. Using the software ImageJ the fluorescence intensity was measured.

2.11.2.3 Deflection - Green Fluorescent Polymer Microspheres

For the mechanical characterisation green-fluorescent polymer microspheres (Green Fluorescent Polymer Microspheres, Diameter 4.8 µm and 9.9 µm, Lot number 40694/39713, Thermo Scientific, USA) were loaded into 2 % agarose hydrogels at a concentration of 0.5 %. Beads were used as surrogates of cells to measure the amount of deflection of cells after applying pressure. Pictures were taken at 0 to 1000 mbar pressure in steps of 100 mbar.

2.11.3 Mechanical stimulation on a chip

For the mechanical stimulation chondrocytes were loaded into a 2 % agarose hydrogel at a concentration of $3*10^6$ cells/mL. Six different conditions were tested (Table 8). To mimic an inflammation, medium containing 10 ng TNF-α and 10 ng IL-β per mL was used. Physiological (400 mbar) and hyper-physiological (800 mbar) mechanical stimulations were compared by application of different pressure conditions.

Table 8: Conditions for the mechanical stimulation experiment. Healthy = normal culture medium; inflamed = culture medium with 1 % TNF-α and 1 % IL-β supplementation

Mechanical stimulation	Pressure [mbar]	Treatment
control	0	healthy
control	0	inflamed
physiological	400	healthy
physiological	400	inflamed
hyper-physiological	800	healthy
hyper-physiological	800	inflamed

The conditions were tested for three biological replicates and always two technical duplicates. The mechanical stimulation was performed daily over two weeks. The pattern was 2 x 30min stimulation with 800 mbar or 400 mbar with a frequency of 1Hz. For the inflamed treatment inflammation medium (2.1.1) was added into the medium wells instead of the normal culture medium.

2.12 Data analysis and visualisation

For data analysis and visualisation the softwares Rstudio (R version 4.0.3)[119], GraphPad Prism (version 5.04)[120] and ImageJ – fiji (version 2.1.1)[121] were used. For statistical analysis paired Student's t-test was used where appropriate. As threshold a p-value of less than 0.05 was considered statistically significant ($p < 0.05$). If measurements were performed in replicates standard deviation was indicated.

3 Results

3.1 Pilot experiment 1 - Hydrogel comparison

Different biopolymers and concentrations were tested to find the optimal scaffold to develop a joint-on-a-chip model.

3.1.1 Microscopic and macroscopic examination

3.1.1.1 Collagen type 1 hydrogels vs fibrin hydrogels

The first experiment had the goal to identify which hydrogels are suitable for the different cell types of a joint and to test three different cell concentrations (Figures 11-13). The results showed that nearly all of the hydrogel-cell construct collapsed after 48h of cultivation. Only fibrin hydrogels laden with chondrocytes were still stable after 48 hours (Figure 11 A4-6). This could be seen on a macro- as well as on a microscopic level (Figures 11-14).

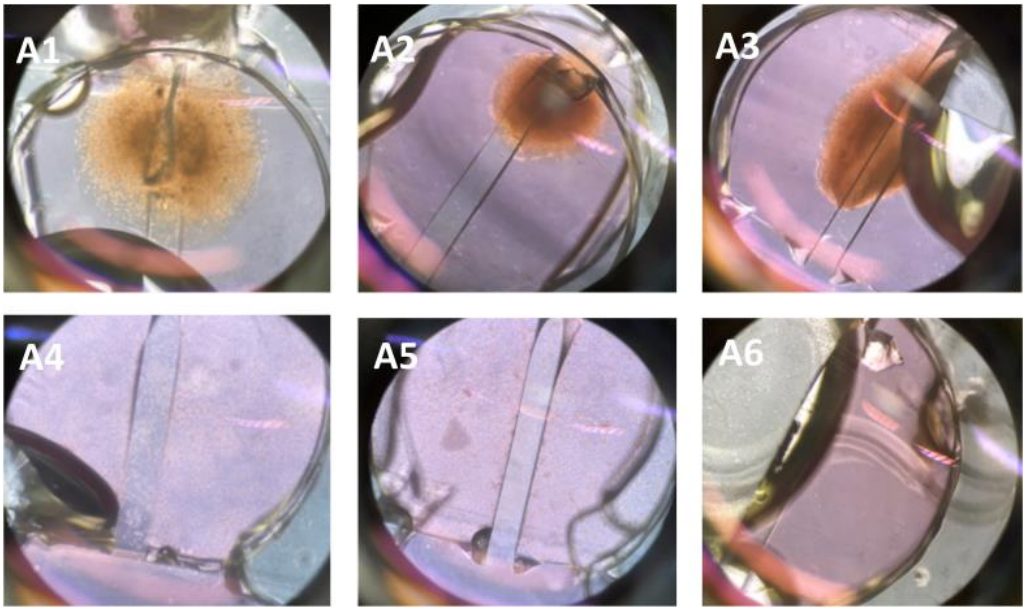

Figure 11: ***Hydrogel test after 48h.*** *4x magnification*
A) Chondrocytes
1-3) collagen hydrogel; 4-6) fibrin hydrogel;
*1&4) 3*10^6 cells; 2&5) 6*10^6 cells; 3&6) 9*10^6 cells*

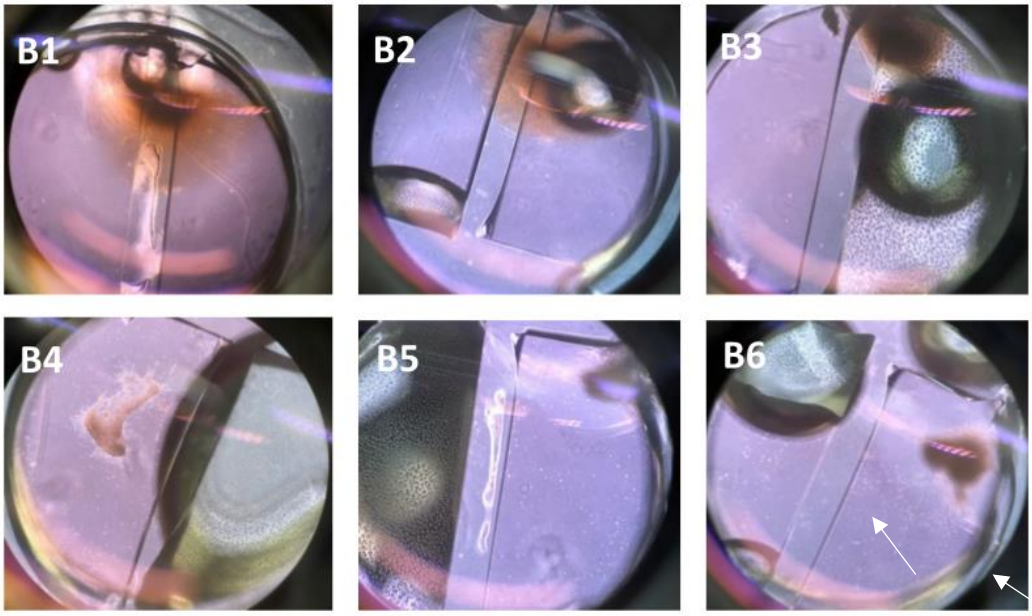

Figure 12: ***Hydrogel test after 48h****. 4x magnification*
B) MSCs; 1-3) collagen hydrogel; 4-6) fibrin hydrogel;
*1&4) 3*106 cells; 2&5) 6*106 cells; 3&6) 9*106 cells*
Arrows indicate where cells migrated out of the hydrogels

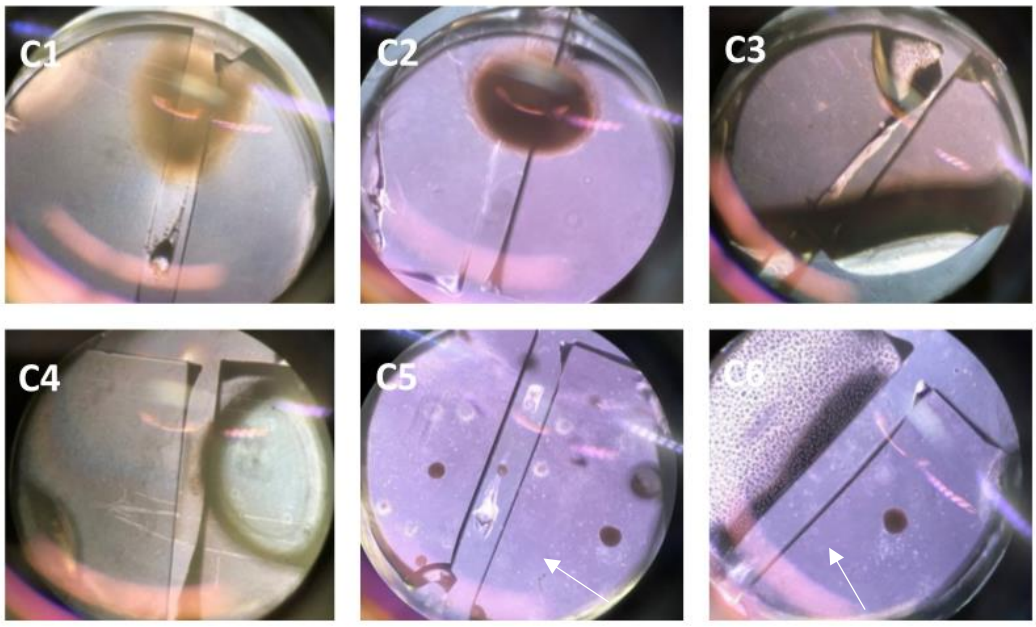

Figure 13: ***Hydrogel test after 48h****. 4x magnification*
C) Synoviocytes; 1-3) collagen hydrogel; 4-6) fibrin hydrogel;
*1&4) 3*106 cells; 2&5) 6*106 cells; 3&6) 9*106 cells*
Arrows indicate where cells migrated out of the hydrogels

Fibrin hydrogels at a fibrinogen concentration of 2.5 mg/mL seemed not useful for MSCs and synoviocytes. It was decided to increase the concentration for the next experiments. Collagen type I hydrogels did not appear to be appropriate for chondrocytes, MSCs, or synoviocytes, since none of the constructs stayed stable. Moreover, we saw that the cells migrated out of the hydrogels to the bottom of the chamber (Figure 12,13: B6, C5-6). Therefore, we decided to use an antimigration agent such as lipidure coating for the next experiments to prevent migration of the cells. Due to the instability of the scaffolds, no conclusion about the optimal cell number could be drawn. Based on previous studies we proceeded with 3 million cells per mL[115].

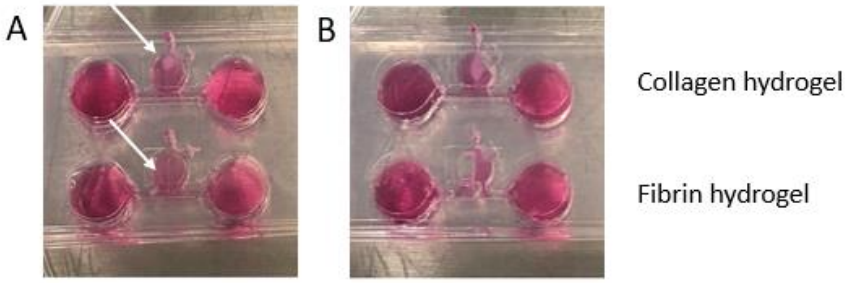

Figure 14: ***Macroscopic example of the hydrogel test for chondrocytes after 48h.*** *On the left cell concentration: 6*10^6 cells and on the right cell concentration: 9*10^6 cells Hydrogel constructs collapsed or dissolved after 48h of cultivation. The upper arrow points to a collapsed collagen hydrogel and the lower arrow to the intact fibrin hydrogel*

3.1.1.2 Stability of fibrin hydrogels

Since fibrin hydrogels collapsed in the first experiment, it was decided to test the stability of fibrin hydrogel with different concentration without cell. The fibrin concentration was increased to better mimic the natural stiffness of articular cartilage and the subchondral bone. After 2 weeks of cultivation hydrogels still displayed a nice morphology. They did not dissolve or collapse, proving the stability of the material itself. No considerable difference could be seen between the different fibrin concentrations (Figure 15).

A 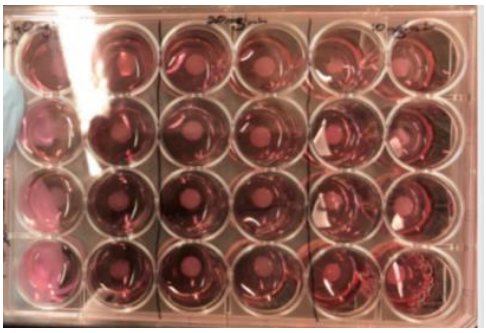 B 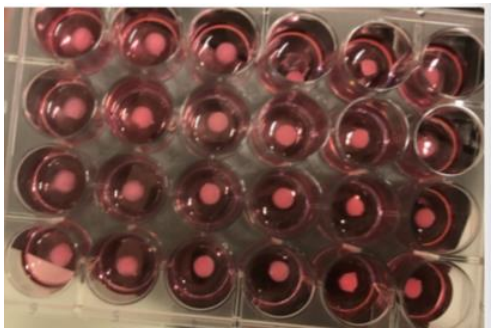

Figure 15: ***Fibrin hydrogels without cells.*** *Determination of the stability of different fibrin concentration; fibrin concentrations from left to right; columns 1-2: 40 mg/mL; columns 3-4: 20 mg/mL; columns 5-6: 10 mg/mL; A) time point 0; B) after 2 weeks*

3.1.1.3 Comparison of different fibrin hydrogels

Fibrin hydrogels were tested from two different companies, namely Sigma Aldrich and TISSEEL. For each three different concentrations were tested (Table 7) on MSC, chondrocytes and synoviocytes. For each condition of the Sigma Aldrich hydrogels three hydrogels were produced and six hydrogels for the TISSEEL hydrogels. The cell-fibrin-constructs were cultured over a time period of 10 days (Sigma Adlrich fibrin gels) or 12 days (TISSEEL fibrin gels). A considerable number (more than half) of hydrogel drops collapsed or completely dissolved by that time point and therefore could not be analyzed (Figure 16). For the remaining hydrogels FDA/PI staining and MTT assay was performed.

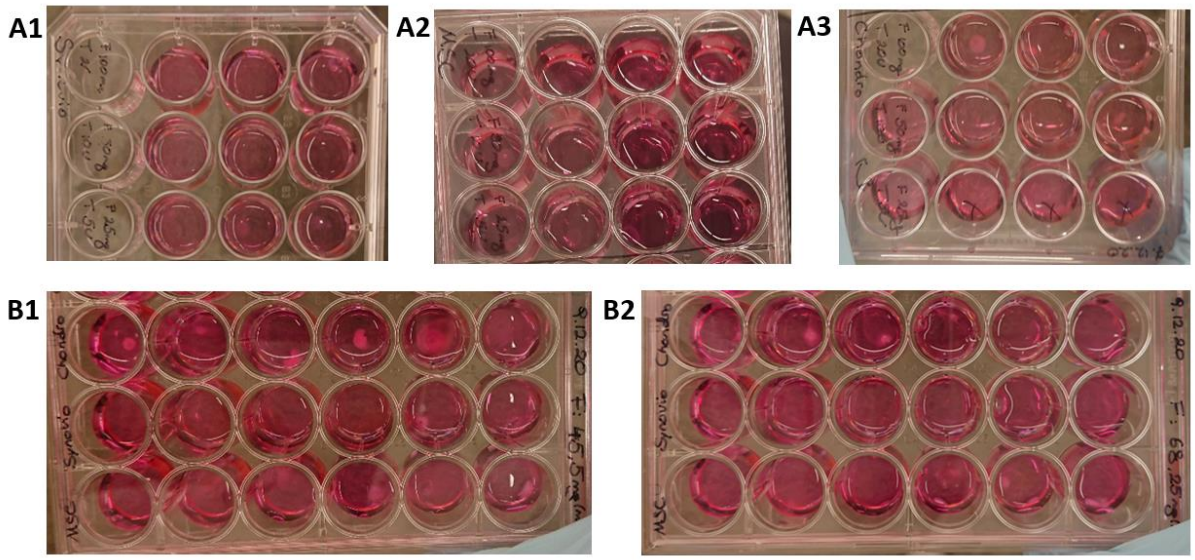

Figure 16: ***fibrin hydrogels;*** *A)Sigma Aldrich hydrogels after 10 days of cultivation; A1) Synoviocytes; A2) MSCs; A3) Chondrocytes; from top to bottom: 100 mg/mL, 50 mg/mL, 25 mg/mL fibrinogen concentration; For each condition at least 3 samples were prepared. In A2 and A3 additional wells were filled to use excess material. B) TISSEEL after 12 days of cultivation; B1) 45.5 mg/mL fibrinogen; B2) 68.25 mg/mL; hydrogel for 79.6 mg/mL not shown; from top to bottom: chondrocytes, synoviocytes, MSCs*

3.1.1.4 Agarose hydrogels

Since the fibrin hydrogels did not appear to be so suitable, another hydrogel scaffold, namely agarose, was tested.

The gel droplets were examined under a light microscope every other day. Shown in figure 17 are agarose drops after 10, 20 and 30 days of cultivation. The drops kept their round morphology and did not dissolve or shrink much. The microscopic examination also revealed that the cells were homogenously distributed in the hydrogel and that the chondrocytes kept their round morphology compared to monolayer culture, where chondrocytes become elongated.

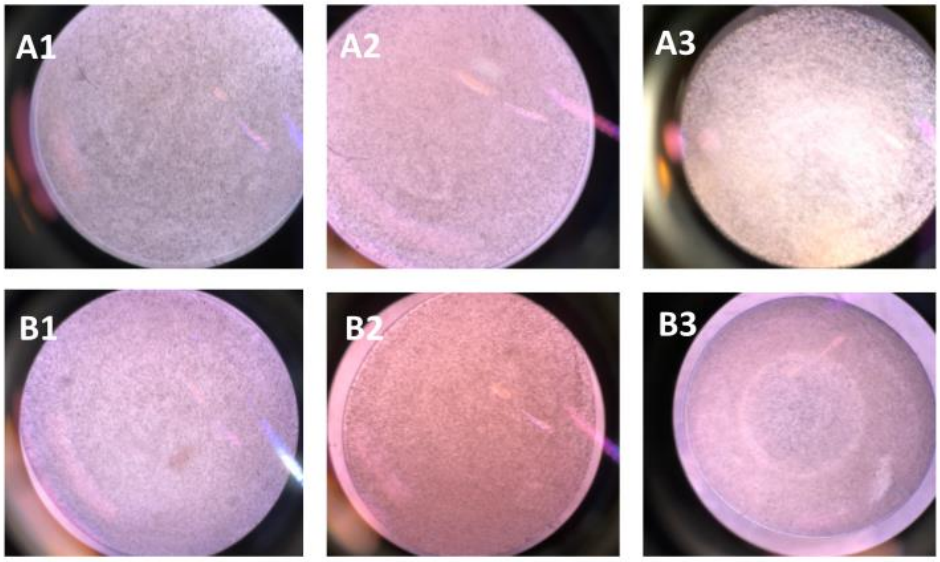

Figure 17: ***Chondrocytes seeded into agarose hydrogels.*** *A) 2 % agarose; B) 4 % agarose; 1) after 10 days in culture; 2) after 20 days in culture; 3) after 30 days in culture*

3.1.1.5 Agarose collagen type II blended hydrogels

Agarose hydrogels appeared to be favorable over fibrin hydrogels due to fact that they were more stable and could be cultivated over a longer time period. Another approach was to test agarose hydrogels blended with collagen type II. As was observed for the agarose hydrogels the blended hydrogels also showed that the cells were homogenously distributed in the hydrogel. However, examining the hydrogel macroscopically it was found that the collagen did not dissolve properly (Figure 18).

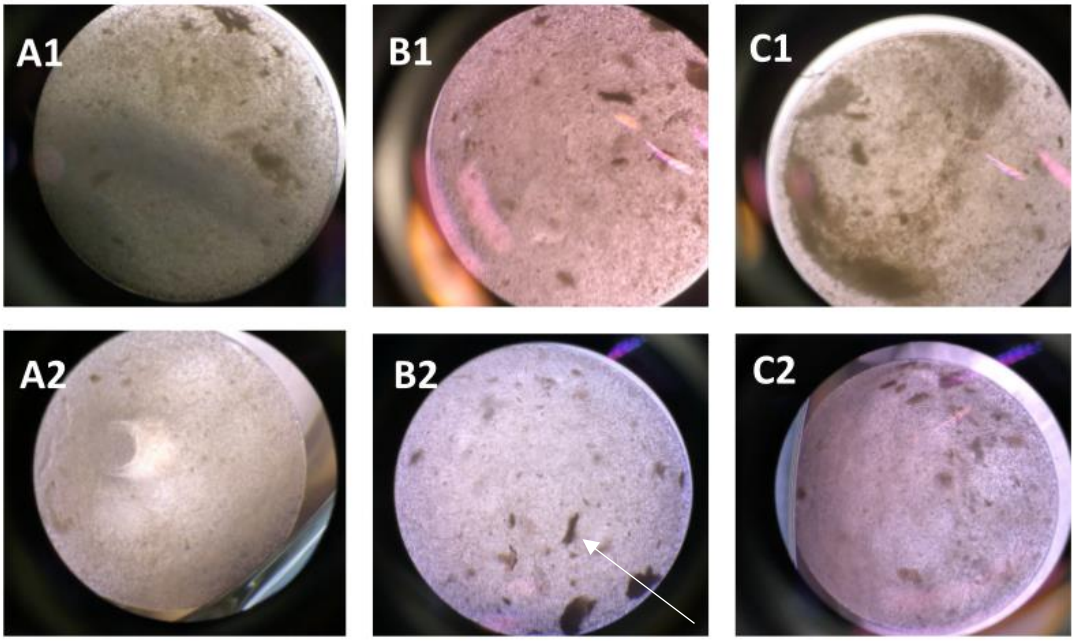

Figure 18: ***Agarose-collagen type II blended hydrogels. A****) 2 % agarose with 2.5 mg/mL collagen II; B) 2 % agarose with 5 mg/mL collagen II; C) 4 % agarose with 5 mg/mL collagen II; 1) after 10 days; 2) after 20 days; arrow showing where collagen did not dissolve properly*

3.1.2 MTT assay

3.1.2.1 Fibrin hydrogels

As can be seen in figure 19, most of the constructs shrunk considerably. However, MTT assays showed that at least some of the cells were still metabolic active after the culture period of 10 or 12 days, respectively to the used hydrogel. Only for MSCs and 2 of the synoviocytes conditions cultured in TISSEEL fibrin hydrogels no color change was observed.

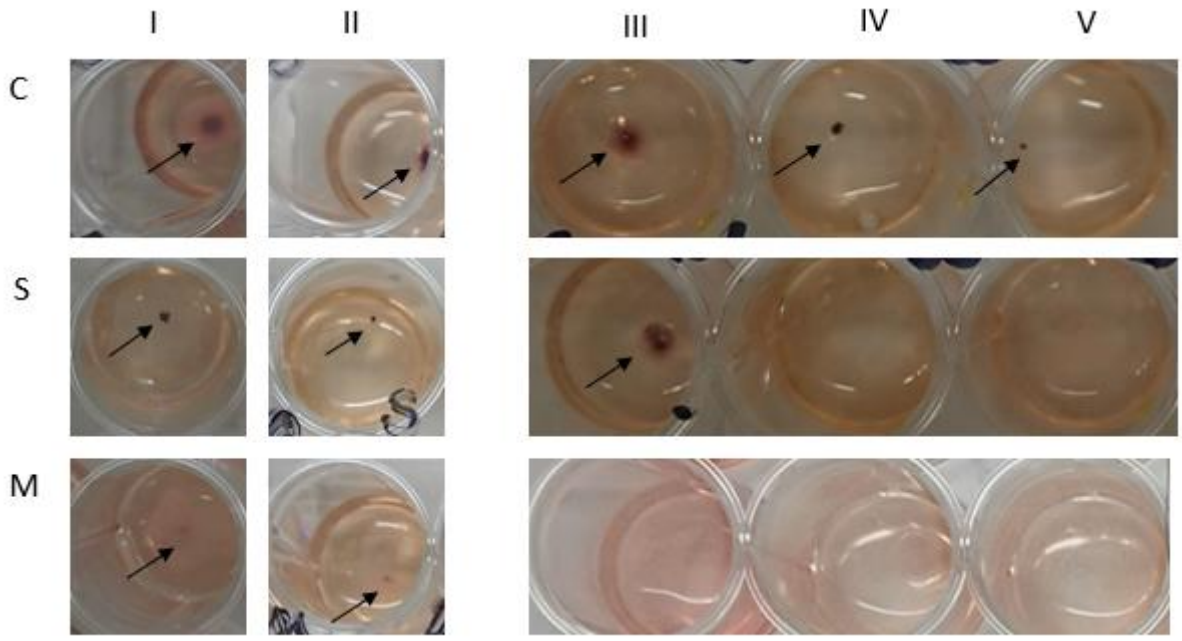

Figure 19: ***MTT assay of fibrin hydrogels*** *after 10 days (Sigma Aldrich fibrin gels) or 12 days (TISSEEL fibrin gels) of cultivation. Arrows pointing to shrunken hydrogels. A color change indicated that the seeded cells were still metabolically active.*

3.1.2.2 Agarose hydrogels

The MTT assay showed that chondrocytes embedded in agarose hydrogels stayed metabolic active even after 30 days of cultivation (Figure 20). This is indicated by the purple color of the construct. It can be seen that staining was weaker after 10 days of cultivation, compared to constructs kept in culture for 30 days. Potentially indicating cell proliferation during the extended culture period.

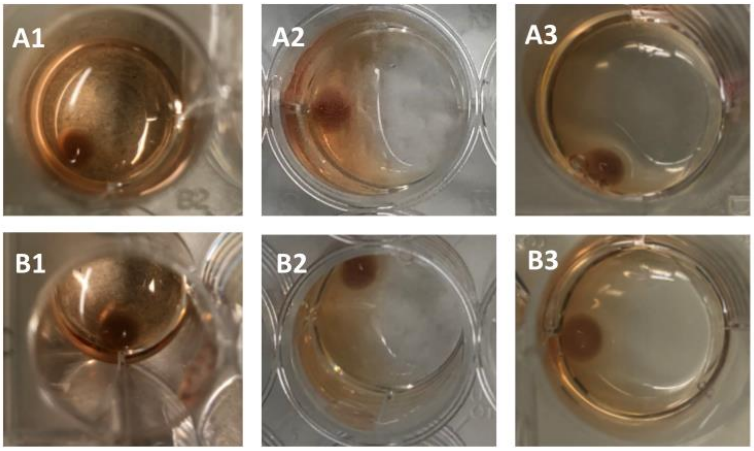

Figure 20: ***MTT assay of agarose chondrocyte constructs.*** *A) 2 % agarose; B) 4 % agarose; 1) after 10 days in culture; 2) after 20 days of culture; 3) after 30 days of culture. A color change indicated that the seeded cells were still metabolically active.*

3.1.2.3 Agarose blended hydrogels

The MTT assay showed that independent of the hydrogel composition chondrocytes stayed metabolically active, hence alive, after 20 days of cultivation (Figure 21).

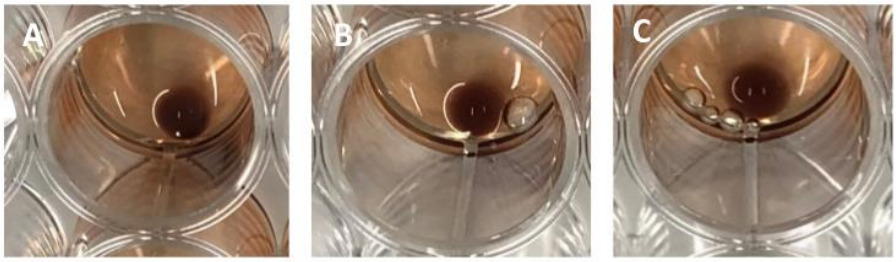

Figure 21: ***MTT assay after 20 days of culture.*** *A) 2 % agarose with 2.5 mg/mL collagen II; B) 2 % agarose with 5 mg/mL collagen II; C) 4 % agarose with 5 mg/mL collagen II. A color change indicated that the seeded cells were still metabolically active.*

3.1.3 Life/dead staining

3.1.3.1 MSCs in fibrin hydrogels

For the cultured MSC-constructs four hydrogels condition were stable enough to be analysed. It can be seen in figure 22 that for the Sigma Aldrich hydrogels more cells died in the lower concentrated hydrogel of 50 mg/mL (44 %) compared to the harder 100 mg/mL (66 %) scaffold (Figure 29). However, the total cell count was very low with only 90 cells. The cells were more distributed compared to the cells seeded into TISSEEL hydrogels (Figure 22 C&D).

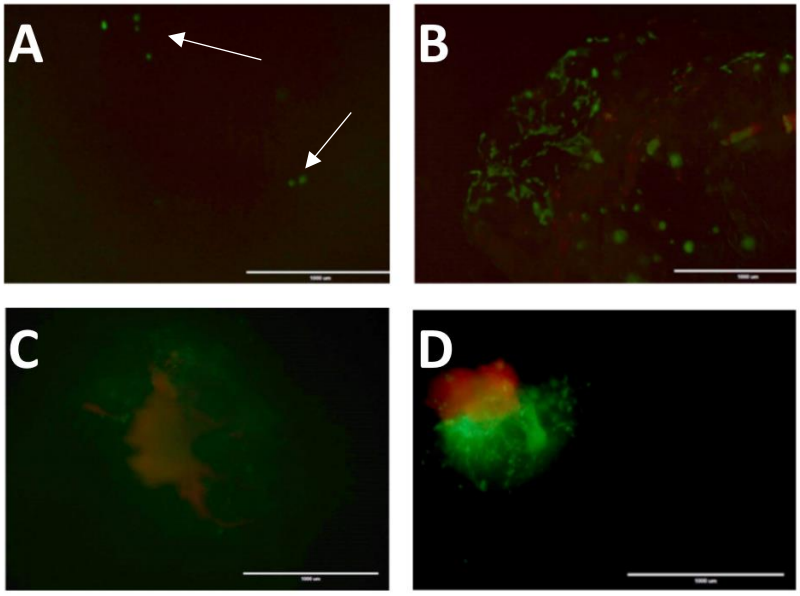

*Figure 22: **Viability staining of fibrin mesenchymal stem cell constructs**: composite of FDA (green) and PI (red) signal; A) Sigma Aldrich fibrin hydrogel concentration 100 mg/mL after 10 days in culture; B) Sigma Aldrich fibrin hydrogel concentration 50 mg/mL after 10 days in culture; C) TISSEEL fibrin hydrogel concentration 45.5 mg/mL after 12 days in culture; D) TISSEEL fibrin hydrogel concentration 68.25 mg/mL after 12 days in culture*

3.1.3.2 Chondrocytes in fibrin hydrogels

A relatively high number of dead cells were found for the Sigma Aldrich hydrogel construct using 50 mg/mL of fibrinogen (Figure 23A), compared to the other conditions. For the other conditions a lot of green fluorescent background signal was seen. The single cells can hardly be distinguished from each other. This may indicate that the survival rate was very low. The collapsed hydrogels were not spheroid but showed various shapes.

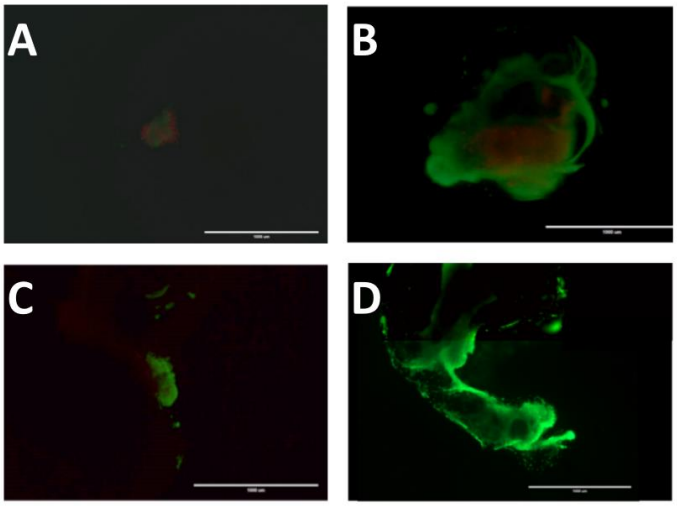

*Figure 23: **Viability staining of fibrin chondrocyte constructs**: composite of FDA (green) and PI (red) signal; A) Sigma Aldrich fibrin hydrogel concentration 50 mg/mL after 10 days in culture; B) Sigma Aldrich fibrin hydrogel concentration 100 mg/mL after 10 days in culture; C) TISSEL fibrin hydrogel concentration 68.25 mg/mL after 12 days in culture; D) TISSEL fibrin hydrogel concentration 79.6 mg/mL after 12 days in culture*

3.1.3.3 Synoviocytes in fibrin hydrogels

Of the in total 18 hydrogels seeded with synoviocytes only two were still stable enough to be analyses using a life/dead assay. In figure 24 a 45.5 mg/mL and 68.25 mg/mL TISSEEL fibrin hydrogel are shown. The construct considerably shrunk. In both conditions some dead cells can be seen. In the 68.25 mg/mL concentrated hydrogel the cell construct was compact and spheroid, whereas the softer 45.5 mg/mL construct was more dispersed.

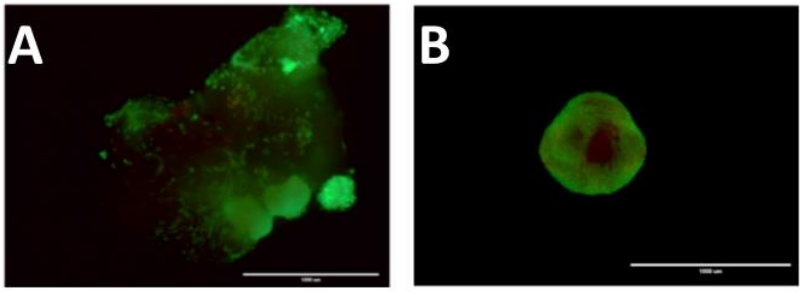

*Figure 24: **Viability staining of fibrin synoviocytes constructs**: composite of FDA (green) and PI (red) signal after 12 days in culture; A) TISSEL fibrin hydrogel concentration 45.5 mg/mL; B) TISSEEL fibrin hydrogel concentration 68.25 mg/mL*

3.1.3.4 Chondrocytes in agarose hydrogel

An FDA/PI assay was performed on the gel constructs to test for cell viability (Figure 25-26). Compared to the fibrin hydrogels (Figures 22-24) these hydrogels stayed stable and did not collapse.

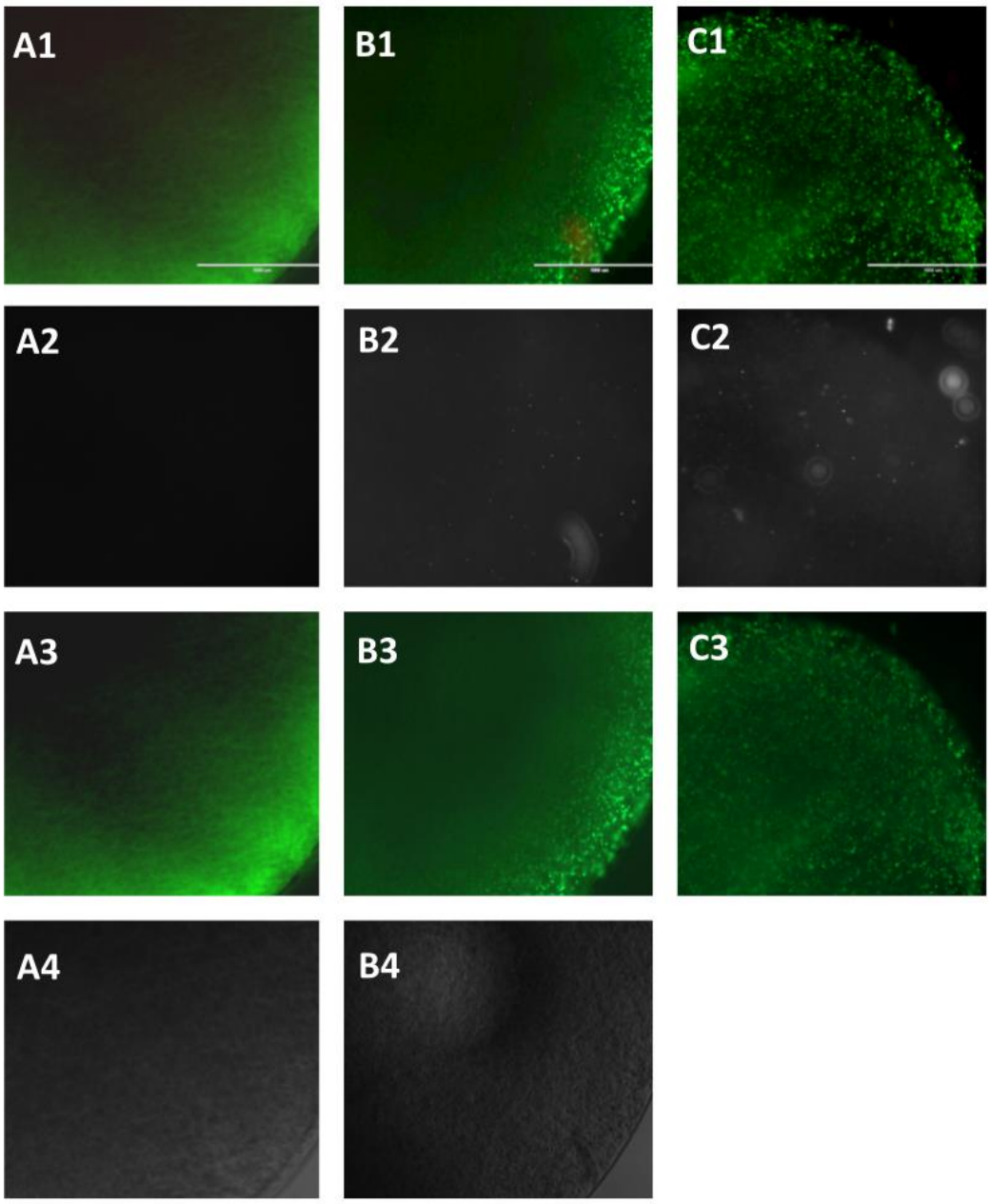

Figure 25: ***Viability staining of 2 % agarose chondrocyte constructs*** *(from top to bottom: composite of FDA and PI signal, PI-signal, FDA-signal, phase-contrast image). A) after 10 days in culture; B) after 20 days in culture; C) after 30 days in culture – phase contrast image not shown; 4x magnification - scalebar only shown for the composite pictures*

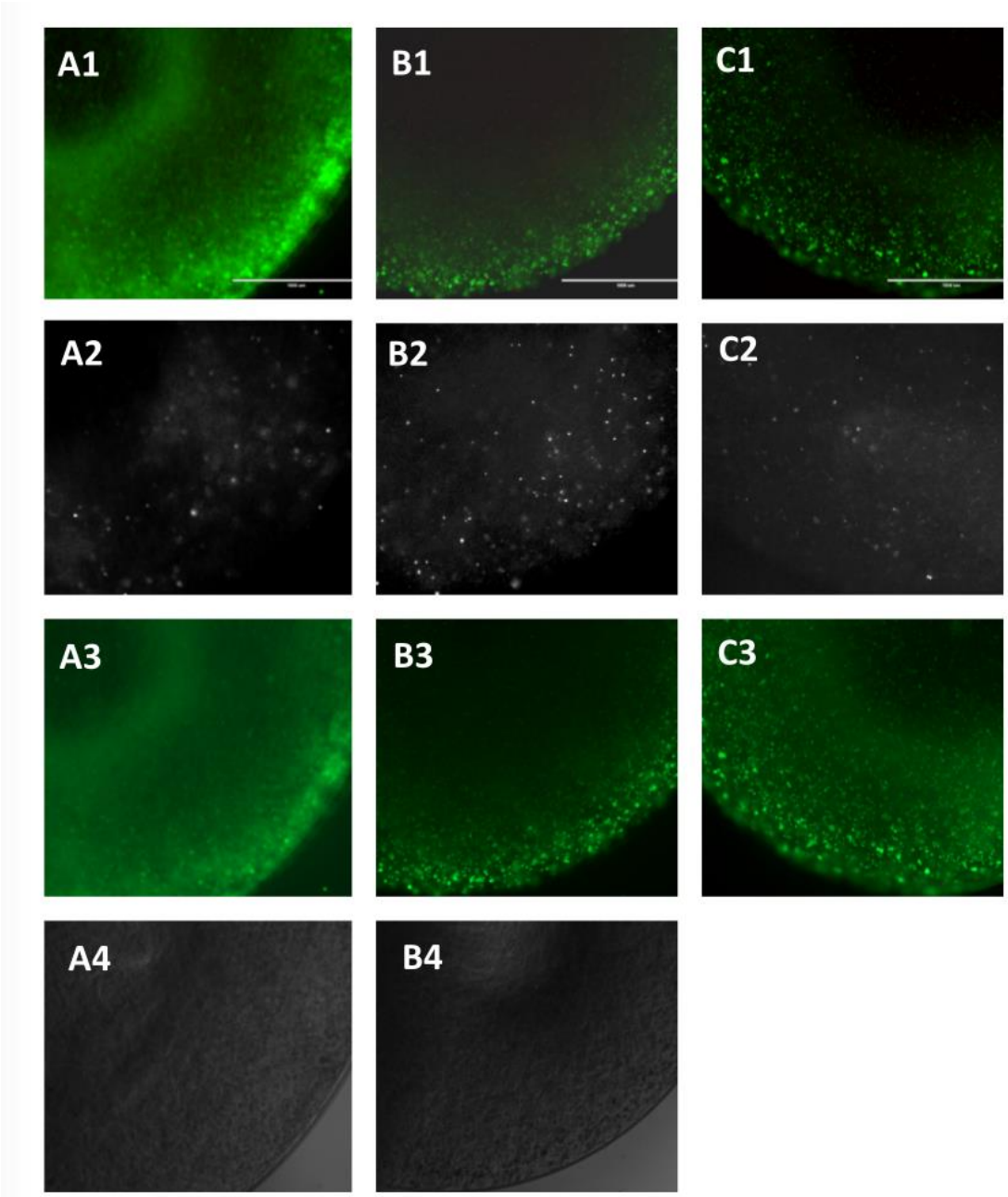

Figure 26: ***Viability staining of 4 % agarose chondrocyte constructs*** *(from top to bottom: composite of FDA and PI signal, PI-signal, FDA-signal, phase-contrast image). A) after 10 days of culture; B) after 20 days of culture; C) after 30 days of culture – phase contrast image not shown; 4x magnification - scalebar only shown for the composite pictures*

Optical examination of the droplets showed that most chondrocytes stayed alive even after 30 days of cultivation. The overlap pictures clearly showed a higher ratio of green fluorescence compared to the red signal, indicating that the majority of cells survived. This observation was confirmed by analysis with the image analyzing tool ImageJ[121] (Figure 26)

3.1.3.5 Chondrocytes in blended hydrogels

In figure 27 and 28 FDA/PI staining of chondrocytes constructs seeded in blended hydrogels after 10 and 20 days of cultivations can be seen. Similar to the agarose hydrogels the blended hydrogels stayed stable even after 20 days of cultivation.

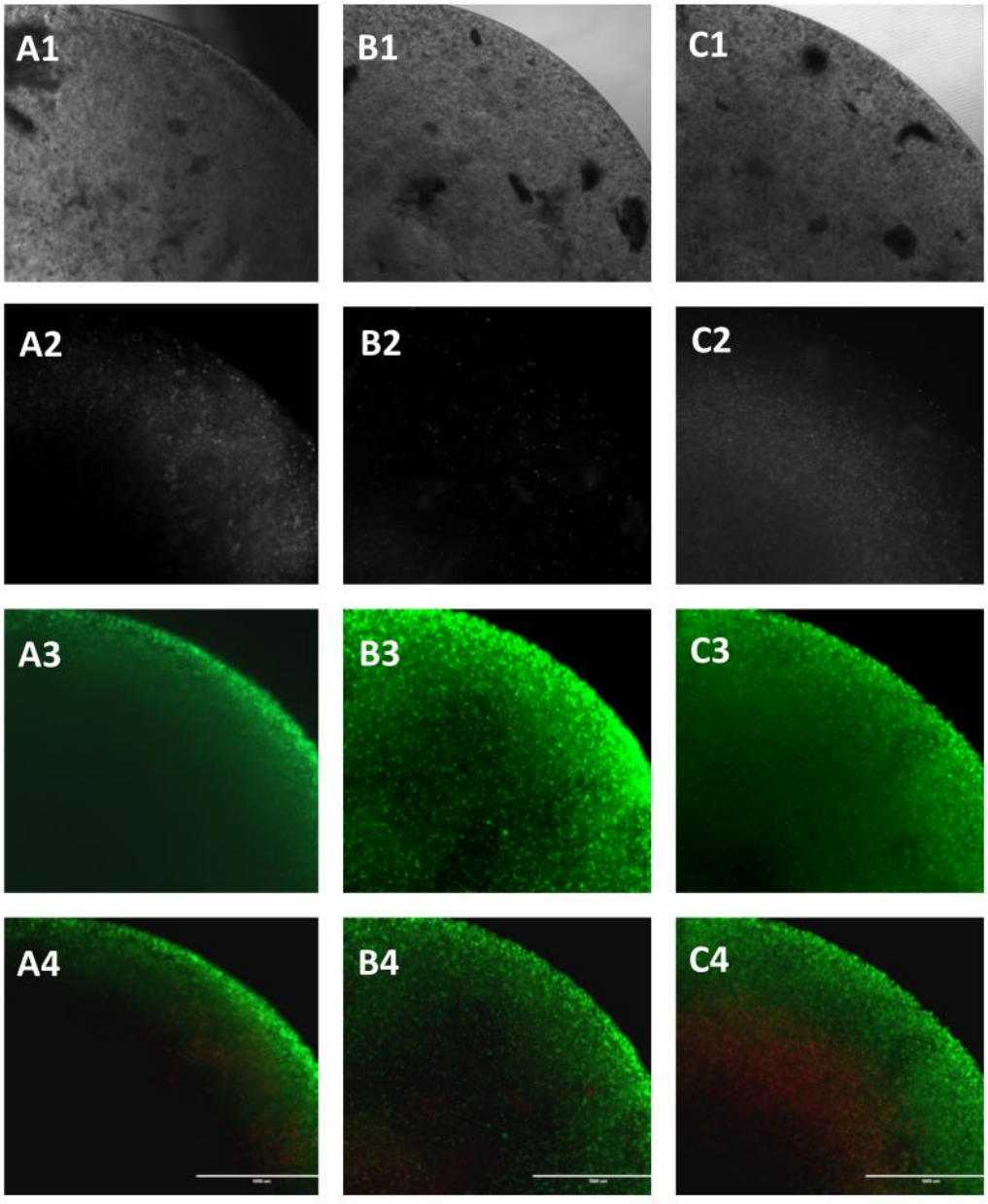

Figure 27: ***Viability staining of agarose-collagen II chondrocyte constructs after 10 days of culture,*** *(from top to bottom: phase-contrast image, PI-signal, FDA-signal, composite of FDA and PI signal); A) 2 % agarose with 2.5 mg/mL collagen II; B) 2 % agarose with 5 mg/mL collagen II; C) 4 % agarose with 5 mg/mL collagen II; 4x magnification - scalebar only shown for the composite pictures*

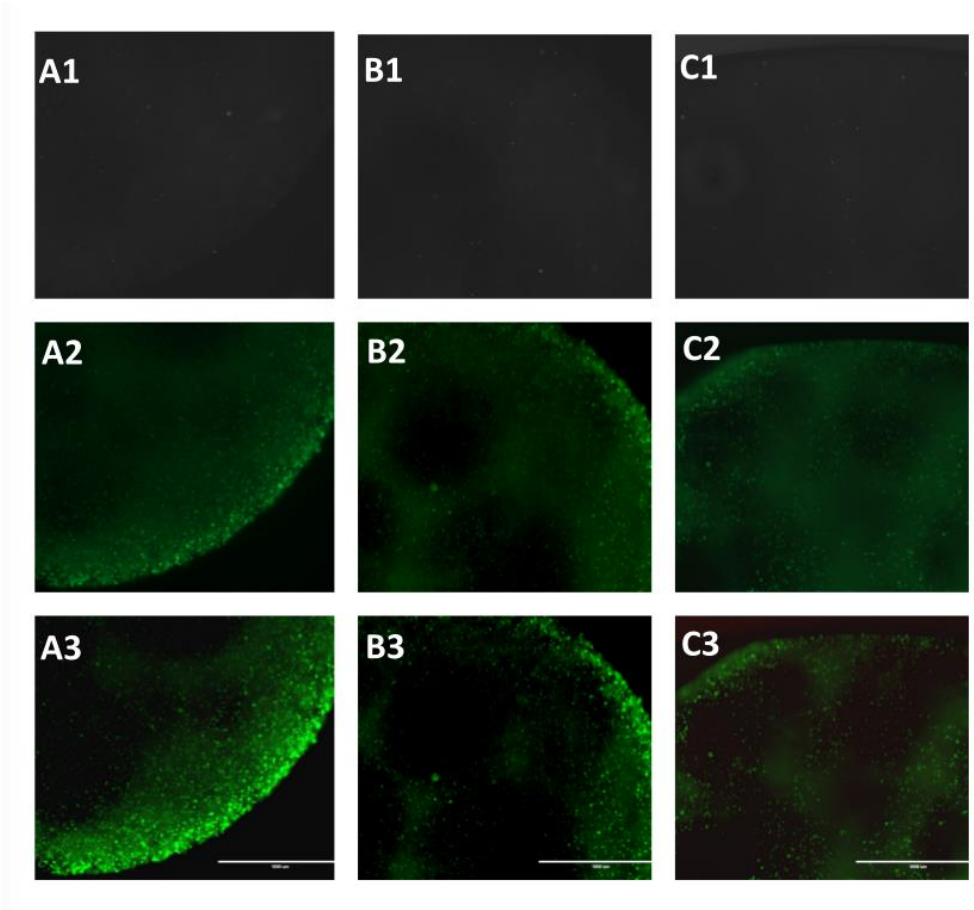

Figure 28: ***Viability staining of agarose-collagen II chondrocyte constructs after 20 days of culture;*** *(from top to bottom: PI-signal, FDA-signal, composite of FDA and PI signal); A) 2 % agarose with 2.5 mg/mL collagen II; B) 2 % agarose with 5 mg/mL collagen II; C) 4 % agarose with 5 mg/mL collagen II; 4x magnification - scalebar only shown for the composite pictures*

3.1.4 Life/dead ratio

3.1.4.1 Fibrin hydrogels

Analysing the life/dead ratio of a tested fibrin hydrogel conditions it can be said that overall, the total cell count was rather low (< 1000) (Figure 29), except for chondrocytes seeded into 79.6 mg/mL TISSEEL fibrin glue hydrogels. For chondrocytes seeded into TISSEEL hydrogels a very high percentage of dead cells was found (>80 %).

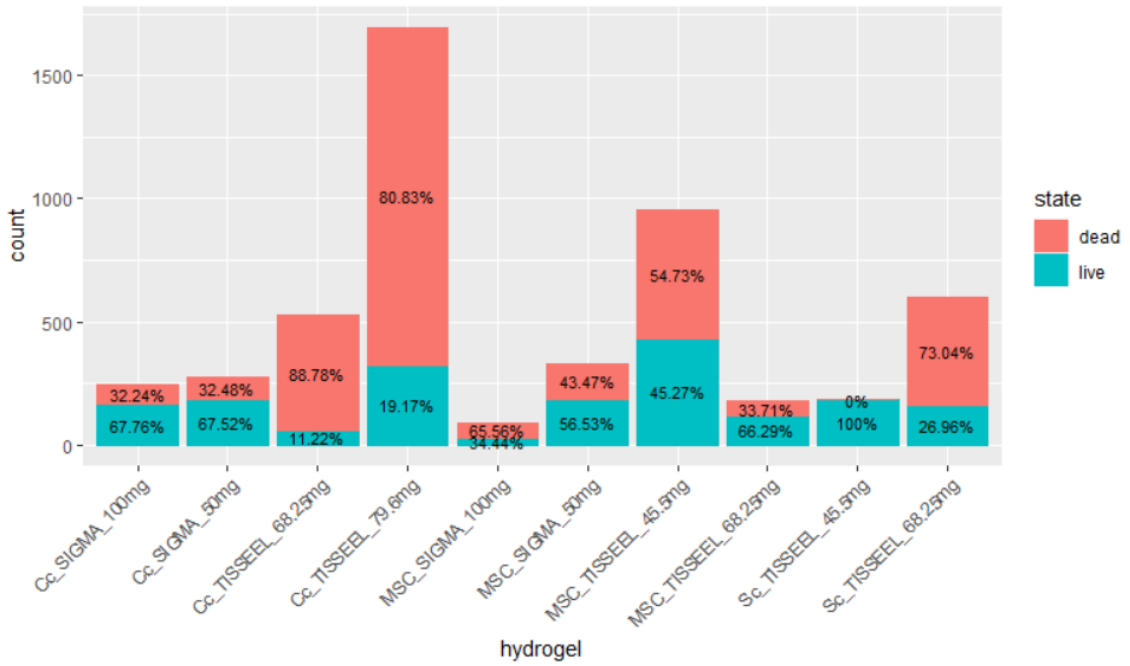

Figure 29: ***Quantification of the live-dead assay*** *for various fibrin hydrogel concentrations and different cell types. Cc = chondrocytes, MSC = Mesenchymal stem cells, Sc =Synoviocytes. In mg the used fibrinogen concentration per mL. The y-axis gives the total cell count measured.*

TISSEEL fibrin glue led to better results for synoviocytes, since all hydrogels using Sigma Aldrich fibrin hydrogels had dissolved completely after 10 days. For chondrocytes and MSCs, no difference could be seen concerning the robustness of the hydrogel. However, the FDA/PI assays showed that, compared to figure 30 and 31, for none of the tested conditions a high number of living cells could be found.

3.1.4.2 Agarose hydrogels

Analysis of the life/dead assay revealed that chondrocytes remain viable when seeded into agarose hydrogels**.** After 10 days of cultivation, only 5 % of the total cell count were found to be dead in both hydrogel conditions tested (Figure 30). Prolonging the culture period decreased cell viability only slightly. After one month of cultivation still, 92 % of the cells were alive.

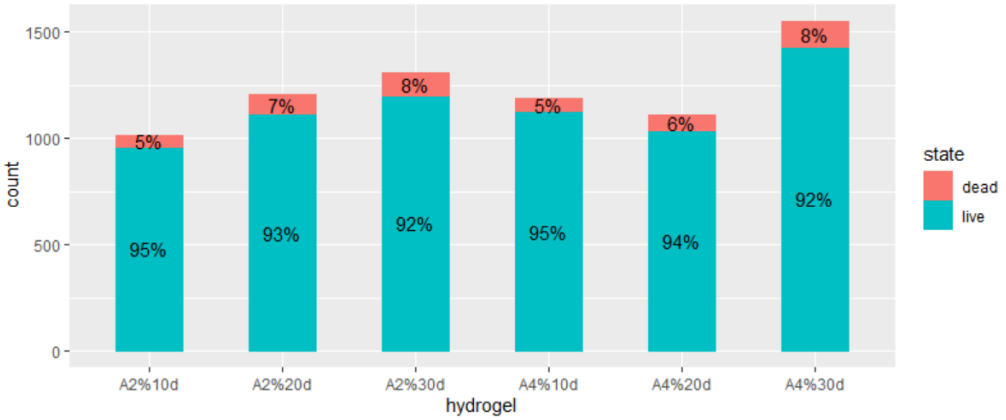

Figure 30: ***Quantification of the live-dead assay results.*** *Using a 2 % or 4 % agarose hydrogel. Results after 10, 20 and 30 days of cultivation. The count gives the total cell count measured.*

3.1.4.3 Agarose collagen type II blended hydrogels

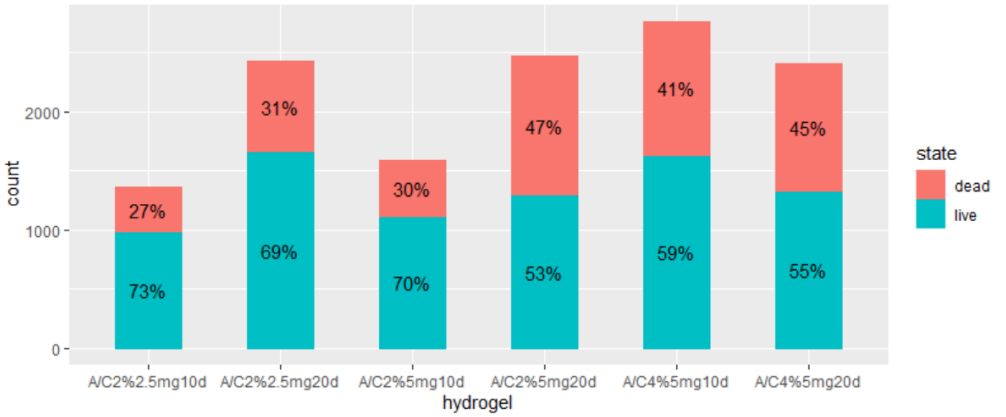

Figure 31: ***Quantification of the live-dead assay*** *results from collagen type II and agarose blended hydrogels. The percentage of live and dead cells is shown. The count gives the total cell count measured.*

The FDA/PI showed that slightly more dead cells were found compared to pure agarose hydrogels. Statistical analysis proved that. A considerably higher amount of dead cells were found in the blended gels with approximately 30 % after 10 days of cultivation and more than 40 % after 20 days of cultivation (Figure 31).

3.1.5 Gene expression of agarose vs blended hydrogels

qPCR analysis was performed on chondrocytes cultured in agarose hydrogels, as well as in blended hydrogels (Figure 32).

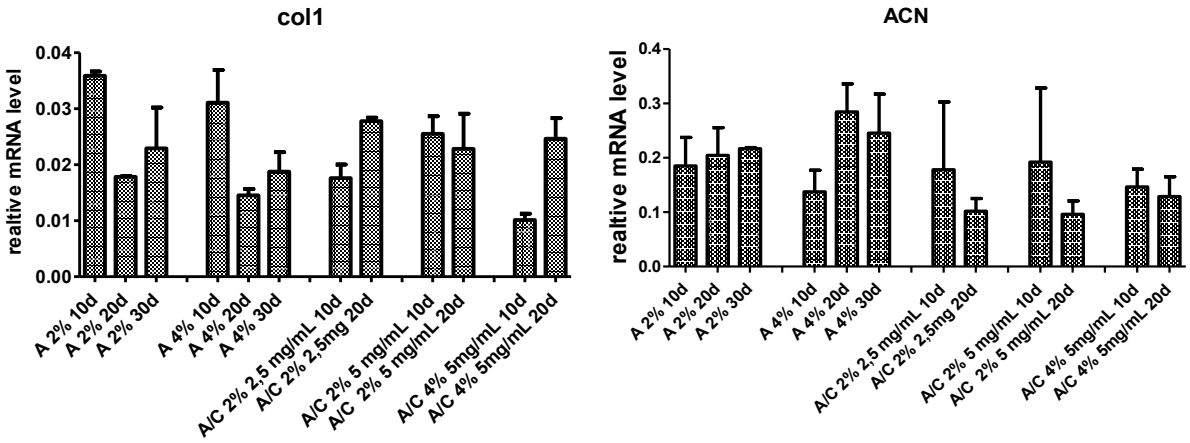

*Figure 32: **Gene expression** analysis of agarose versus agarose-collagen blended gels at different concentrations and time points. A = agarose hydrogels; A/C = blended hydrogels; in % the portion of agarose and in milligram used fibrinogen concentration per mL; culture period 10 to 30 days; col1 = collagen type 1 as marker for dedifferentiation; ACN = aggrecan as marker for chondrogenic phenotype; error bars showing the standard deviation*

All conditions showed a higher expression of the chondrogenic marker aggrecan and a low expression of collagen type I. Chondrocytes in agarose hydrogels showed a slightly higher expression of aggrecan compared to the ones in blended hydrogels. However no significant difference between the results was found.

For the agarose hydrogels the aggrecan expression increased slightly with culture time, with exception of the 4 % agarose hydrogel where the ACN expression decreased from 20 to 30 days. The collagen type 1 expression decreased for the agarose hydrogel from day 10 to day 20 but increased afterward again. Opposite behavior was found in agarose collagen blended hydrogels. There the expression of cartilage marker aggrecan decreased with culture time and col1 increased.

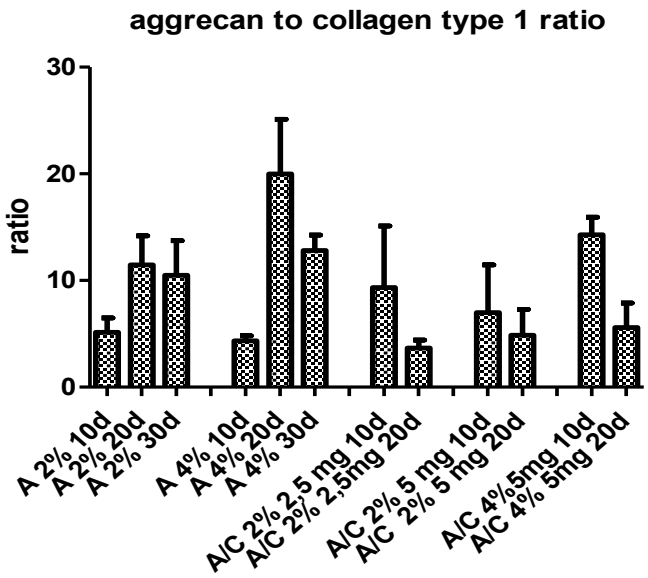

Figure 33: ***Influence of culture time and hydrogel scaffold on the differentiation index of chondrocytes.*** *A = agarose hydrogels; A/C = blended hydrogels; in % the portion of agarose and in milligram used fibrinogen concentration per mL; culture period 10 to 30 days; Col1 = collagen type 1 as marker for dedifferentiation; ACN = aggrecan as marker for chondrogenic phenotype; error bars showing the standard deviation*

The aggrecan to collagen 1 ratio can be used to identify if the cells de-differentiated (Figure 33). A decrease in the aggrecan to collagen 1 (ACN/Col1) ratio indicates a de-differentiation toward the fibroblastic phenotype[122]. For the blended hydrogels a decrease could be observed with culture time. The highest ratio was found in the 4 % agarose hydrogels after 20 days of culture.

3.2 Pilot 2 – Characterisation of agarose hydrogels

3.2.1 Cell homogeneity in hydrogels - cell tracker

Chondrocytes treated with cell tracker dye were used to analyse if the cells are homogeneously distributed in the agarose hydrogels after loading them onto a microfluidic chip. Results can be seen in Figure 34. It can be seen that cells were evenly distributed within the chambers. In figure 34 D it can be seen that during the loading process some of the hydrogel leaked into the medium channel and the connected medium reservoir.

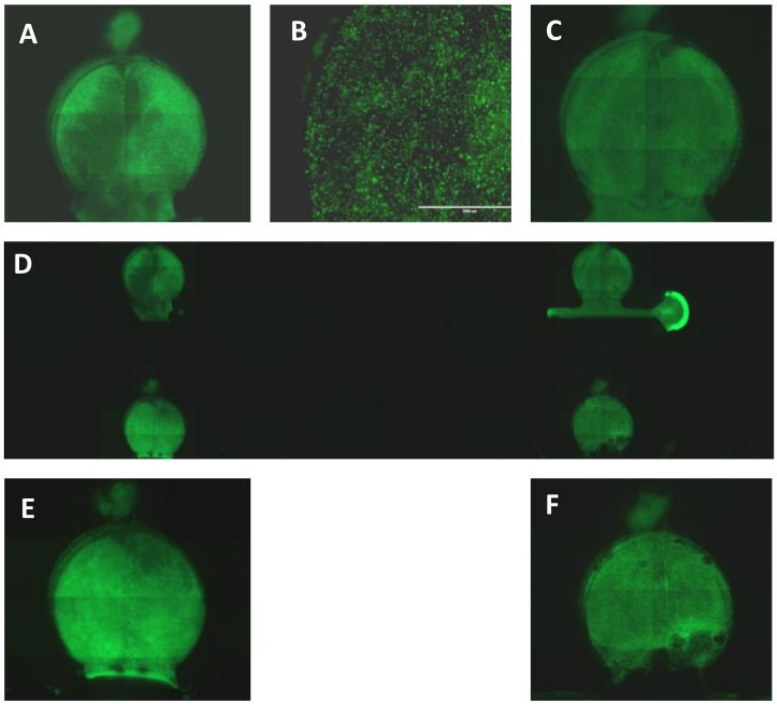

*Figure 34: **Cell tracker staining** shows that cells are homogenously distributed within the hydrogel. Showing a scan picture of the whole chip (D), of the individual chambers (A, C, E, F) and a 4x magnification of one chamber (B). One chamber has a diameter of 5 mm. The length of the whole chip is 26 x 76 mm.*

3.2.2 Rate of diffusion into the hydrogel

The diffusion rate analysis of the TISSEEL and the agarose hydrogels revealed a lower diffusion rate the higher the concentration of the biomaterial. In figure 35 an example is shown how the fluorescein solution diffused into a 4 % agarose hydrogel over time.

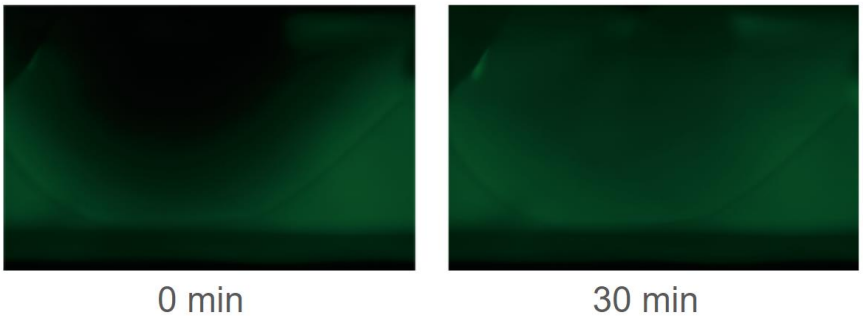

*Figure 35: Example of time laps picture for analysis of the **diffusion gradient**. Showing how the fluorescein solution diffuses into a 4 % agarose gel over time; 4x magnification*

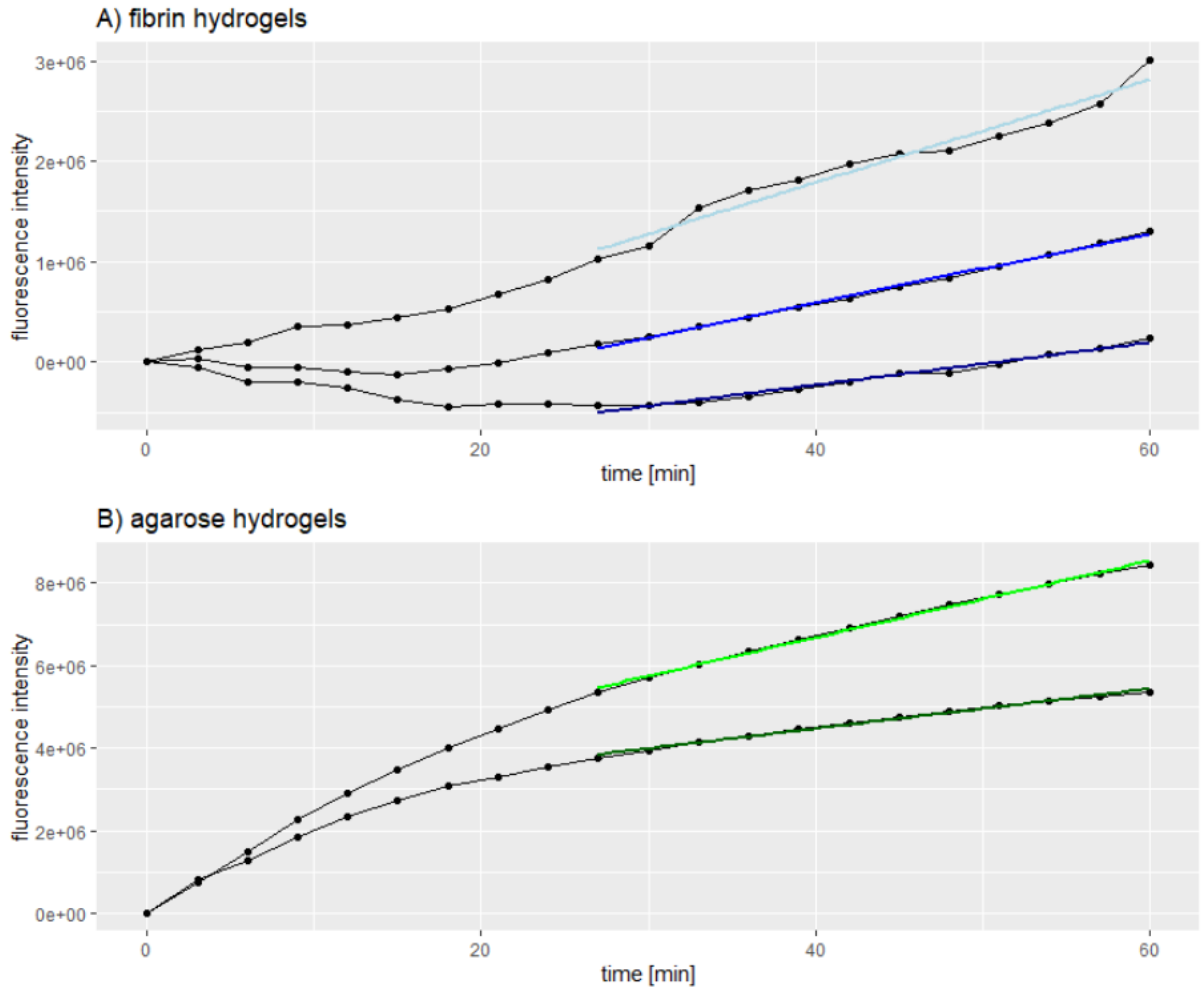

Figure 36: A) ***relative diffusion analysis*** *for TISSEEL fibrin hydrogels; lightblue: 45.5 mg/mL – R^2 = 0.989; medium blue: 68.25 mg/mL – R^2 = 0.9977; darkblue: 79.6 mg/mL – R^2 = 0.989. B) Diffusion rate analysis for agarose hydrogels; light green: 2 % agarose – R^2 = 0.9955; darkgreen: 4 % agarose – R^2 = 0.9911*

The first time points behaved aberrant (toe region) therefore it was decided to exclude these time-points from the linear fit (Figure 36). Comparing the measured relative fluorescence intensity values per minute (Table 9) it can be seen that there is a linear relationship between hydrogel concentration and intensity change per minute. A 2 % agarose hydrogel had an approximately two times higher intensity change compared to the 4 % agarose hydrogel. A similar observation was made for the fibrin hydrogels.

Table 9: Relative intensity change over time

Hydrogel	Relative intensity per minute
45.5 mg/mL TISSEEL	49663
68.25 mg/mL TISSEEL	34999.2
79.6 mg/mL TISSEEL	22481.4
2 % agarose	93136
4 % agarose	48179

The measured diffusion rate per minute for each hydrogel concentration is shown in figure 37. No significant difference was measured between the different concentrations.

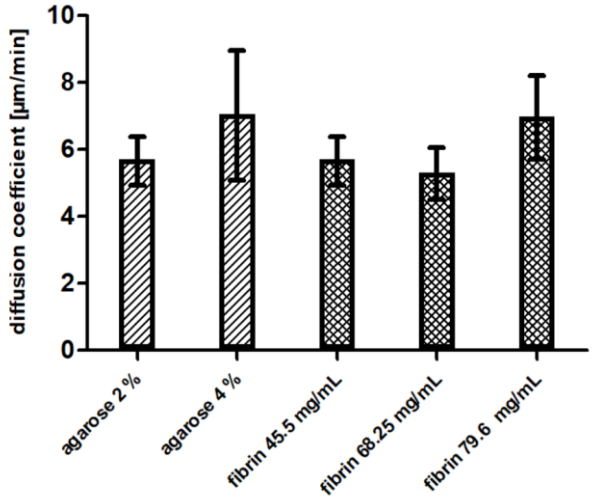

*Figure 37: **Diffusion coefficient** in µm per minute for agarose and TISSEEL hydrogel concentrations on a microfluidic chip; error bars showing the standard deviation*

3.2.3 Elastic modulus of the hydrogels

The elastic modulus was analysed using a tonometer, which measured the rigidity in millimeters of mercury (mmHg). To be comparable to values reported in the literature resulting values were converted into kilo Pascal (kPA) (Table 10). The rigidity increased with the concentration of the biopolymer in the hydrogel. 4 % agarose gels have a similar rigidity to the 68.25 mg/mL fibrin hydrogels (Figure 38).

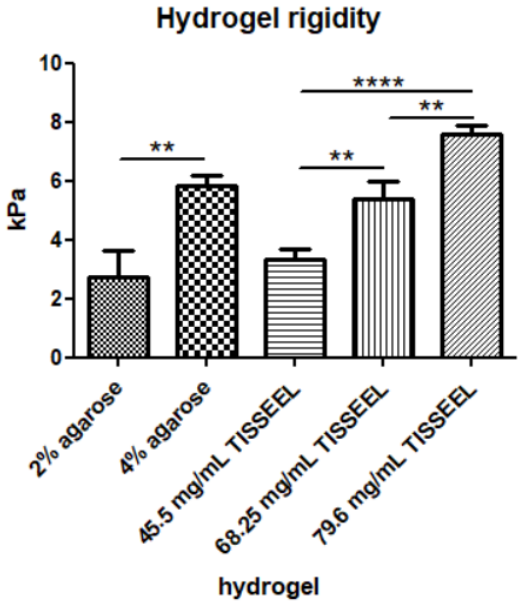

*Figure 38: **Elastic modulus** of the different hydrogel types; error bars showing the standard deviation; significance cutoff: "**": p < 0.01; "****": p < 0.0001*

Table 10: Rigidity of the different hydrogels, n=3

		Rigidity		
Hydrogel	concentration	mmHg	kPa	% RSD
agarose	2 %	20.33	2.71	34.89
	4 %	43.67	5.82	6.61
TISSEEL	45.5 mg/mL	25.0	3.33	10.58
	68.25 mg/mL	40.67	5.42	11.45
	79.6 mg/mL	56.0	7.47	3.51

3.3 Pilot 3 – Mechanical stimulation on a chip

3.3.1 Chip designs for mechanical studies

In order to investigate the effects of mechanical stimulation on chondrocytes, a novel microfluidic joint-on-a-chip was designed. A pneumatic chamber was added which could be dilated by applying air pressure was installed. Through this, a compressive force acts on the chondrocyte laden hydrogel which simulates a mechanical stimulus comparable to movement. In figure 39 a manufactured chip is shown for each design version.The microfluidic chip was built out of

eleven PDMS layers in the first draft and twelve in the second. The additional layer was added to make sure that the pneumatic chamber only dilated downwards to the organoid chamber.

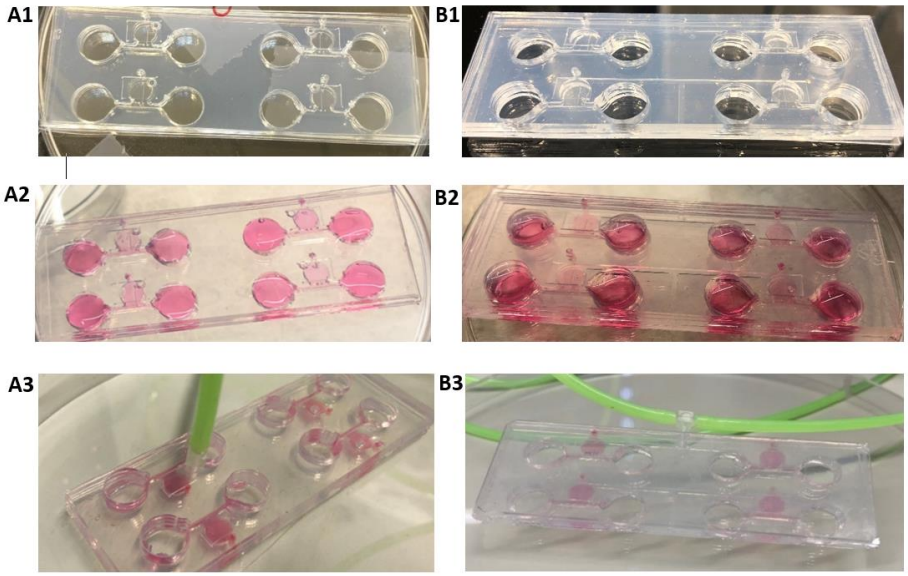

Figure 39: **Microfluidic chips**. A) first design; B) second design; 1) empty chip; 2) chip loaded with hydrogel and filled medium reservoirs; 3) chip connected to the pressure system

Through several modification steps, we were able to establish a device suitable four studying biomechanical stimulation of chondrocytes. Each microfluidic chip hosted for technical replicates, which allow for multiplexing. In the first design, each pneumatic chamber was controllable independently from the others. However, the inlet on top of the chip proved to be not very suitable interface, because the connection to the pressure system was not very solid. Through changing the design to an inlet on the side, we were not only able to regulate the pressure flow more precisely, but this also allowed placing of a glass slide on top of the chip. This protected the cell constructs from contamination and helped in directing the force induced by the pressure completely to the organoid.

3.3.2 Compression capability characterization

Before the microfluidic chip could be used for mechanical stimulation studies, characterisation of the system was required. In the following experiments, the novel microfluidic chip was validated. For pressure controlling the Fluigent system was used. We performed several characterisation steps to prove that the system is compatible with our joint-on-a-chip model.

3.3.2.1 Signal transmission

First, we investigated if any delay between the software command and the appearance of the signal at the actuator happened. A minimal delay was found between applied pressure and the signal received by the actuator, with a minimal standard deviation (Figure 40). Extrapolation for 0.5, 1 and 2 Hz were performed for each wave type using a linear model (Table 11).

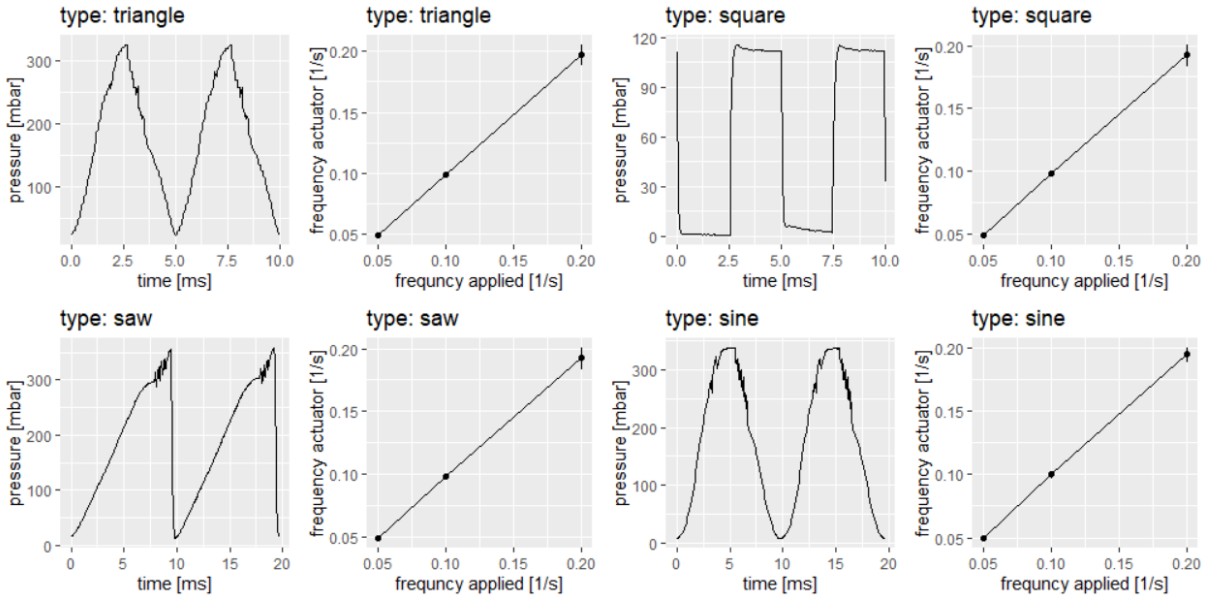

Figure 40: ***Different types of pressure curves****, which can be applied through the Fluigent MAT software and* ***signal transmission*** *for different frequencies. Error bars showing the standard deviation*

Table 11: Period and frequency applied versus signal received by the actuator. Measurements were performed by 10 technical replicates. Extrapolation performed by using a linear model; sine: R^2=0.9996; triangle: R^2=1; square: R^2=0.9999; saw: R^2=0.9999

	frequency [s^{-1}]			extrapolation frequency [s^{-1}]	
wave type	applied	actuator mean	std	applied	actuator
sine	0.05	0.050	$5.37 * 10^{-3}$	0.5	0.493
	0.1	0.100	$2.31 * 10^{-3}$	1	0.986
	0.2	0.195	$5.17 * 10^{-3}$	2	1.971
triangle	0.05	0.050	$5.29 * 10^{-3}$	0.5	0.484
	0.1	0.099	$1.84 * 10^{-3}$	1	0.965
	0.2	0.197	$7.87 * 10^{-3}$	2	1.928
square	0.05	0.049	$4.99 * 10^{-4}$	0.5	0.478
	0.1	0.098	$2.00 * 10^{-3}$	1	0.954
	0.2	0.192	$8.12 * 10^{-3}$	2	1.905
saw	0.05	0.050	$5.29 * 10^{-4}$	0.5	0.478
	0.1	0.099	$5.17 * 10^{-3}$	1	0.954
	0.2	0.193	$7.81 * 10^{-3}$	2	1.905

3.3.2.2 Compression of the organoid chamber

The amount of deflection of the PDMS layer separating the pneumatic chamber from the organoid chamber was determined by measuring the change in fluorescence intensity. The higher the compression force the more fluorescein solution was pressed out of the chamber and the fluorescence intensity decreased (Figure 41).

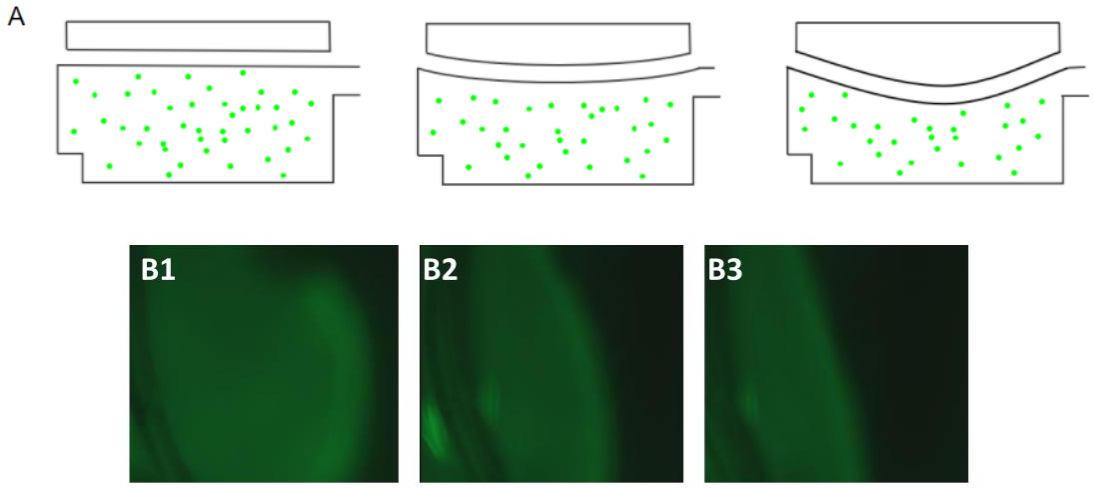

Figure 41: ***Compression of the organoid chamber using a fluorescein solution*** *A) schematic representation of how the blown-up pneumatic chamber presses on the organoid chamber; B) example pictures of measurement. 1) no pressure applied; 2) 500 mbar applied; 3) 1000 mbar applied; 4x magnification*

A non-linear relationship between pressure and deflection was observed. The change, in the beginning, was higher compared to effects of pressure changes between 700 and 1000 mbar (Figure 42).

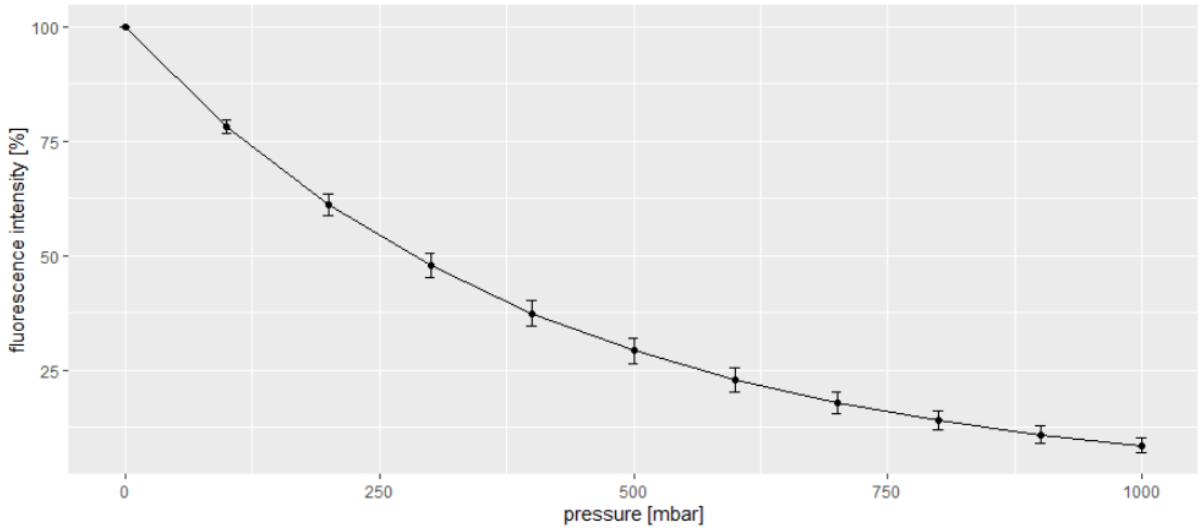

Figure 42: ***Relative fluorescence intensity per pressure;*** *n=2; error bars showing the standard deviation*

3.3.2.3 Compression measurement using green Fluorescent Polymer Microspheres

Using green fluorescence beads as surrogates, the deflection of the 2 % agarose hydrogel was measured. In figure 43 an example is shown how the particles moved from a relaxed state without any pressure to a compressed state after application of 500 mbar.

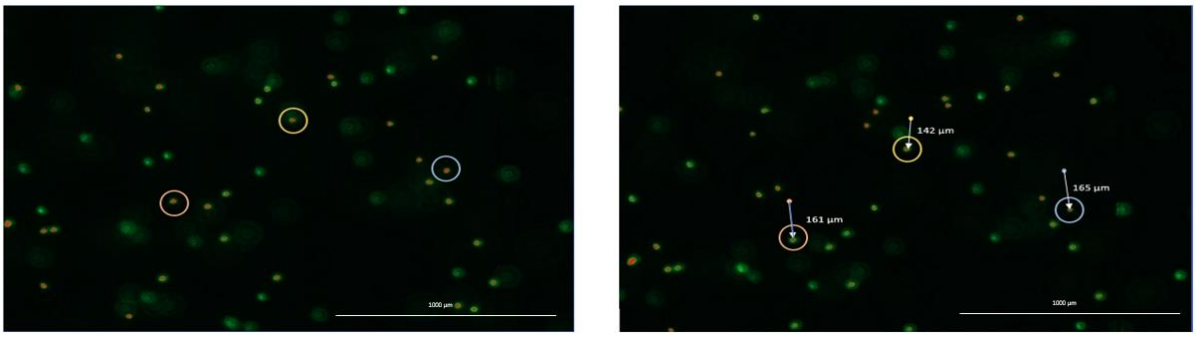

Figure 43: Example of ***particle movement*** *after application of a 500 mbar pressure*

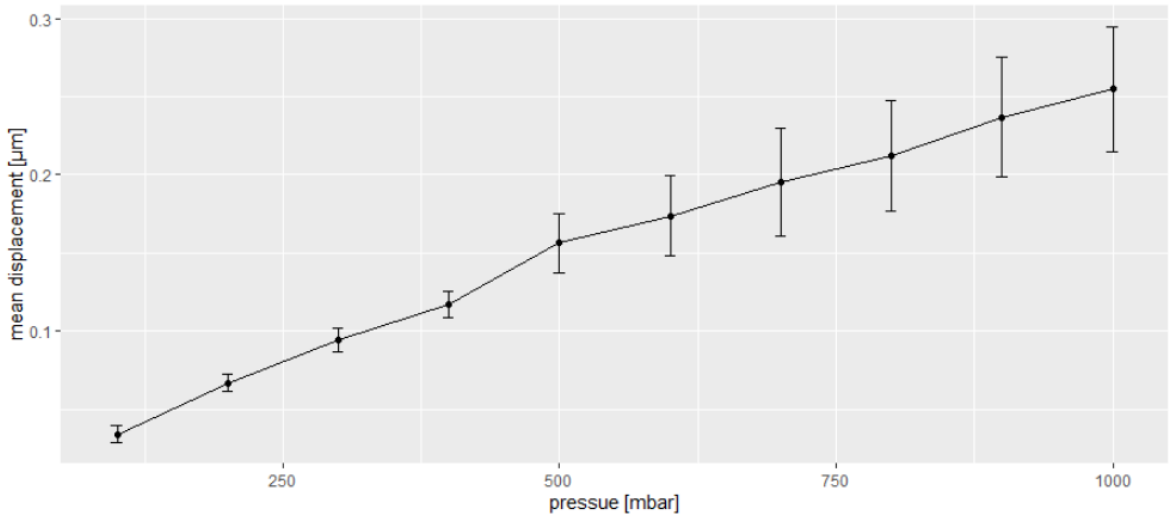

Figure 44: ***Mean displacement of particles per pressure****; error bars showing the standard deviation*

Between pressures of 100 to 400 mbar the movement of the beads was minimal with a low standard deviation between measurements (Figure 44). After 500 mbar the beads started to move no longer uniform in the same direction. Up to pressures of 400 mbar a compressive force is mimic, while beyond 400 mbar the hydrogel constructs are squeezed through the pressure, indicated by the observed altered particle movement.

3.3.3 Trauma model

Tests showed that prolonged pressures beyond 500 mbar led to the destruction of the hydrogels. In figure 45A an intact hydrogel is shown, compared to 45B where clear destruction can be seen after application of 800 mbar. In 45C the macroscopic destruction of the hydrogels can be seen in the top row and intact hydrogels in the bottom row.

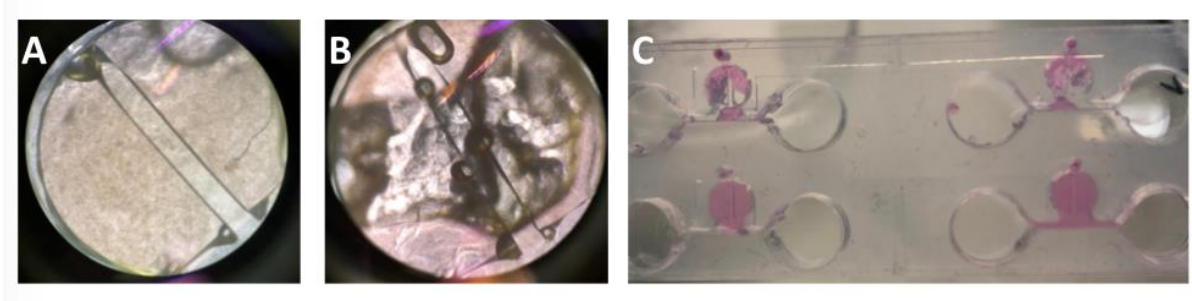

Figure 45: ***Destruction of the hydrogel at too high pressure.*** *A) 4x magnification of intact hydrogel B) 4x magnification of destructed hydrogel C) microfluidic chips with destructed (top) and intact hydrogels (bottom)*

3.3.4 Mechanical stimulation of chondrocytes

Chondrocytes were loaded onto a microfluidic chip using a 2 % agarose hydrogel to test for effects of mechanical stimulation. The constructs were stimulated with either 400 mbar mimicking a physiological pressure, or 800 mbar to mimic hyper-physiological stress.

This experiment was performed using three biological and two technical replicates for each condition. However, extracted RNA yield was rather low (0 - 12 ng/µL per sample). Therefore, it was necessary to pool the replica and to reduce the number of tested markers.

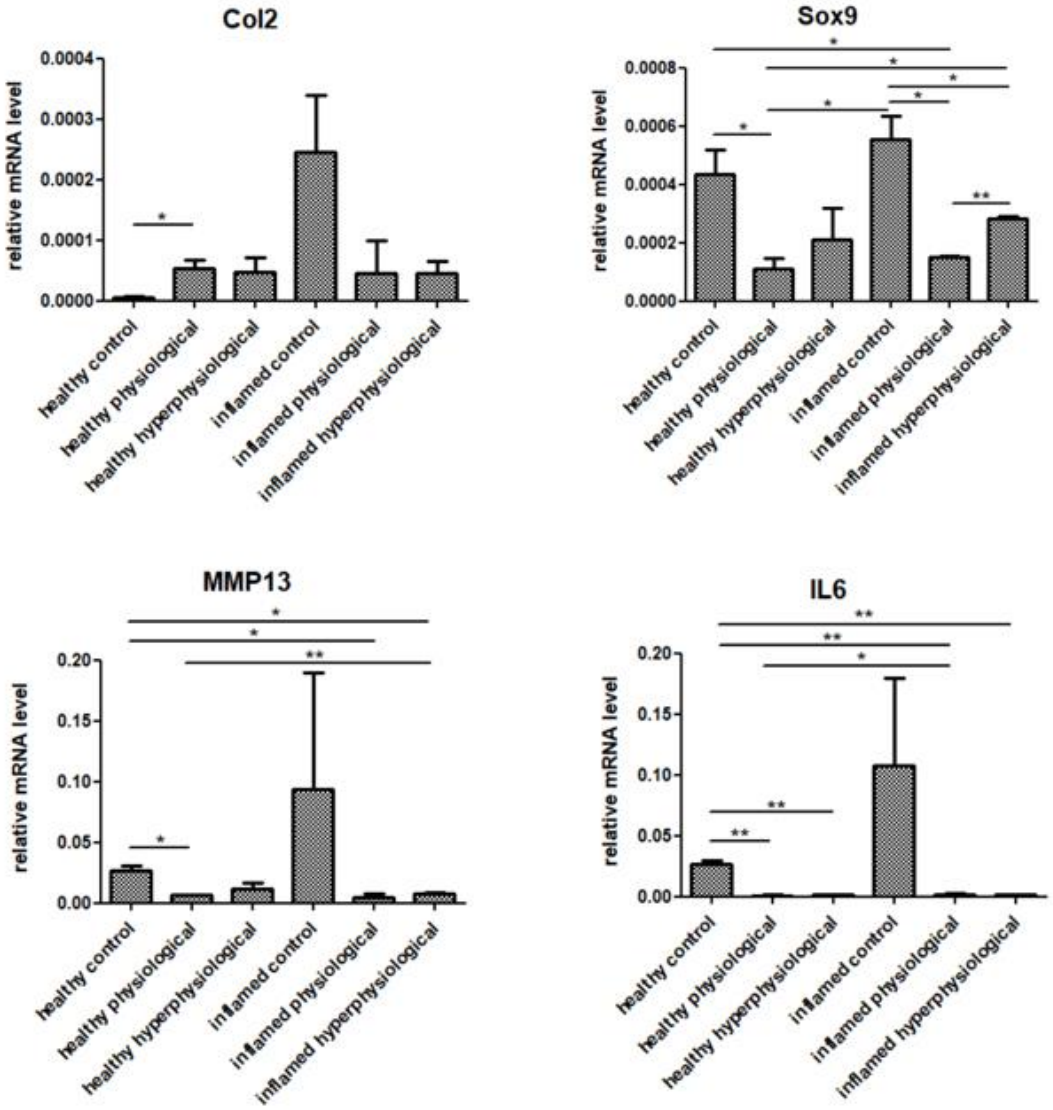

Figure 46: ***Gene expression analysis;*** *control = no pressure; physiological = 400 mbar pressure; hyper-physiological = 800 mbar pressure; inflamed = cytokine stimulation; Col2 and Sox9 = cartilage marker; MMP13 and IL6 = inflammation marker; significance cutoff: "*": p < 0.05; "**": p < 0.01; error bars showing the standard deviation*

Measured expression levels for cartilage markers Col2 and Sox9 were extremely low (<0.0007). As can be seen in figure 46 for Col2 the only significant difference was found between healthy control and physiological mechanically stimulated samples, were an increase in expression was measured. All other comparisons were not significantly different. An opposite behaviour was found for the other cartilage marker, Sox9, where a significantly higher expression was found in the healthy control compared to the healthy physiological stimulated samples. For Sox9 the same was also found for the inflamed treatment. However, here between physiological and hyper-physiological stimulation the Sox9 expression increased again. No aggrecan expression could be anaylsed, because the marker did not work properly in this run.

Looking at the inflammation markers it can be said that MMP13 and IL6, were significantly higher in healthy control compared to the healthy physiological treatment and for IL6 also compared to the hyper physiological treatment. Moreover, the highest expression was found in the inflamed control samples. However, these samples have a very high standard deviation. For all mechanical stimulated samples, the measured IL6 expression was minimal (<0.0022).

4 Discussion

Osteoarthritis is a highly prevalent joint disease, with a significant disease burden in human as well as in veterinary patients. Development of effective treatment options has been largely unsuccessful[86]. A major reason for this is that we still not fully understand the etiology and pathogenesis of OA. Therefore, it is very important to develop and validate experimental models of OA, which can be used to study disease onset and progression as wells as to test potential therapeutics. In this study, we managed to successfully establish a functional, mechanically stimulated microfluidic joint-on-a-chip model. We tested various hydrogel types and concentrations to find the most suitable scaffold for different cell types of the joint (chondrocytes, synoviocytes, MSCs) and for mechanical stimulation of chondrocytes.

In first pilot experiment it was tested if collagen or fibrin hydrogel would be an ideal scaffold for joint cells. However, after 48 hours of incubation, nearly all cell constructs collapsed or completely dissolved, showing that these scaffolds were not suitable. Collagen is a very soft scaffold[123], whereas cartilage and bone are very hard substances[124]. The elastic modulus for collagen hydrogels was found to be around 2.7 kPa[125], for the subchondral bone to be between 1.6 and 2.3 GPa[126] and for articular cartilage to be about 2.21 GPa[127]. Therefore, it does not sufficiently mimic the natural environment. Fibrin is not a natural component of the ECM however in previous studies it proved to be a suitable scaffold[115]. Nonetheless, the concentration of fibrinogen which was used in the first preliminary experiment appeared to be too low to create a stable matrix. In order to mimic the natural environment more closely, fibrinogen concentrations were increased in the follow-up experiments.

Cells seeded into fibrin hydrogel were not very stable over a longer culture period. It was found that already after 10 days of incubation the construct shrunk considerably. The shrinkage of fibrin hydrogels laden with cells was also observed in other studies[128]. The group of O'Cearbhaill et al. seeded MSCs into fibrin hydrogels. They observed cell compaction in the constructs over a 9-day culture period. Moreover, they found that the shrinkage of the constructs appears to be cell density depended. They showed that at lower densities of 100 000 cells/mL nearly no contraction was observed, whereas densities of 1 000 000 cells/mL led to massive compaction. They suggested that the shrinkage of the fibrin hydrogels is due to the fact that the cells remodeled the scaffold[129]. This would explain why we observed such a drastic shrinkage of the constructs. However, Rosser et al., who developed a nutrient gradient-based

microfluidic 3D chondrocyte culture-on-a-chip, seeded chondrocytes into TISSEEL fibrin hydrogel. They managed to culture the construct for 21 days without any reported shrinkage. But compared to our studies (fibrin concentrations: 25-100 mg/mL) they used a lower fibrinogen concentration of 20 mg/mL[115]. The stability of fibrin hydrogels could be improved by optimizing the concentration of calcium ions, the pH, by lowering the cell density or by addition of protease inhibitors[130]. Temperature and pH have a high impact on the stability of fibrin hydrogels. Both contribute to the denaturation of fibrinogen molecules. At a pH below 5.5 fibrin hydrogels can not be formed. Decreasing the temperature from 37 °C to 15 °C has been shown to increase the rate of fibrinogenesis[131]. A disadvantage of using fibrin hydrogels is that they need two compounds for polymerization, namely fibrinogen and thrombin[131]. This can lead to unhomogenized distributions of polymer density and the laden cells.

Mechanical stimulation is a key factor for chondrogenic homeostasis and for the onset of osteoarthritis[51]. To study the effect of mechanical stimulation on chondrocytes, agarose hydrogels were chosen since no satisfying results could be achieved with fibrin hydrogels and agarose has been reported to be an ideal matrix for chondrocytes, especially when used for mechanical stimulation studies[101]. This could be confirmed in this study. The life/dead staining revealed that after 10 days of incubation 95 % of the cells were still viable and after 30 days still 92 % of the cells were alive. Also, no shrinkage of the constructs was observed, compared to fibrin hydrogels. Moreover, there are several advantages to choose agarose hydrogels. Agarose proved to be a suitable scaffold to mimic cartilage, because of adjustable mechanical properties and swelling ratios. Upon static and dynamic loading similar mechanical behaviors are found in agarose compared to cartilage[37]. For example, both are hydrated material and exhibit strain dependent hydraulic permeability. Therefore, with increased deformation through applied forces the resistance to water transport through the material increases[37].

A major problem in 3D cultures is the inadequate nutrients and oxygen supply, which dismisses chondrocytes growth. Guaccio et al. investigated this phenomena and found that the oxygen consumption rate in agarose gels is doubled compared to collagen gels[132]. Therefore, agarose scaffolds closer mimic what is found in the natural environment of chondrocytes. Moreover, it enables a stabilized phenotype and an enhanced proteoglycan precipitation was reported[133].

Through high pressure tissue destruction was observed. However, agarose is reported to have a high pressure tolerance (Young's modulus > 0.5 MPa) compared to native tissues, such as bone (1-20 GPa) and cartilage (10-20 GPa)[37].

In monolayer cultures, chondrocytes typically undergo dedifferentiation, which is marked by induction of collagen type I expression together with a decrease in collagen type II and aggrecan expression[134]. The gene expression analysis of our agarose chondrocyte constructs showed that the chondrogenic dedifferentiation marker col1 was only expressed to a very low amount (< 0.04 fold change). The expression of the chondrogenic marker aggrecan was significantly higher (acan/col1 = 9). Indicating that the chondrocytes maintained their phenotype and no unwanted fibrocartilage formation was induced[79]. Similar behavior was also found in the 3D chondrocyte culture by Rosser et al. After 21 days of cultivation they measured an aggrecan expression level of approximately 1 and a collagen type I expression of 0.3, which is roughly a acan/col1 ratio of 3.3[115]. However, it must be said that in contrast to Rosser et al. we used agarose as scaffold whereas they used TISSEEL fibrin glue.

Comparing the properties of the agarose hydrogels to the TISSEEL fibrin glue produced hydrogels we found that depending on the concentration a similar rigidity (~2.5 -7.5 kPa) was measured. However, both were still a lot softer compared to what is found in natural articular cartilage (2.21 GPa)[127]. It was found that chondrocytes seeded into harder hydrogels have an increased growth and exhibit more proliferation markes[135]. To increase the rigidity, we tried a 50 % agarose hydrogel. However, the agarose powder did not even dissolve properly.

Using a fluorescein solution it was measured how the relative fluorescence intensity changed during diffusing into the different hydrogels. It was found that a linear relationship exists between density and diffusion. The relative intensity change of a 2 % agarose hydrogel was approximately twice as in the 4 % agarose hydrogel. This is probably related to the pore size. It is reported that a 4 % agarose has a pore size of 70 nm and a 2 % hydrogel has a size of 150 nm[136]. The pore diameter of articular cartilage was found to be between 11 and 14 nm[137].

The aim of *in vitro* studies is to mimic the natural environment as closely as possible. A relatively new approach is to use blended hydrogels. In studies using cells of the intervertebral disks it was found that a mixture of collagen and agarose shows favourable properties[103]. Blended hydrogels provided similar mechanical properties as standard agarose hydrogels, with the advantage that blended hydrogels promoted cell adhesion. Hence, a more native like tissue was assembled which still allowed for exploration of biomechanical influences[102]. We could not confirm the beneficial advantage of using agarose collagen type II blended hydrogels. However, a reason for the unexpected outcome, could be that the collagen did not dissolve properly.

Using again a fluoresceine solution the compression capacity of different pressures was investigated. A non-linear relationship between pressure and deflection was observed. The reason for this could be the elastic properties of the PDMS foil. In articular cartilage, it was observed that dynamic strain during normal activity ranges from 15 to 35 %. Higher strain between 50 – 70 % causes injury and for strains of 70 to 90 % cell death was reported[55]. Destruction of the hydrogels was observed following stimulation with high pressures (> 500 mbar). This strain may therefore be used as a trauma model, where tissue destruction occurs.

Moreover, the effect of compression on cells was investigated using green fluorescence beads as surrogates. Different pressures were applied and displacement of the beads was measured. A non-linear relationship was observed. For pressures between 100 and 400 mbar excursion of the beads was only minimal with a low standard deviation between measurements. At 500 mbar and greater pressure the beads started to move in a slightly different direction and also at a different level. Indicating that through pressures up to 400 mbar a compression force is mimic, while beyond 400 mbar the hydrogel construct gets squeezed through the pressure.

Based on the preliminary findings a final mechanical experiment was performed. However, the yield of extracted RNA was relatively low (0 – 12 ng/µL per sample). It has been reported previously that it is very hard to isolate sufficient amounts of high quality RNA from cell-hydrogel complexes and that hydrogel contaminates hinder downstream applications, such as qPCR[138]. Reasons for the low RNA yield could be that RNA is a very polar molecules as well as the ECM molecules used for the hydrogels. RNA is negatively charged and undergoes ionic complexing with positively charged regions of the matrix[139]. Hence, the attraction between the molecule is very high. This makes the isolation of RNA from 3D cultures harder compared to monolayer cultures. So far, no golden standard has been found to most efficiently extract RNA from hydrogels[138].

Due to the low yield of RNA no expression of collagen type I could be measured. Meaning that no conclusions about possible dedifferentiation of the chondrocytes can be drawn. Instead, we focused on expression levels of chondrocyte markers col2, sox9 and aggrecan, as well as inflammation markers IL6 and MMP13. However, expression levels of Col2 and Sox9 were extremely low (<0.0007). This is probably related to the low yield of RNA and the low quality. Burgess et al. found that the amount of RNA is crucial for good quality qPCRs[138].

In OA the amount of collagen type II in the matrix decreases with disease progression[140]. This was also found in our study for the inflamed samples. For col2 expression the only significant

difference was found between the healthy control and samples stimulated with physiological pressure. For Sox9, a significantly higher expression was found in the control compared to the mechanically stimulated samples. However, a higher col2 expression was found in the mechanical stimulated samples compared to the control.

In this study, we were able to develop a functional joint-on-a-chip model. Through the addition of a pneumatic chamber, a variety of complex mechanical stimulations can be tested for their effect on chondrocytes. However, further optimization steps will be required, before this system can be used as a disease model to screen and test new therapeutics, in order to facilitate development of new drugs and treatment options.

An important next step would be to increase the RNA yield obtained from samples. This could be achieved by using more technical replicates and pooling the samples. Alternatively other analysing methods could be used such as RNAseq instead of qPCR for gene expression analysis. The advantage of using RNAseq approaches would be that compared to qPCR a lower amount of RNA is needed to analyse much more genes. Moreover, novel transcripts, alternative spliced isoforms, splice sites and small and noncoding RNA could be analysed[141].

Through the destruction of the hydrogel due to high pressure, a lot of material is lost. Another future improvement could focus on that. Possible solutions could be to make the connection between the medium channel and the organoid chamber smaller and by that prevent the loss of fragments or to use a permeable membrane to separate the organoid chamber from the medium channel. It could also be investigated if the hydrogel elasticity could be improved. Generally, higher concentrated hydrogels have better mechanical properties and do not tear so easily[128]. However, 2 % agarose hydrogels are widely used for mechanical studies on chondrocytes[101]. Reasons for not using higher concentrated hydrogels are that with higher density the cell migration and ingrowth into the matrix becomes more difficult[128].

So far, only few OA model have been developed using microfluidic technology[86]. Occetta et al. developed a 3D human cartilage-on-a-chip[9] model to investigate OA induced through mechanical stimulation (Figure 4). Similar to our OA-on-a-chip they also used PDMS to construction the chip. Their chip comprised two chambers separated by a flexible PDMS membrane. The upper chamber hosted the organoid and the bottom chamber acted as actuation compartment. In contrast to our system, they had a separate culture chamber, which consisted out of a 300 µm wide central channel hosting the microtissue and flanking it two channels for the medium supply. Two rows of T-shaped hanging posts separate the medium channels from the culture

channel in the top compartment. Through pressure application to the bottom compartment the PDMS membrane deforms, and a compressive force acts on the microtissue. Their device allows for confined compression of 10 and 30 %. Compared to our microfluidic chip, where each organoid had an individual pneumatic chamber on top, the cartilage-on-a-chip from Occetta et al. pressurized the bottom compartment. Moreover, we had a direct connection of the medium channel to the organoid chamber and our device hosted four technical replicates. Another difference is that they used human chondrocytes, whereas we derived our cells from horses. As hydrogel scaffold they used a poly ethylene glycol (PEG)-based hydrogel. This 3D enzymatically cross-linked and MMP-degradable PEG- based hydrogel was established in previous studies of this group. According to them the use of PEG as hydrogel base had the advantage that it allowed for high standardisation with respect to naturally derived biomaterials and through chemically modification allowed for tissue remodelling through physiologically relevant processes. For the hydrogel preparation they seeded $50*10^6$ cells/mL into a 2 % PEG hydrogel. Hence, they used a considerably higher cell number compared to the $3*10^6$ cells/mL we used. Analysis showed that their microtissues where rich in aggrecan and collagen type II[9]. However, since no conclusive results could be obtained in our preliminary experiments, it still needs to be investigated if our system provides the same rich aggrecan and collagen type II expression.

Another microfluidic OA model was developed by Rosser et al. They established a nutrient gradient-based 3D chondrocyte culture-on-a-chip[115]. In contrast to our system, they did not include any mechanical stimulation into their device, but rather focused on improving the *in vitro* environment for chondrocytes. With their model they proved to be able to mimic native cartilage, with its different zones and alternative cell densities. The cell number we chose for our experiments was on the basis of this study. Also their basic chip design was similar to ours in terms of that the organoid chamber was directly connected to a medium supply channel[115]. However, through the biomechanical stimulation our system is able to more closely mimic the native onset of OA.

Osteoarthritis is a disease of the whole joint. A big advantage of microfluidic system is that they allow co-culture of different cells to study interaction and cross talk among multiple microtissues[86]. To our knowledge so far only two OA co-culture chips have been developed. Lin et al. used pluripotent stem cells and a dual-flow bioreactor to create an osteochondral tissue chip[38]. They seeded an intermediate phenotype of mesenchymal progenitors into a 15 % methacrylated gelatin hydrogel and loaded this onto the microbioreactor. Through supplementation

of chondrogenic medium to the top of the construct and osteogenic medium to the bottom they managed to establish an osteochondral tissue, with chondrocytes and osteoblasts after 28 days of differentiation. He et al. developed a human stem cell derived microfluidic model that consisted out of three units: osteochondral unit, synovial and adipose tissues. The different tissues were connected to one medium channel and through that they could study interaction between the different tissues. The current limitations of these co-culture models are that they induce OA through chemical signalling. Therefore, a future improvement of our joint-on-a-chip model could be to induce additional compartments of other tissues of the joint.

In the next step, our system should be combined with a co-culture system, that allows for simultaneous culturing of different cell types of the joint. In particular, compartments to mimic the synovium and the subchondral bone should be added. The replication of the communication between the different cell types together with the mechanical stimulation of our system would allow for a more complete understanding of OA pathogenesis.

Another approach in further enhancing the system would be to mimic the differences in mechanical properties found in natural joint tissues. Differences in Poisson's ratio, equilibrium shear moduls, tensile Young's modulus and aggregate moduls were found between different joint locations and also between different zones of articular cartilage[142].

The obtained preliminary results will serve as the basis for a future joint-on-a-chip models which can be used to investigate novel treatment approaches and perform drug screening. Ultimately serving the One Health approach in finding a suitable therapy for human as well as veterinary patients suffering from osteoarthritis and potentially contribute to the reduction in animal trails at the same time.

Summary

Osteoarthritis (OA) is a highly prevalent joint disease, which affects about 300 million people worldwide, which is roughly 4 % of the population. This makes it one of the most diagnosed diseases in human general practice. Osteoarthritis is characterized by cartilage degradation which is mainly induced by mechanical stress on the joints. Chronic pain, impaired locomotion, and high socioeconomic costs are associated with this disease. Especially elderly people are affected by osteoarthritis. Therefore, with the increase in global lifespan also the prevalence of OA will increase. Currently, no therapy is available to stop the progressive loss of articular cartilage. Thus, there is a large unmet need for a disease-modifying regenerative treatment for OA.

OA not only occurs in humans but in various domesticated animals such as the horse, dog, sheep etc. In equine patients, locomotion disorders such as osteoarthritis are very common and often result in dropping out from athletic use. Hence, not only humans but also horses would-be beneficiaries of new treatment strategies.

The development of new therapies requires test modalities that allow to study the pathophysiology of the disease on the one hand and investigate the effect of newly developed drugs on the other hand. Organs on a chip are small in vitro bioreactors, which closely mimic organs and tissues and allow for high throughput screening of drugs. A dynamic OA-on-a-chip model could therefore be a useful tool to drive OA research and treatment development forward.

In this project, a pneumatic polydimethylsiloxane (PDMS-) based microfluidic OA on a chip model was developed and validated. The system allows application of multiple compression conditions to mimic joint loading and four technical replicates on a single chip. It was found that agarose hydrogels were most suitable as scaffolds for the creation of mechanically stimulated chondrocyte organoids on microfluidic chips. The developed microfluidic joint-on-a-chip was used to study healthy versus inflamed primary equine chondrocytes grown as 3D articular microtissues and subjected to dynamic mechanical force to closely mimic a natural articular environment. The effects of physiological and hyper-physiological mechanical stress were investigated over a period of two weeks.

Through the development of an in vitro joint-on-a-chip model we created a miniature bioreactor that can be used to gain further understanding of the onset and progression of OA and the role of biomechanical forces on articular chondrocytes. In future, this system can be used as a disease model for screening of novel treatment options for OA.

Zusammenfassung

Osteoarthritis (OA) ist eine hochprävalente Gelenkerkrankung, von der weltweit etwa 300 Millionen Menschen betroffen sind, was ungefähr 4 % der Bevölkerung sind. Dies macht OA zu einer der am häufigsten diagnostizierten Erkrankungen in der Allgemeinmedizin. Arthrose ist durch Knorpelabbau gekennzeichnet, der vor allem durch mechanische Belastung der Gelenke verursacht wird. Chronische Schmerzen, Bewegungsstörungen und hohe sozioökonomische Kosten sind mit dieser Erkrankung assoziiert. Vor allem ältere Menschen sind von OA betroffen. Daher wird mit der derzeit beobachteten Zunahme der globalen Lebenserwartung auch die Prävalenz von OA zunehmen. Gegenwärtig gibt es keine Therapie, um den fortschreitenden Verlust des Gelenkknorpels zu stoppen. Somit besteht ein großer ungedeckter Bedarf an einer krankheitsmodifizierenden regenerativen Behandlung für OA.

OA kommt nicht nur beim Menschen vor, sondern auch bei verschiedenen domestizierten Tieren wie dem Pferd, dem Hund, dem Schaf etc. Bei Pferden ist OA sehr häufig und führt oft zum Ausscheiden aus der sportlichen Nutzung. Daher würden nicht nur Menschen, sondern auch Pferde von neuen Behandlungsstrategien profitieren.

Die Entwicklung neuer Therapien erfordert Testmodalitäten, die es erlauben, einerseits die Pathophysiologie der Erkrankung zu studieren und andererseits die Wirkung neu entwickelter Medikamente zu untersuchen. Organe auf einem Chip sind kleine *In-vitro*-Bioreaktoren, die Organe und Gewebe imitieren und ein Hochdurchsatz-Screening von Medikamenten ermöglichen. Ein dynamisches OA-on-a-Chip-Modell könnte daher ein nützliches Werkzeug sein, um die OA Forschung und Entwicklung neuer Medikamente voranzutreiben.

In diesem Projekt wurde ein pneumatisches Polydimethylsiloxan (PDMS-) basiertes mikrofluidisches OA auf einem Chip Modell entwickelt und validiert. Das System ermöglicht mehrere Kompressionsbedingungen, um die Gelenksbelastung nachzuahmen in vier technische Replikate auf einem einzigen Chip. Es wurde festgestellt, dass Agarose-Hydrogele als Matrix für die Kreation von mechanisch angeregten Chondrozyten-Organoiden auf mikrofluidischen Chips am besten geeignet waren. Der entwickelte mikrofluidische Joint-on-a-Chip wurde verwendet, um gesunde und entzündete primäre equine Chondrozyten zu untersuchen, die als 3D-Gelenkmikrogewebe gezüchtet und einer dynamischen mechanischen Kraft ausgesetzt wurden, um eine natürliche Gelenksumgebung nahe zu imitieren. Die Auswirkungen physiologischer und hyperphysiologischer mechanischer Belastungen wurden über einen Zeitraum von zwei Wochen untersucht.

Durch die Entwicklung eines in vitro Joint-on-a-Chip-Modells wurde ein Miniatur-Bioreaktor entwickelt, mit dem sich die Entstehung und Progression von OA und die Rolle biomechanischer Kräfte auf Gelenks-Chondrozyten weiter erforschen lassen. Dieses System kann zukünftig als Krankheitsmodell für das Screening neuer Behandlungsoptionen für OA verwendet werden.

5 List of References

1. Bertoni L, Jacquet-Guibon S, Branly T, et al. An experimentally induced osteoarthritis model in horses performed on both metacarpophalangeal and metatarsophalangeal joints: technical, clinical, imaging, biochemical, macroscopic and microscopic characterization. *PLoS One*. 2020;15(6):e0235251. doi:10.1371/journal.pone.0235251

2. Mathiessen A, Conaghan PG. Synovitis in Osteoarthritis: Current Understanding with Therapeutic Implications. *Arthritis Research and Therapy* 2017;19(1):1-9. doi.org/10.1186/s13075-017-1229-9

3. Frisbie D., Synovial Joint Biology and Pathobiology, Equine Surgery, Fourth Edition. *Elsevier Inc.* 2012;4:1096-1114 doi.org/10.1016/B978-1-4377-0867-7.00078-8

4. Shen J, Abu-Amer Y, O'Keefe RJ, McAlinden A. Inflammation and epigenetic regulation in osteoarthritis. *Connect Tissue Res*. 2017;58(1):49-63. doi:10.1080/03008207.2016.1208655

5. Kloppenburg M, Berenbaum F. Osteoarthritis year in review 2019: epidemiology and therapy. *Osteoarthr Cartil*. 2020;28(3):242-248. doi:10.1016/j.joca.2020.01.002

6. Caron, John P., 'Osteoarthritis', in Diagnosis and Management of Lameness in the Horse: Second Edition. *Elsevier Inc.* 2010;(2):655–68 doi:10.1016/B978-1-4160-6069-7.00061-4

8. Souza MV de. Osteoarthritis in horses - Part 1: relationship between clinical and radiographic examination for the diagnosis. *Brazilian Arch Biol Technol*. 2016;59(0). doi:10.1590/1678-4324-2016150024

9. Occhetta P, Mainardi A, Votta E, et al. Hyperphysiological compression of articular cartilage induces an osteoarthritic phenotype in a cartilage-on-a-chip model. *Nat Biomed Eng*. 2019;3(7):545-557. doi:10.1038/s41551-019-0406-3

10. Xia B, Di Chen, Zhang J, Hu S, Jin H, Tong P. Osteoarthritis Pathogenesis: A Review of Molecular Mechanisms. *Calcif Tissue Int*. 2014;95(6):495-505. doi:10.1007/s00223-014-9917-9

11. Munjal A, Bapat S, Hubbard D, Hunter M, Kolhe R, Fulzele S. Advances in Molecular biomarker for early diagnosis of Osteoarthritis. *Biomol Concepts*. 2019;10(1):111-119. doi:10.1515/bmc-2019-0014

12. Johnson CI, Argyle DJ, Clements DN. In vitro models for the study of osteoarthritis. *Vet J*. 2016;209:40-49. doi:10.1016/j.tvjl.2015.07.011

13. Kidd JA, Barr ARS. Osteoarthritis in the horse. *EQUINE Vet Educ*. 2001;13(3):160-168.

14. McIlwraith CW, Frisbie DD, Kawcak CE. The horse as a model of naturally occurring osteoarthritis. *Bone Joint Res*. 2012;1(11):297-309. doi:10.1302/2046-3758.111.2000132

15. Wong DM, Davis JL, White N a. Tutorial Article. *Equine Vet Educ*. 2011;23(2):88-100. http://doi.wiley.com/10.1111/j.2042-3292.2010.00173.x

16. McCoy AM. Animal Models of Osteoarthritis: Comparisons and Key Considerations. *Vet Pathol*. 2015;52(5):803-818. doi:10.1177/0300985815588611

17. Decker RS, Koyama E, Pacifici M. Genesis and morphogenesis of limb synovial joints and articular

cartilage. *Matrix Biol*. 2014;39:5-10. doi:10.1016/j.matbio.2014.08.006

18. Mathiessen A, Conaghan PG. Synovitis in osteoarthritis: Current understanding with therapeutic implications. *Arthritis Res Ther*. 2017;19(1). doi:10.1186/s13075-017-1229-9

19. Castrogiovanni P, Di Rosa M, Ravalli S, et al. Moderate physical activity as a prevention method for knee osteoarthritis and the role of synoviocytes as biological key. *Int J Mol Sci*. 2019;20(3). doi:10.3390/ijms20030511

20. Li G, Yin J, Gao J, et al. Subchondral bone in osteoarthritis: Insight into risk factors and microstructural changes. *Arthritis Res Ther*. 2013;15(6):223. doi:10.1186/ar4405

21. Castañeda S, Roman-Blas JA, Largo R, Herrero-Beaumont G. Subchondral bone as a key target for osteoarthritis treatment. *Biochem Pharmacol*. 2012;83(3):315-323. doi:10.1016/j.bcp.2011.09.018

22. Holopainen JT, Brama PAJ, Halmesmäki E, et al. Changes in subchondral bone mineral density and collagen matrix organization in growing horses. *Bone*. 2008;43(6):1108-1114. doi:10.1016/j.bone.2008.07.254

23. Lee D, Erickson A, You T, Dudley AT, Ryu S. Pneumatic microfluidic cell compression device for high-throughput study of chondrocyte mechanobiology. *Lab Chip*. 2018;18(14):2077-2086. doi:10.1039/c8lc00320c

24. Komeili A, Abusara Z, Federico S, Herzog W. A compression system for studying depth-dependent mechanical properties of articular cartilage under dynamic loading conditions. *Med Eng Phys*. 2018;60:103-108. doi:10.1016/j.medengphy.2018.07.004

25. Montagne K, Onuma Y, Ito Y, Aiki Y, Furukawa KS, Ushida T. High hydrostatic pressure induces pro-osteoarthritic changes in cartilage precursor cells: A transcriptome analysis. *PLoS One*. 2017;12(8):1-17. doi:10.1371/journal.pone.0183226

26. Musumeci G. The effect of mechanical loading on articular cartilage. *J Funct Morphol Kinesiol*. 2016;1(2):154-161. doi:10.3390/jfmk1020154

27. Patel JM, Wise BC, Bonnevie ED, Mauck RL. A Systematic Review and Guide to Mechanical Testing for Articular Cartilage Tissue Engineering. *Tissue Eng - Part C Methods*. 2019;25(10):593-608. doi:10.1089/ten.tec.2019.0116

28. Shahin K, Doran PM. Tissue engineering of cartilage using a mechanobioreactor exerting simultaneous mechanical shear and compression to simulate the rolling action of articular joints. *Biotechnol Bioeng*. 2012;109(4):1060-1073. doi:10.1002/bit.24372

29. Sophia Fox AJ, Bedi A, Rodeo SA. The basic science of articular cartilage: Structure, composition, and function. *Sports Health*. 2009;1(6):461-468. doi:10.1177/1941738109350438

30. Singh P, Marcu KB, Goldring MB, Otero M. Phenotypic instability of chondrocytes in osteoarthritis: on a path to hypertrophy. *Ann N Y Acad Sci*. 2019;1442(1):17-34. doi:10.1111/nyas.13930

31. Kozhemyakina E, Lassar AB, Zelzer E. A pathway to bone: Signaling molecules and transcription factors involved in chondrocyte development and maturation. *Dev*. 2015;142(5):817-831. doi:10.1242/dev.105536

32. Le LTT, Swingler TE, Clark IM. Review: The role of microRNAs in osteoarthritis and chondrogenesis. *Arthritis Rheum*. 2013;65(8):1963-1974. doi:10.1002/art.37990

33. Sun MMG, Beier F. Chondrocyte hypertrophy in skeletal development, growth, and disease. *Birth Defects Res Part C - Embryo Today Rev*. 2014;102(1):74-82. doi:10.1002/bdrc.21062

34. Nims RJ, Cigan AD, Albro MB, Hung CT, Ateshian GA. Synthesis rates and binding kinetics of matrix products in engineered cartilage constructs using chondrocyte-seeded agarose gels. *J Biomech*. 2014;47(9):2165-2172. doi:10.1016/j.jbiomech.2013.10.044

35. Zhou S, Cui Z, Urban JPG. Factors influencing the oxygen concentration gradient from the synovial surface of articular cartilage to the cartilage-bone interface: A modeling study. *Arthritis Rheum*. 2004;50(12):3915-3924. doi:10.1002/art.20675

36. Messina OD, Vidal Wilman M, Vidal Neira LF. Nutrition, osteoarthritis and cartilage metabolism. *Aging Clin Exp Res*. 2019;31(6):807-813. doi:10.1007/s40520-019-01191-w

37. Salati MA, Khazai J, Tahmuri AM, et al. Agarose-Based biomaterials: Opportunities and challenges in cartilage tissue engineering. *Polymers (Basel)*. 2020;12(5):1-15. doi:10.3390/POLYM12051150

38. Lin Z, Li Z, Li EN, et al. Osteochondral Tissue Chip Derived From iPSCs: Modeling OA Pathologies and Testing Drugs. *Front Bioeng Biotechnol*. 2019;7. doi:10.3389/fbioe.2019.00411

39. Scanzello CR, Goldring SR. The role of synovitis in osteoarthritis pathogenesis. *Bone*. 2012;51(2):249-257. doi:10.1016/j.bone.2012.02.012

40. Berenbaum F. Osteoarthritis as an inflammatory disease (osteoarthritis is not osteoarthrosis!). *Osteoarthr Cartil*. 2013;21(1):16-21. doi:10.1016/j.joca.2012.11.012

41. Sniekers YH, Intema F, Lafeber FPJG, et al. A role for subchondral bone changes in the process of osteoarthritis; A micro-CT study of two canine models. *BMC Musculoskelet Disord*. 2008;9:20. doi:10.1186/1471-2474-9-20

42. Suri S, Walsh DA. Osteochondral alterations in osteoarthritis. *Bone*. 2012;51(2):204-211. doi:10.1016/j.bone.2011.10.010

43. Jr DH, Brower R, medicine KJ-C in podiatric, 2001 undefined. Articular cartilage. Anatomy, injury, and repair. *europepmc.org*. Accessed May 29, 2021. https://europepmc.org/article/med/11344979

44. Babarina A V., Möllers U, Bittner K, Vischer P, Bruckner P. Role of the subchondral vascular system in endochondral ossification: Endothelial cell-derived proteinases derepress late cartilage differentiation in vitro. *Matrix Biol*. 2001;20(3):205-213. doi:10.1016/S0945-053X(01)00132-9

45. Wang T, He C. Pro-inflammatory cytokines: The link between obesity and osteoarthritis. *Cytokine Growth*

Factor Rev. 2018;44:38-50. doi:10.1016/j.cytogfr.2018.10.002

46. Iwanaga T, Shikichi M, Kitamura H, Yanase H, Nozawa-Inoue K. Morphology and functional roles of synoviocytes in the joint. *Arch Histol Cytol*. 2000;63(1):17-31. doi:10.1679/aohc.63.17

47. Nelson BB, Goodrich LR. Treatment of Joint Disease. In: *Robinson's Current Therapy in Equine Medicine: Seventh Edition*. Elsevier Inc.; 2015:798-804. doi:10.1016/B978-1-4557-4555-5.00187-4

48. Mathiessen A, Conaghan PG. Synovitis in osteoarthritis: Current understanding with therapeutic implications. *Arthritis Res Ther*. 2017;19(1):1-9. doi:10.1186/s13075-017-1229-9

49. Sokolove J, Lepus CM. Role of inflammation in the pathogenesis of osteoarthritis: Latest findings and interpretations. *Ther Adv Musculoskelet Dis*. 2013;5(2):77-94. doi:10.1177/1759720X12467868

50. Xie Y, Liu X, Wang S, Wang M, Wang G. Proper mechanical stimulation improve the chondrogenic differentiation of mesenchymal stem cells: Improve the viscoelasticity and chondrogenic phenotype. *Biomed Pharmacother*. 2019;115. doi:10.1016/j.biopha.2019.108935

51. Sun HB. Mechanical loading, cartilage degradation, and arthritis. *Ann N Y Acad Sci*. 2010;1211:37-50. doi:10.1111/j.1749-6632.2010.05808.x

52. Galois L, Etienne S, Grossin L, et al. Moderate-impact exercise is associated with decreased severity of experimental osteoarthritis in rats. *Rheumatology*. 2003;42(5):692-694. doi:10.1093/rheumatology/keg094

53. Dolzani P, Assirelli E, Pulsatelli L, Meliconi R, Mariani E, Neri S. Ex vivo physiological compression of human osteoarthritis cartilage modulates cellular and matrix components. *PLoS One*. 2019;14(9):1-16. doi:10.1371/journal.pone.0222947

54. Mosher TJ, Smith HE, Collins C, et al. Change in knee cartilage T2 at MR imaging after running: A feasibility study. *Radiology*. 2005;234(1):245-249. doi:10.1148/radiol.2341040041

55. Sanchez-Adams J, Leddy HA, McNulty AL, O'Conor CJ, Guilak F. The Mechanobiology of Articular Cartilage: Bearing the Burden of Osteoarthritis. *Curr Rheumatol Rep*. 2014;16(10):1-9. doi:10.1007/s11926-014-0451-6

56. Smith RL, Lin J, Trindade MCD, et al. Time-dependent effects of intermittent hydrostatic pressure on articular chondrocyte type II collagen and aggrecan mRNA expression. *J Rehabil Res Dev*. 2000;37(2):153-161.

57. Loening AM, James IE, Levenston ME, et al. Injurious mechanical compression of bovine articular cartilage induces chondrocyte apoptosis. *Arch Biochem Biophys*. 2000;381(2):205-212. doi:10.1006/abbi.2000.1988

58. Chen CT, Burton-Wurster N, Lust G, Bank RA, Tekoppele JM. Compositional and metabolic changes in damaged cartilage are peak- stress, stress-rate, and loading-duration dependent. *J Orthop Res*. 1999;17(6):870-879. doi:10.1002/jor.1100170612

59. Davisson T, Kunig S, Chen A, Sah R, Ratcliffe A. Static and dynamic compression modulate matrix

metabolism in tissue engineered cartilage. *J Orthop Res*. 2002;20(4):842-848. doi:10.1016/S0736-0266(01)00160-7

60. Sinha R, Verdonschot N, Koopman B, Rouwkema J. Tuning Cell and Tissue Development by Combining Multiple Mechanical Signals. *Tissue Eng Part B Rev*. 2017;23(5):494-504. doi:10.1089/ten.teb.2016.0500

61. Paggi CA, Venzac B, Karperien M, Leijten JCH, Le Gac S. Monolithic microfluidic platform for exerting gradients of compression on cell-laden hydrogels, and application to a model of the articular cartilage. *Sensors Actuators, B Chem*. 2020;315(February):127917. doi:10.1016/j.snb.2020.127917

62. Wang JHC, Li B. Mechanics rules cell biology. *Sport Med Arthrosc Rehabil Ther Technol*. 2010;2(1):1-7. doi:10.1186/1758-2555-2-16

63. Griffin TM, Scanzello CR. Innate inflammation and synovial macrophages in osteoarthritis pathophysiology. *Clin Exp Rheumatol*. 2019;37(5):57-63.

64. Guilak F. Biomechanical factors in osteoarthritis. *Best Pract Res Clin Rheumatol*. 2011;25(6):815-823. doi:10.1016/j.berh.2011.11.013

65. Lieberthal J, Sambamurthy N, Scanzello CR. Inflammation in joint injury and post-traumatic osteoarthritis. *Osteoarthr Cartil*. 2015;23(11):1825-1834. doi:10.1016/j.joca.2015.08.015

66. Farahat MN, Yanni G, Poston R, et al. Cytokine expression in synovial membranes of patients with rheumatoid arthritis and osteoarthritis. *Ann Rheum Dis*. 1993;52:870-875. doi:10.1136/ard.52.12.870

67. Brown TD, Johnston RC, Saltzman CL, Marsh JL, Buckwalter JA. Posttraumatic osteoarthritis: A first estimate of incidence, prevalence, and burden of disease. *Journal of Orthopaedic Trauma*. 2006;20(10):739-744. doi:10.1097/01.bot.0000246468.80635.ef

68. Liu-Bryan R, Terkeltaub R. The growing array of innate inflammatory ignition switches in osteoarthritis. *Arthritis Rheum*. 2012;64(7):2055-2058. doi:10.1002/art.34492

69. Martel-Pelletier J, Alaaeddine N, Pelletier J-P. Cytokines and their role in the pathophysiology of osteoarthritsis. *Frontiers in Bioscience*. 1999;4:694-701. doi: 10.2741/a387

70. Goldring MB. Osteoarthritis and Cartilage: The Role of Cytokines. *Curr Rheumatol Rep*. 2000;2:459-465.

71. Miller RE, Miller RJ, Malfait AM. Osteoarthritis joint pain: The cytokine connection. *Cytokine*. 2014;70(2):185-193. doi:10.1016/j.cyto.2014.06.019

72. Donell S. Subchondral bone remodelling in osteoarthritis. *EFORT Open Rev*. 2019;4(6):221-229. doi:10.1302/2058-5241.4.180102

73. Hui AY, Mccarty WJ, Masuda K, Firestein GS, Sah RL. A Systems Biology Approach to Synovial Joint Lubrication in Health, Injury, and Disease. *Wiley Interdiscip Rev Syst Biol Med*. 2012;4(1):15-37. doi:10.1002/wsbm.157

74. Hunter DJ, McDougall JJ, Keefe FJ. The Symptoms of Osteoarthritis and the Genesis of Pain. *Rheum Dis Clin North Am*. 2008;34(3):623-643. doi:10.1016/j.rdc.2008.05.004

75. McIlwraith CW, Kawcak CE, Frisbie DD, et al. Biomarkers for equine joint injury and osteoarthritis. *J Orthop Res*. 2018;36(3):823-831. doi:10.1002/jor.23738

76. Califf RM. Minireview Biomarker definitions and their applications. *Exp Biol Med*. 2018;243:213-221. doi:10.1177/1535370217750088

77. He Y, Siebuhr AS, Brandt-Hansen NU, et al. Type X collagen levels are elevated in serum from human osteoarthritis patients and associated with biomarkers of cartilage degradation and inflammation. *BMC Musculoskelet Disord*. 2014;15(1):1-10. doi:10.1186/1471-2474-15-309

78. Verma P, Dalal K. Serum cartilage oligomeric matrix protein (COMP) in knee osteoarthritis: A novel diagnostic and prognostic biomarker. *J Orthop Res*. 2013;31(7):999-1006. doi:10.1002/jor.22324

79. Hiemer B, Genz B, Jonitz-Heincke A, et al. Devitalisation of human cartilage by high hydrostatic pressure treatment: Subsequent cultivation of chondrocytes and mesenchymal stem cells on the devitalised tissue. *Sci Rep*. 2016;6(April):1-12. doi:10.1038/srep33747

80. Kivett L, Taintor J, Wright J. Evaluation of the safety of a combination of oral administration of phenylbutazone and firocoxib in horses. *J Vet Pharmacol Ther*. 2014;37(4):413-416. doi:10.1111/jvp.12097

81. Foland JW, Mcilwraith CW, Trotter GW, Powers BE, Lamar CH. Effect of Betamethasone and Exercise on Equine Carpal Joints With Osteochondral Fragments. *Vet Surg*. 1994;23(5):369-376. doi:10.1111/j.1532-950X.1994.tb00497.x

82. Contino EK. Management and Rehabilitation of Joint Disease in Sport Horses. *Vet Clin North Am - Equine Pract*. 2018;34(2):345-358. doi:10.1016/j.cveq.2018.04.007

83. King MR, Haussler KK, Kawcak CE, et al. Biomechanical and histologic evaluation of the effects of underwater treadmill exercise on horses with experimentally induced osteoarthritis of the middle carpal joint. *Am J Vet Res*. 2017;78(5):558-569. doi:10.2460/ajvr.78.5.558

84. Yovich J V., Trotter GW, McIlwraith CW, Norrdin RW. Effects of polysulfated glycosaminoglycan on chemical and physical defects in equine articular cartilage. *Am J Vet Res*. 1987;48(9):1407-1414.

85. Madry H, Ochi M, Cucchiarini M, Pape D, Seil R. Large animal models in experimental knee sports surgery: focus on clinical translation. *J Exp Orthop*. 2015;2(1):1-12. doi:10.1186/s40634-015-0025-1

86. He, Yuchen, Zhong Li, Peter G. Alexander,et al. Pathogenesis of Osteoarthritis: Risk Factors, Regulatory Pathways in Chondrocytes, and Experimental Models. *Biology* 2020;9(8):1–32 doi.org/10.3390/biology9080194

87. Wayne Mcilwraith C, Fortier LA, Frisbie DD, Nixon AJ. Equine models of articular cartilage repair. *Cartilage*. 2011;2(4):317-326. doi:10.1177/1947603511406531

88. Das C Hansen KC and Tyler JK LMS. 乳鼠心肌提取 HHS Public Access. *Physiol Behav*. 2017;176(3):139-148. doi:10.1016/j.physbeh.2017.03.040

89. Justice MJ, Dhillon P. Using the mouse to model human disease: Increasing validity and reproducibility. *DMM Dis Model Mech*. 2016;9(2):101-103. doi:10.1242/dmm.024547

90. Neuhold LA, Killar L, Zhao W, et al. Postnatal expression in hyaline cartilage of constitutively active human collagenase-3 (MMP-13) induces osteoarthritis in mice. *J Clin Invest*. 2001;107(1):35-44. doi:10.1172/JCI10564

91. Cuddy LC, Lewis DD, Kim SE, et al. Contact mechanics and three-dimensional alignment of normal dog elbows. *Vet Surg*. 2012;41(7):818-828. doi:10.1111/j.1532-950X.2012.01036.x

92. Sansone V, Applefield RC, De Luca P, et al. Does a high-fat diet affect the development and progression of osteoarthritis in mice? A systematic review. *Bone Joint Res*. 2019;8(12):582-592. doi:10.1302/2046-3758.812.BJR-2019-0038.R1

93. Glasson SS, Blanchet TJ, Morris EA. The surgical destabilization of the medial meniscus (DMM) model of osteoarthritis in the 129/SvEv mouse. *Osteoarthr Cartil*. 2007;15(9):1061-1069. doi:10.1016/j.joca.2007.03.006

94. De Croos JNA, Dhaliwal SS, Grynpas MD, Pilliar RM, Kandel RA. Cyclic compressive mechanical stimulation induces sequential catabolic and anabolic gene changes in chondrocytes resulting in increased extracellular matrix accumulation. *Matrix Biol*. 2006;25(6):323-331. doi:10.1016/j.matbio.2006.03.005

95. Novakofski KD, Torre CJ, Fortier LA. Interleukin-1α, -6, and -8 decrease Cdc42 activity resulting in loss of articular chondrocyte phenotype. *J Orthop Res*. 2012;30(2):246-251. doi:10.1002/jor.21515

96. Pearson MJ, Herndler-Brandstetter D, Tariq MA, et al. IL-6 secretion in osteoarthritis patients is mediated by chondrocyte-synovial fibroblast cross-talk and is enhanced by obesity. *Sci Rep*. 2017;7(1):1-11. doi:10.1038/s41598-017-03759-w

97. Samvelyan HJ, Hughes D, Stevens C, Staines KA. Models of Osteoarthritis: Relevance and New Insights. *Calcif Tissue Int*. 2020;1:3. doi:10.1007/s00223-020-00670-x

98. Powley IR, Patel M, Miles G, et al. Patient-derived explants (PDEs) as a powerful preclinical platform for anti-cancer drug and biomarker discovery. *Br J Cancer*. 2020;122(6):735-744. doi:10.1038/s41416-019-0672-6

99. Gilbert SJ, Singhrao SK, Khan IM, et al. Enhanced tissue integration during cartilage repair in vitro can be achieved by inhibiting chondrocyte death at the wound edge. *Tissue Eng - Part A*. 2009;15(7):1739-1749. doi:10.1089/ten.tea.2008.0361

100. Fitzgerald JB, Jin M, Dean D, Wood DJ, Zheng MH, Grodzinsky AJ. Mechanical Compression of Cartilage Explants Induces Multiple Time-dependent Gene Expression Patterns and Involves Intracellular Calcium and Cyclic AMP. *J Biol Chem*. 2004;279(19):19502-19511. doi:10.1074/jbc.M400437200

101. Anderson DE, Johnstone B. Dynamic mechanical compression of chondrocytes for tissue engineering: A critical review. *Front Bioeng Biotechnol*. 2017;5(DEC). doi:10.3389/fbioe.2017.00076

102. Cambria E, Brunner S, Heusser S, et al. Cell-Laden Agarose-Collagen Composite Hydrogels for Mechanotransduction Studies. *Front Bioeng Biotechnol*. 2020;8(April):1-14. doi:10.3389/fbioe.2020.00346

103. Ulrich TA, Jain A, Tanner K, MacKay JL, Kumar S. Probing cellular mechanobiology in three-dimensional culture with collagen-agarose matrices. *Biomaterials*. 2010;31(7):1875-1884. doi:10.1016/j.biomaterials.2009.10.047

104. Hunter CJ, Mouw JK, Levenston ME. Dynamic compression of chondrocyte-seeded fibrin gels: Effects on matrix accumulation and mechanical stiffness. *Osteoarthr Cartil*. 2004;12(2):117-130. doi:10.1016/j.joca.2003.08.009

105. Chen WH, Lo WC, Hsu WC, et al. Synergistic anabolic actions of hyaluronic acid and platelet-rich plasma on cartilage regeneration in osteoarthritis therapy. *Biomaterials*. 2014;35(36):9599-9607. doi:10.1016/j.biomaterials.2014.07.058

106. Bischof JE, Spritzer CE, Caputo AM, et al. In vivo cartilage contact strains in patients with lateral ankle instability. *J Biomech*. 2010;43(13):2561-2566. doi:10.1016/j.jbiomech.2010.05.013

107. Eckstein F, Tieschky M, Faber S, Englmeier KH, Reiser M. Functional analysis of articular cartilage deformation, recovery, and fluid flow following dynamic exercise in vivo. *Anat Embryol (Berl)*. 1999;200(4):419-424. doi:10.1007/s004290050291

108. Eckstein F, Hudelmaier M, Putz R. The effects of exercise on human articular cartilage. *J Anat*. 2006;208(4):491-512. doi:10.1111/j.1469-7580.2006.00546.x

109. Grodzinsky AJ, Levenston ME, Jin M, Frank EH. Cartilage tissue remodeling in response to mechanical forces. *Annu Rev Biomed Eng*. 2000;2(2000):691-713. doi:10.1146/annurev.bioeng.2.1.691

110. Lujan TJ, Wirtz KM, Bahney CS, Madey SM, Johnstone B, Bottlang M. A novel bioreactor for the dynamic stimulation and mechanical evaluation of multiple tissue-engineered constructs. *Tissue Eng - Part C Methods*. 2011;17(3):367-374. doi:10.1089/ten.tec.2010.0381

111. Lee DA, Bader DL. Compressive strains at physiological frequencies influence the metabolism of chondrocytes seeded in agarose. *J Orthop Res*. 1997;15(2):181-188. doi:10.1002/jor.1100150205

112. Ma HP, Deng X, Chen DY, et al. A microfluidic chip-based co-culture of fibroblast-like synoviocytes with osteoblasts and osteoclasts to test bone erosion and drug evaluation. *R Soc Open Sci*. 2018;5(9). doi:10.1098/rsos.180528

113. Canadas RF, Marques AP, Reis RL, Oliveira JM. Bioreactors and microfluidics for osteochondral interface maturation. In: *Advances in Experimental Medicine and Biology*. Vol 1059. Springer New York LLC; 2018:395-420. doi:10.1007/978-3-319-76735-2_18

114. Lee D, Erickson A, Dudley AT, Ryu S. *A Microfluidic Platform for Stimulating Chondrocytes with Dynamic Compression*. Vol 2019.; 2019. doi:10.3791/59676

115. Rosser J, Bachmann B, Jordan C, et al. Microfluidic nutrient gradient–based three-dimensional chondrocyte culture-on-a-chip as an in vitro equine arthritis model. *Mater Today Bio*.

2019;4(April):100023. doi:10.1016/j.mtbio.2019.100023

116. Fluigent. Cartilage on Chip. 2019;(Figure 1). https://www.utwente.nl/en/techmed/research/domains/bioengineering-technologies/

117. Fluigent GmbH. User's Manual - Microfluidic Automation Tool 2021:1-47.

118. Allevi3D. Live/Dead Quantification Using Fiji – Step-By-Step Guide. Published 2020. https://www.allevi3d.com/livedead-assay-quantification-fiji/

119. RStudio Team. Rstudio: Integrated Development Environment for R. *Rstudio, PBC, Boston, MA*. Published online 2020. http://www.rstudio.com/

120. GraphPad S. GraphPad Prism. *San Diego, Calif USA*. Published online 2021. www.graphpad.com

121. Schindelin J, Arganda-Carreras I, Frise E, et al. Fiji: An open-source platform for biological-image analysis. *Nat Methods*. 2012;9(7):676-682. doi:10.1038/nmeth.2019

122. Barlič A, Drobnič M, Maličev E, Kregar-Velikonja N. Quantitative analysis of gene expression in human articular chondrocytes assigned for autologous implantation. *J Orthop Res*. 2008;26(6):847-853. doi:10.1002/jor.20559

123. Caliari SR, Burdick JA. A practical guide to hydrogels for cell culture. *Nat Methods*. 2016;13(5):405-414. doi:10.1038/nmeth.3839

124. Roberts JJ, Martens PJ. Engineering biosynthetic cell encapsulation systems. In: *Biosynthetic Polymers for Medical Applications*. Elsevier Inc.; 2016:205-239. doi:10.1016/B978-1-78242-105-4.00009-2

125. Engler A, Bacakova L, Newman C, Hategan A, Griffin M, Discher D. Substrate compliance versus ligand density in cell on gel responses. *Biophys J*. 2004 Jan;86(1 Pt 1):617-28. doi: 10.1016/S0006-3495(04)74140-5.

126. Mente PL, Lewis JL. Elastic modulus of calcified cartilage is an order of magnitude less than that of subchondral bone. *J Orthop Res*. 1994;12(5):637-647. doi:10.1002/jor.1100120506

127. Silver FH, Bradica G, Tria A. Elastic energy storage in human articular cartilage: Estimation of the elastic modulus for type II collagen and changes associated with osteoarthritis. *Matrix Biol*. 2002;21(2):129-137. doi:10.1016/S0945-053X(01)00195-0

128. Schneider-Barthold C, Baganz S, Wilhelmi M, Scheper T, Pepelanova I. Hydrogels based on collagen and fibrin - Frontiers and applications. *BioNanoMaterials*. 2016;17(1-2):3-12. doi:10.1515/bnm-2015-0025

129. O'Cearbhaill ED, Murphy M, Barry F, McHugh PE, Barron V. Behavior of human mesenchymal stem cells in fibrin-based vascular tissue engineering constructs. In: *Annals of Biomedical Engineering*. Vol 38. Springer; 2010:649-657. doi:10.1007/s10439-010-9912-x

130. Huang S, Fu X. Naturally derived materials-based cell and drug delivery systems in skin regeneration. *J Control Release*. 2010;142(2):149-159. doi:10.1016/j.jconrel.2009.10.018

131. Coradin T, Wang K, Law T, Trichet L. Type I collagen-fibrin mixed hydrogels: Preparation, properties and biomedical applications. *Gels*. 2020;6(4):1-22. doi:10.3390/gels6040036

132. Guaccio A, Borselli C, Oliviero O, Netti PA. Oxygen consumption of chondrocytes in agarose and collagen gels: A comparative analysis. *Biomaterials*. 2008;29(10):1484-1493. doi:10.1016/j.biomaterials.2007.12.020

133. Cigan AD, Roach BL, Nims RJ, et al. High seeding density of human chondrocytes in agarose produces tissue-engineered cartilage approaching native mechanical and biochemical properties. *J Biomech*. 2016;49(9):1909-1917. doi:10.1016/j.jbiomech.2016.04.039

134. Stewart MC, Saunders KM, Burton-Wurster N, Macleod JN. Phenotypic Stability of Articular Chondrocytes In Vitro: The Effects of Culture Models, Bone Morphogenetic Protein 2, and Serum Supplementation. *J Bone Miner Res*. 2000;15(1):166-174. doi:10.1359/jbmr.2000.15.1.166

135. Levental I, Georges PC, Janmey PA. Soft biological materials and their impact on cell function. *Soft Matter*. 2007;3(3):299-306. doi:10.1039/b610522j

136. Gustavsson PE, Son POL. Chapter 6 Monolithic Polysaccharide Materials. In: *Journal of Chromatography Library*. Vol 67. Elsevier; 2003:121-141. doi:10.1016/S0301-4770(03)80022-2

137. Majda D, Bhattarai A, Riikonen J, et al. New approach for determining cartilage pore size distribution: NaCl-thermoporometry. *Microporous Mesoporous Mater*. 2017;241:238-245. doi:10.1016/j.micromeso.2017.01.005

138. Burgess KA, Workman VL, Elsawy MA, Miller AF, Oceandy D, Saiani A. RNA extraction from self-assembling peptide hydrogels to allow qPCR analysis of encapsulated cells. *PLoS One*. 2018;13(6). doi:10.1371/journal.pone.0197517

139. Wang L, Stegemann JP. Extraction of high quality RNA from polysaccharide matrices using cetlytrimethylammonium bromide. *Biomaterials*. 2010;31(7):1612-1618. doi:10.1016/j.biomaterials.2009.11.024

140. Miosge N, Hartmann M, Maelicke C, Herken R. Expression of collagen type I and type II in consecutive stages of human osteoarthritis. *Histochem Cell Biol*. 2004;122(3):229-236. doi:10.1007/s00418-004-0697-6

141. Wang Z, Gerstein M, Snyder M. RNA-Seq: A revolutionary tool for transcriptomics. *Nat Rev Genet*. 2009;10(1):57-63. doi:10.1038/nrg2484

142. Little CJ. Fabrication of Composite Scaffolds Impregnated with an Optimized Fibrin-Alginate Hydrogel for Cartilage Tissue Engineering. *Master Thesis - University of Saskatchewan Saskatoon 2012:1-140*

List of Figures

List of Tables